

Coherent Soft Imitation Learning

Joe Watson^{1*}, Sandy H. Huang² and Nicolas Heess²

¹Technical University of Darmstadt, Germany, ²DeepMind, *Work done during an internship at DeepMind

Imitation learning methods seek to learn from an expert either through behavioral cloning (BC) of the policy or inverse reinforcement learning (IRL) of the reward. Such methods enable agents to learn complex tasks from humans that are difficult to capture with hand-designed reward functions. Choosing BC or IRL for imitation depends on the quality and state-action coverage of the demonstrations, as well as additional access to the Markov decision process. Hybrid strategies that combine BC and IRL are not common, as initial policy optimization against inaccurate rewards diminishes the benefit of pretraining the policy with BC. This work derives an imitation method that captures the strengths of both BC and IRL. In the entropy-regularized ('soft') reinforcement learning setting, we show that the behaviour-cloned policy can be used as both a shaped reward and a critic hypothesis space by inverting the regularized policy update. This *coherency* facilities fine-tuning cloned policies using the reward estimate and additional interactions with the environment. This approach conveniently achieves imitation learning through initial behaviour cloning, followed by refinement via RL with online or offline data sources. The simplicity of the approach enables graceful scaling to high-dimensional and vision-based tasks, with stable learning and minimal hyperparameter tuning, in contrast to adversarial approaches.

Keywords: inverse reinforcement learning, behavioral cloning, learning from demonstration

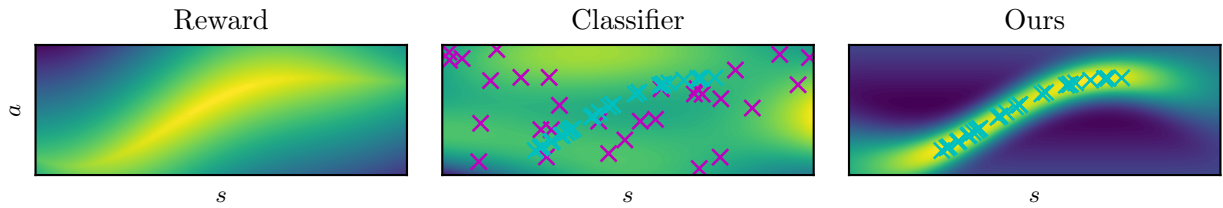


Figure 1 | By using regression rather than classification, our approach effectively infers a shaped reward from expert data, whereas classification-based methods require additional non-expert data and may struggle to resolve the difference between expert (x) and non-expert (x) samples.

1. Introduction

Imitation learning (IL) methods [Osa et al., 2018] provide algorithms for learning skills from expert demonstrations in domains such as robotics [Schaal, 1999], either through direct mimicry (behavioral cloning, BC [Pomerleau, 1991]) or inferring the latent reward (inverse reinforcement learning, IRL [Kalman, 1964, Ng and Russell, 2000, Abbeel and Ng, 2004]) assuming a Markov decision process (MDP) [Puterman, 2014, Sutton and Barto, 2018]. While BC is straightforward to implement, it is susceptible to covariate shift during evaluation [Ross and Bagnell, 2011]. IRL overcomes this problem, but tackles the harder problem of jointly learning a reward and policy from interactions. So far, these two approaches to imitation have been largely separated [Zheng et al., 2022], as optimizing the policy with an evolving reward estimate counteracts the benefit of pre-training the policy [Orsini et al., 2021]. The benefit of combining the two approaches is sample-efficient learning, which would allow any BC policy to be further improved using additional experience.

Contribution. Our IL method naturally combines BC and IRL by using the perspectives of entropy-regularized reinforcement learning (RL) [Peters et al., 2010, Fox et al., 2016, Van Hoof et al., 2017, Abdolmaleki

et al., 2018, Haarnoja et al., 2018, Bas-Serrano et al., 2021] and gradient-based IRL [Pirotta and Restelli, 2016, Ramponi et al., 2020]. Our approach uses a BC policy to define an estimate of a shaped reward for which it is optimal, that can then be used to finetune the policy with additional knowledge, such as online interactions, offline data or a dynamics model. Using the cloned policy to specify the reward avoids the need for careful regularization and hyperparameter tuning associated with adversarial imitation learning [Orsini et al., 2021, Zhang et al., 2022], and we estimate a shaped variant of the *true* reward, rather than design a heuristic proxy, e.g. [Reddy et al., 2019, Brantley et al., 2020]. In summary,

1. We use entropy-regularized RL to derive an estimate of a shaped reward from a cloned policy, which can be used to improve the policy to overcome the covariate shift problem.
2. We introduce approximate stationary stochastic process policies to implement this approach for continuous control by constructing specialized neural network architectures.
3. We show strong performance on online and offline imitation for high-dimensional and image-based continuous control tasks.

2. Background & related work

A Markov decision process is a tuple $\langle \mathcal{S}, \mathcal{A}, \mathcal{P}, r, \gamma, \mu_0 \rangle$, where \mathcal{S} is the state space, \mathcal{A} is the action space, $\mathcal{P} : \mathcal{S} \times \mathcal{A} \times \mathcal{S} \rightarrow \mathbb{R}^+$ is the transition model, $r : \mathcal{S} \times \mathcal{A} \rightarrow \mathbb{R}$ is the reward function, γ is the discount factor, and μ_0 is the initial state distribution $s_0 \sim \mu_0(\cdot)$. When evaluating a policy $\pi \in \Pi$, we use the occupancy measure $\rho_\pi(s, a) \triangleq \pi(a | s) \mu_\pi(s)$, $\mu_\pi(s) \triangleq \sum_{t=0}^{\infty} \gamma^t \mu_t^\pi(s)$ where $\mu_{t+1}^\pi(s') = \int \mathcal{P}(s' | s, a) \pi(a | s) \mu_t^\pi(s) ds da$. This measure is used to compute infinite-horizon discounted expectations, $\mathbb{E}_{s, a \sim \rho_\pi}[f(s, a)] = \mathbb{E}_{s_{t+1} \sim \mathcal{P}(\cdot | s_t, a_t), a_t \sim \pi(\cdot | s_t)}[\sum_{t=0}^{\infty} \gamma^t f(s_t, a_t)]$. Densities $d_\pi(s, a) = (1 - \gamma) \rho_\pi(s, a)$ and $\nu_\pi(s) = (1 - \gamma) \mu_\pi(s)$ are normalized measures. When the reward is unknown, imitation can be performed from a dataset \mathcal{D} of transitions (s, a, s') as demonstrations, obtained from the discounted occupancy measure of the expert policy $\pi_* = \arg \max_\pi \mathbb{E}_{s, a \sim \rho_\pi}[r(s, a)]$. The policy could be inferred directly, or by inferring a reward and policy jointly, referred to as behavioral cloning and inverse reinforcement learning respectively.

Behavioral cloning. The simplest approach to imitation is to directly mimic the behaviour using regression [Pomerleau, 1991], $\min_{\pi \in \Pi} l(\pi, \mathcal{D}) + \lambda \Psi(\pi)$, with some loss function l , hypothesis space Π and regularizer Ψ . This method is effective with sufficient data coverage and an appropriate hypothesis space, but suffers from compounding errors and cannot improve unless querying the expert [Ross and Bagnell, 2011]. The MIMIC-EXP algorithm of Rajaraman et al. [2020] motivates BC as the optimal no-interaction policy when fitting the demonstration distribution while having a uniform policy outside of the data distribution.

Inverse reinforcement learning. Rather than just inferring the policy, IRL infers the reward and policy jointly, and relies on access to the underlying MDP [Russell, 1998, Ng and Russell, 2000]. IRL iteratively finds a reward for which the expert policy is optimal compared to the set of possible policies, while also finding the policy that maximizes this reward function. Using additional data beyond the demonstrations, such as environment interactions, the learned policy seeks to match or even improve upon the expert [Abbeel and Ng, 2004]. To avoid repeatedly solving the inner RL problem, one can consider the game-theoretic approach [Syed and Schapire, 2007], where the optimization problem is a two-player zero-sum game where the policy and reward converge to the saddle point minimizing the ‘apprenticeship error’ $\min_{\pi \in \Pi} \max_{r \in \mathcal{R}} \mathbb{E}_{\mathcal{D}}[r] - \mathbb{E}_{\rho_\pi}[r]$. This approach is attractive as it learns the policy and reward concurrently. Moreover, in practice, saddle point optimization can suffer from difficult optimization when scaling to high dimensions and exhibit instabilities and hyperparameter sensitivity [Orsini et al., 2021]. Compared to BC, IRL methods theoretically scale to longer task horizons by overcoming compounding errors through environment interactions [Xu et al., 2020].

Maximum entropy inverse reinforcement learning & soft policy iteration. IRL is an under-specified problem [Russell, 1998], in particular in regions outside of the demonstration distribution. An effective way to address this is *causal entropy* regularization [Ziebart, 2010], by applying the principle of maximum entropy [Jaynes, 1982] to IRL (ME-IRL). Moreover, the entropy-regularized formulation has an elegant closed-form solution [Ziebart, 2010]. The approach can be expressed as an equivalent constrained minimum relative entropy problem for policy $q(\mathbf{a} \mid \mathbf{s})$ against a uniform prior $p(\mathbf{a} \mid \mathbf{s}) = \mathcal{U}_{\mathcal{A}}(\mathbf{a})$ using the Kullback-Leibler (KL) divergence and a constraint matching expected features ϕ , with Lagrangian

$$\min_{q, \mathbf{w}} \int_{\mathcal{S}} \nu_q(\mathbf{s}) \mathbb{D}_{\text{KL}}[q(\mathbf{a} \mid \mathbf{s}) \parallel p(\mathbf{a} \mid \mathbf{s})] d\mathbf{s} + \mathbf{w}^\top (\mathbb{E}_{\mathbf{s}, \mathbf{a} \sim \mathcal{D}}[\phi(\mathbf{s}_t, \mathbf{a}_t)] - \mathbb{E}_{\mathbf{s}, \mathbf{a} \sim \rho_q}[\phi(\mathbf{s}, \mathbf{a})]). \quad (1)$$

The constraint term can be interpreted apprenticeship error, where $\mathbf{w}^\top \phi(\mathbf{s}, \mathbf{a}) = r_{\mathbf{w}}(\mathbf{s}, \mathbf{a})$. Solving Equation 1 using dynamic programming yields the ‘soft’ Bellman equation [Ziebart, 2010],

$$\mathcal{Q}(\mathbf{s}, \mathbf{a}) = r_{\mathbf{w}}(\mathbf{s}, \mathbf{a}) + \gamma \mathbb{E}_{\mathbf{s}' \sim \mathcal{P}(\cdot \mid \mathbf{s}, \mathbf{a})} [\mathcal{V}(\mathbf{s}')] , \quad \mathcal{V}(\mathbf{s}) = \log \int_{\mathcal{A}} \exp(\mathcal{Q}(\mathbf{s}, \mathbf{a})) p(\mathbf{a} \mid \mathbf{s}) d\mathbf{a}. \quad (2)$$

Using Jensen’s inequality and importance sampling, this target is typically replaced with a lower-bound [Marino et al., 2021], which has the same optimum and samples from the optimized policy rather than the initial policy like many practical deep RL algorithms [Haarnoja et al., 2018]:

$$\mathcal{Q}(\mathbf{s}, \mathbf{a}) = r_{\mathbf{w}}(\mathbf{s}, \mathbf{a}) + \gamma \mathbb{E}_{\mathbf{a}' \sim q(\cdot \mid \mathbf{s}'), \mathbf{s}' \sim \mathcal{P}(\cdot \mid \mathbf{s}, \mathbf{a})} [\mathcal{Q}(\mathbf{s}', \mathbf{a}') - (\log q(\mathbf{a}' \mid \mathbf{s}') - \log p(\mathbf{a}' \mid \mathbf{s}'))]. \quad (3)$$

The policy update blends the exponentiated advantage function ‘pseudo-likelihood’ with the prior, as a form of regularized Boltzmann policy [Haarnoja et al., 2018] that resembles a Bayes posterior [Barber, 2012],

$$q(\mathbf{a} \mid \mathbf{s}) \propto \exp(\mathcal{Q}(\mathbf{s}, \mathbf{a}) - \mathcal{V}(\mathbf{s})) p(\mathbf{a} \mid \mathbf{s}). \quad (4)$$

These regularized updates can also be used for RL , where the problem is posed as a KL -regularized RL objective, $\max_q \mathbb{E}_{\mathbf{s}, \mathbf{a} \sim \rho_q} [\mathcal{Q}(\mathbf{s}, \mathbf{a})] - \alpha \mathbb{D}_{\text{KL}}[q(\mathbf{a} \mid \mathbf{s}) \parallel p(\mathbf{a} \mid \mathbf{s})]$, where a temperature term α controls the strength of the regularization. This regularized policy update is known as soft- [Fox et al., 2016, Haarnoja et al., 2018] or posterior policy iteration [Rawlik et al., 2013, Watson and Peters, 2022] (SPI , PPI), as it resembles a Bayesian update. In the function approximation setting, the update is performed in a variational fashion by minimizing the reverse KL divergence between the parametric policy q_{θ} and the critic-derived update at sampled states \mathbf{s}_n [Haarnoja et al., 2018],

$$\mathcal{J}(\theta) = \sum_n \mathbb{D}_{\text{KL}}[q_{\theta}(\mathbf{a} \mid \mathbf{s}_n) \parallel \exp(\alpha^{-1} \mathcal{Q}(\mathbf{s}_n, \mathbf{a}) - \mathcal{V}(\mathbf{s}_n))].$$

The above objective can be optimized using reparameterized gradients [Haarnoja et al., 2018]. A complete derivation of soft policy iteration and ME-IRL is provided in Appendix I.1.

Gradient-based inverse reinforcement learning. An alternative IRL strategy is a gradient-based approach (GIRL), that avoids saddle-point optimization by learning a reward function such that the BC policy’s policy gradient is zero [Pirotta and Restelli, 2016], which satisfies first-order optimality. However, this approach does not offer a remedy for the ill-posed nature of IRL . Moreover, the Hessian is required for the sufficient condition of optimality [Metelli et al., 2017], which is undesirable for policies with many parameters.

Related work. Prior state-of-the-art methods have combined the game-theoretic IRL objective [Syed and Schapire, 2007] with entropy-regularized RL . These methods can be as viewed as minimizing a divergence between the expert and policy, and include GAIL [Ho and Ermon, 2016], AIRL [Fu et al., 2018a], $f\text{-MAX}$ [Ghasemipour et al., 2019], DAC [Kostrikov et al., 2019], valuedICE [Kostrikov et al., 2020], IQLearn [Garg et al., 2021] and proximal point imitation learning (PPIL , [Vianco et al., 2022]). These methods differ through their choice of on-policy policy gradient (GAIL) or off-policy actor-critic (DAC , IQLearn , PPIL),

and also how the minimax optimization is implemented, e.g. using a classifier (GAIL, DAC, AIRL), implicit reward functions (valuedICE, IQLearn) or Lagrangian dual objective (PPIL). Alternative approaches to entropy-regularized IL use the Wasserstein metric (PWIL) [Dadashi et al., 2021], labelling of sparse proxy rewards (SQIL) [Reddy et al., 2019], feature matching [Ziebart, 2010, Boularias et al., 2011, Wulfmeier et al., 2015, Arenz et al., 2016], maximum likelihood [Finn et al., 2016] and matching state marginals [Ni et al., 2020] to specify the reward. Prior works at the intersection of IRL and BC include policy matching [Neu and Szepesvári, 2007], policy-based GAIL classifiers [Barde et al., 2020], annealing between a BC and GAIL policy [Jena et al., 2020] and discriminator-weighted BC [Xu et al., 2022]. Our approach is inspired by gradient-based IRL [Pirotta and Restelli, 2016, Metelli et al., 2017, Ramponi et al., 2020], which avoids the game-theoretic objective and instead estimates the reward by analysing the policy update steps with respect to the BC policy. An entropy-regularized GIRL setting was investigated in the context of learning from policy updates [Jacq et al., 2019]. For further discussion on related work, see Appendix A.

3. Coherent imitation learning

For efficient and effective imitation learning, it is desirable to combine the simplicity of behavioral cloning with the structure of the MDP, as this would provide a means to initialize and then refine an imitating policy with additional knowledge of the MDP. In this section, we propose such a method by connecting BC and IRL, inspired by GIRL. By inverting the entropy-regularized policy update in Equation 4, the cloned policy is optimal for the derived reward, a quality we refer to as *coherence*. However, before discussing the inversion step, it is also important to discuss how to design and fit the BC policy in the KL-regularized setting so that this notion of coherence is faithfully captured.

Pseudo-likelihoods in imitation learning. As discussed in Section 2, ME-IRL and KL-regularized RL are closely related, which can be reinforced using the idea of ‘pseudo-posteriors’ [Watson and Peters, 2022, van Campenhout and Cover, 1981, Guedj, 2019, Alquier et al., 2016, Knoblauch et al., 2022].

Definition 1. *Pseudo-posteriors are solutions to KL-constrained or minimum divergence problems with an additional scalar objective or vector-valued constraint term and Lagrange multipliers λ ,*

$$\begin{aligned} \max_q \quad & \mathbb{E}_{\mathbf{x} \sim q(\cdot)}[f(\mathbf{x})] - \lambda (\mathbb{D}_{KL}[q(\mathbf{x}) \parallel p(\mathbf{x})] - \epsilon) & \rightarrow & q_{\lambda}(\mathbf{x}) \propto \exp(\lambda^{-1} f(\mathbf{x})) p(\mathbf{x}). \\ \min_q \quad & \mathbb{D}_{KL}[q(\mathbf{x}) \parallel p(\mathbf{x})] - \boldsymbol{\lambda}^{\top} (\mathbb{E}_{\mathbf{x} \sim q(\cdot)}[f(\mathbf{x})] - \mathbf{f}^*) & \rightarrow & q_{\lambda}(\mathbf{x}) \propto \exp(\boldsymbol{\lambda}^{\top} \mathbf{f}(\mathbf{x})) p(\mathbf{x}). \end{aligned}$$

The $\exp(\boldsymbol{\lambda}^{\top} \mathbf{f}(\mathbf{x}))$ term is an unnormalized ‘pseudo-likelihood’, as it facilitates Bayesian inference to solve a regularized optimization problem specified by f .

Optimizing the policy distribution, the top objective captures KL-regularized RL, where f is a measure of the return and the regularization is implemented as a constraint with bound ϵ or soft penalty with constant λ . The bottom objective is the form seen in ME-IRL (Equation 1), where f is the feature space that define the reward model. Contrasting these pseudo-posterior policies against Bayesian approaches to BC, e.g. [Oh et al., 2023, Rudner et al., 2021], they can be compared against their choice of likelihood and prior. The pseudo-likelihoods in entropy-regularized IL methods produce an effective imitating policy by incorporating the MDP structure and trajectory distribution, compared to just the action prediction error typically captured by BC regression likelihoods. This point is expanded in Appendix B.

Stochastic process regression. Viewing the policy update in Equation 4 as a pseudo-posterior, behavioural cloning requires fitting the stochastic process $q(\mathbf{a} \mid \mathbf{s})$ that should embody the qualities of the specified policy prior $p(\mathbf{a} \mid \mathbf{s})$, e.g. maximum entropy regularization. While this design is straightforward to achieve in the tabular setting, it is less straightforward in the continuous setting when using function approximation. However, we can adopt ideas from Gaussian process theory to approximate such policies (Section 4). In both settings, this quality is incorporated by regularizing the regression in a Bayesian-like

fashion. This approach uses a common hypothesis space $p(\mathbf{a} | \mathbf{s}, \mathbf{w})$ (e.g. a neural network architecture or features) and latent weight distribution $p(\mathbf{w})$ such that the predictive distribution matches our policy prior, i.e. $p(\mathbf{a} | \mathbf{s}) = \int p(\mathbf{a} | \mathbf{s}, \mathbf{w}) p(\mathbf{w}) d\mathbf{w}$. In our context, behaviour cloning requires fitting $q(\mathbf{a} | \mathbf{s})$ to the demonstrations. To this end, we use its predictive distribution in order to perform conditional density estimation, rather than adopt a typical Bayesian approach to regression [Barber, 2012, Rasmussen and Williams, 2006]. Therefore, our behavioural cloning objective combines maximizing the data likelihood with respect to the predictive distribution, as well as KL regularization against the prior weight distribution, to perform regularized heteroscedastic regression [Le et al., 2005],

$$\max_{\theta} \mathbb{E}_{\mathbf{a}, \mathbf{s} \sim \mathcal{D}} [\log q_{\theta}(\mathbf{a} | \mathbf{s})] - \lambda \mathbb{D}_{\text{KL}}[q_{\theta}(\mathbf{w}) || p(\mathbf{w})], \quad q_{\theta}(\mathbf{a} | \mathbf{s}) = \int p(\mathbf{a} | \mathbf{s}, \mathbf{w}) q_{\theta}(\mathbf{w}) d\mathbf{w}. \quad (5)$$

This objective has been used to fit parametric Gaussian processes, with a similar motivation [Jankowiak et al., 2020]. Given this policy, we can ask the same question as Pirotta and Restelli [2016] did for GIRL,

For what reward and value function is this policy optimal?

Rather than using policy gradients [Pirotta and Restelli, 2016], the closed-form update of the policy provided by KL -regularized RL provides a means of conveniently answering this question analytically [Jacq et al., 2019].

Inverting soft policy iteration and reward shaping. The closed-form solution to the pseudo-posterior in Definition 1 can be inverted to provide expressions for the critic and reward (Theorem 1).

Theorem 1. (*KL-regularized policy improvement inversion*). *Let p and q_{α} be the prior and pseudo-posterior policy given by posterior policy iteration (Equation 4). The critic can be expressed as*

$$\mathcal{Q}(\mathbf{s}, \mathbf{a}) = \alpha \log \frac{q_{\alpha}(\mathbf{a} | \mathbf{s})}{p(\mathbf{a} | \mathbf{s})} + \mathcal{V}_{\alpha}(\mathbf{s}), \quad \mathcal{V}_{\alpha}(\mathbf{s}) = \alpha \log \int_{\mathcal{A}} \exp \left(\frac{1}{\alpha} \mathcal{Q}(\mathbf{s}, \mathbf{a}) \right) p(\mathbf{a} | \mathbf{s}) d\mathbf{a}. \quad (6)$$

Substituting into the KL-regularized Bellman equation lower-bound from Equation 2,

$$r(\mathbf{s}, \mathbf{a}) = \alpha \log \frac{q_{\alpha}(\mathbf{a} | \mathbf{s})}{p(\mathbf{a} | \mathbf{s})} + \mathcal{V}_{\alpha}(\mathbf{s}) - \gamma \mathbb{E}_{\mathbf{s}' \sim \mathcal{P}(\cdot | \mathbf{s}, \mathbf{a})} [\mathcal{V}_{\alpha}(\mathbf{s}')]. \quad (7)$$

The $\mathcal{V}_{\alpha}(\mathbf{s})$ term is the ‘soft’ value function. We assume $q_{\alpha}(\mathbf{a} | \mathbf{s}) = 0$ whenever $p(\mathbf{a} | \mathbf{s}) = 0$.

For the proof see Appendix I.2. Jacq et al. [2019] derived a similar inversion, but for a maximum entropy policy iteration between two policies, rather than PPI between the prior and posterior. As in Jacq et al. [2019], these expressions for the reward and critic are useful as they can be viewed as a valid form of shaping (Lemma 1), where $\alpha(\log q(\mathbf{a} | \mathbf{s}) - \log p(\mathbf{a} | \mathbf{s}))$ is a shaped ‘coherent’ reward.

Lemma 1. (*Reward shaping, Ng et al. [1999]*). *For a reward function $r : \mathcal{S} \times \mathcal{A} \rightarrow \mathbb{R}$ with optimal policy $\pi \in \Pi$, for a bounded state-based potential function $\Psi : \mathcal{S} \rightarrow \mathbb{R}$, a reward function \tilde{r} shaped by the potential function satisfying $r(\mathbf{s}, \mathbf{a}) = \tilde{r}(\mathbf{s}, \mathbf{a}) + \Psi(\mathbf{s}) - \gamma \mathbb{E}_{\mathbf{s}' \sim \mathcal{P}(\cdot | \mathbf{s}, \mathbf{a})} [\Psi(\mathbf{s}')] \mathbf{s}$ has a shaped critic $\tilde{\mathcal{Q}}$ satisfying $\mathcal{Q}(\mathbf{s}, \mathbf{a}) = \tilde{\mathcal{Q}}(\mathbf{s}, \mathbf{a}) + \Psi(\mathbf{s})$ and the same optimal policy as the original reward.*

Combining Lemma 1 and Theorem 1, estimating the pseudo-posterior policy q using behavioral cloning and constructing the scaled log policy ratio yields a shaped reward, with the soft value function as the corresponding potential $\Psi(\mathbf{s}) = \mathcal{V}_{\alpha}(\mathbf{s})$. This shaped reward can be used to improve the policy with RL (Figure 1), as it encourages behaving like the expert, while having a value of 0 when outside the data’s state distribution, which encourages policies that return to the demonstration’s state distribution when outside it. We refer to this approach as *coherent* soft imitation learning (CSIL, Algorithm 1) as the initial cloned policy is optimal for the coherent reward and critic.

Algorithm 1: Coherent soft imitation learning (CSIL)

Data: Expert demonstrations \mathcal{D} , initial temperature α , refinement temperature, β , parametric policy class $q_\theta(a | s)$, prior policy $p(a | s)$, regression regularizer Ψ , iterations N

Result: $q_{\theta_N}(a | s)$, matching or improving the initial policy $q_{\theta_1}(a | s)$

Train initial policy from demonstrations, $\theta_1 = \arg \max_{\theta} \mathbb{E}_{s, a \sim \mathcal{D}} [\log q_\theta(a | s) - \Psi(\theta)]$;

Define shaped coherent reward, $\tilde{r}_\theta(s, a) = \alpha(\log q_\theta(a | s) - \log p(a | s))$;

Choose reference policy $\pi(a | s)$ to be $p(a | s)$ or $q_{\theta_1}(a | s)$ and initialize the shaped critic, $\tilde{Q}_1(s, a) = \tilde{r}_\theta(s, a) + \gamma(\tilde{Q}_1(s', a') - \alpha(\log q_{\theta_1}(a' | s') - \log \pi(a' | s')))$, $s, a, s', a' \sim \mathcal{D}$;

for $n = 1 \rightarrow N$ **do**

- | Compute \tilde{Q}_n with soft policy iteration where $q_{\theta_n}(a | s) \propto \exp(\beta^{-1} \tilde{Q}_n(s, a)) \pi(a | s)$

end

On a high level, Algorithm 1 can be summarized by the following steps,

1. Perform regularized BC on the demonstrations with a parametric stochastic policy $q_\theta(a | s)$.
2. Define the coherent reward, $r(s, a) = \alpha(\log q(a | s) - \log p(a | s))$, with temperature α .
3. With temperature $\beta < \alpha$, perform SPI to improve on the BC policy with the coherent reward.

Using β is required to improve the policy after inverting it with temperature α . This approach is in contrast to combining BC and prior actor-critic IRL methods, where the process of learning the reward and critic from scratch can lead to ‘unlearning’ the initialized policy [Orsini et al., 2021]. While our method does not seek to learn the true reward function, and instead opts for one shaped by the environment used to generate demonstrations, in practice this is a reasonable compromise. Rather than perform true IRL, CSIL is designed to learn *policy recovery*, as the shaped reward encourages returning to the demonstration distribution when outside, which is the goal of prior imitation methods e.g. [Reddy et al., 2019, Brantley et al., 2020]. In the entropy-regularized setting, an IRL method has the drawback of requiring demonstrations generated from two different environments or discount factors to accurately infer the true reward [Cao et al., 2021], which is often not readily available in practice, e.g. when teaching a single robot a task. Moreover, additional MLPS could be used to estimate the true (unshaped) reward from data [Fu et al., 2018b, Jacq et al., 2019] if desired. Finally, as we are simply using a shaped estimate of the true reward with entropy-regularized RL, CSIL inherits the theoretical properties of these regularized algorithms [Haarnoja et al., 2018, Geist et al., 2019].

Partial expert coverage, minimax optimization and regularized regression. The reward shaping theory from Lemma 1 shows that an advantage function can be used as a shaped reward function when the state potential is a value function. By inverting the soft policy update, the log policy ratio acts as a form of its advantage function. However, in practice we do not have access to the complete advantage function, but rather an estimate, due to finite samples and partial state coverage. If the expert demonstrations provide only partial coverage of the state-action space, then the role of an inverse reinforcement learning algorithm is to learn using additional knowledge of the MDP, e.g. online samples, a dynamics model or an offline dataset, to improve the reward estimate. However, since the log policy ratio is obtained purely from demonstration data, how can it be a useful shaped reward estimate? We show that the use of entropy regularization in the initial behavioral cloning step can play an equivalent role to the saddle-point optimization in game-theoretic IRL (Theorem 2).

Theorem 2. (Coherent inverse reinforcement learning as KL-regularized behavioral cloning). A KL-regularized game-theoretic IRL objective, with policy $q_\theta(a | s)$ and coherent reward parameterization $r_\theta(s, a) = \alpha(\log q_\theta(a | s) - \log p(a | s))$ where $\alpha \geq 0$, is lower bounded by a scaled KL-regularized behavioral cloning objective and a constant term when the optimal policy, posterior and prior share a hypothesis

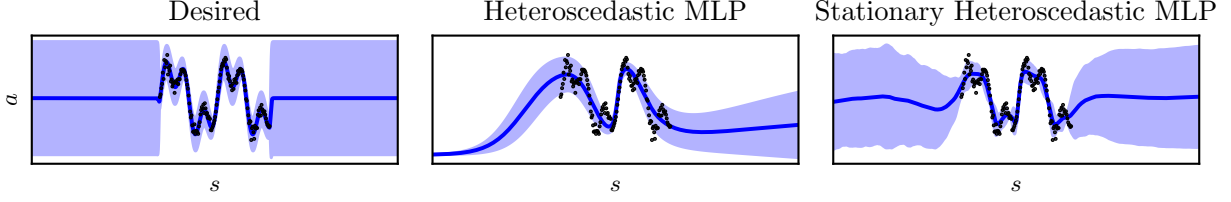


Figure 2 | For the coherent reward to be effective, the stochastic policy should return to the prior distribution outside of the data distribution (left). The typical heteroscedastic parametric policies have undefined out-of-distribution behaviour and typically collapse to the action limits due to the network extrapolation and tanh transformation (middle). By approximating stationary Gaussian processes, we can design policies that exhibit the desired behavior with minimal network modifications (right).

space $p(\mathbf{a} \mid \mathbf{s}, \mathbf{w})$ and finite parameters \mathbf{w} ,

$$\mathbb{E}_{\mathbf{s}, \mathbf{a} \sim \mathcal{D}} [r_{\theta}(\mathbf{s}, \mathbf{a})] - \mathbb{E}_{\mathbf{a} \sim q_{\theta}(\cdot \mid \mathbf{s}), \mathbf{s} \sim \mu_{q_{\theta}}(\cdot)} [r_{\theta}(\mathbf{s}, \mathbf{a}) - \beta(\log q_{\theta}(\mathbf{a} \mid \mathbf{s}) - \log p(\mathbf{a} \mid \mathbf{s}))] \geq \alpha (\mathbb{E}_{\mathbf{s}, \mathbf{a} \sim \mathcal{D}} [\log q_{\theta}(\mathbf{a} \mid \mathbf{s})] - \lambda \mathbb{D}_{KL}[q_{\theta}(\mathbf{w}) \parallel p(\mathbf{w})] + \mathbb{E}_{\mathbf{s}, \mathbf{a} \sim \mathcal{D}} [\log p(\mathbf{a} \mid \mathbf{s})]).$$

where $\lambda = (\alpha - \beta)/\alpha$ and $\mathbb{E}_{\mathbf{s}, \mathbf{a} \sim \mathcal{D}} [\log p(\mathbf{a} \mid \mathbf{s})]$ is constant. The regression objective bounds the IRL objective for a worst case on-policy state distribution $\mu_q(\mathbf{s})$, which motivates its scaling through β . If \mathcal{D} has sufficient coverage, no RL finetuning or KL regularization is required, so $\beta = \alpha$. If \mathcal{D} does not have sufficient coverage, then let $\beta < \alpha$ so $\lambda > 0$ to regularize the BC fit and finetune the policy with RL accordingly with additional soft policy iteration steps.

The proof is provided in Appendix I.3. In the tabular setting, it is straightforward for the cloned policy to retain the prior behaviour outside of the expert’s data distribution. However, in the continuous setting where function approximation is typically adopted, this behaviour is harder to capture.

4. Continuous control policies as stationary processes

Maximum entropy methods used in reinforcement learning can be recast as a minimum relative entropy problem against a regularizing prior policy with a uniform action distribution, i.e. a prior policy $p(\mathbf{a} \mid \mathbf{s}) = \mathcal{U}_{\mathcal{A}}(\mathbf{a}) \forall \mathbf{s} \in \mathcal{S}$, where $\mathcal{U}_{\mathcal{A}}$ is the uniform distribution over \mathcal{A} . Achieving such a policy in the tabular setting is straightforward, as the policy can be updated independently for each state. However, for continuous states, such a policy construction is far more difficult due to function approximation capturing correlations between states. To achieve the desired behaviour, we can use stationary process theory (Definition 2) to construct an appropriate function space (Figure 2).

Definition 2. (Stationary process, [Cox and Miller \[1977\]](#)). A process $f : \mathcal{X} \rightarrow \mathcal{Y}$ is stationary if its joint distribution in $\mathbf{y} \in \mathcal{Y}$, $p(\mathbf{y}_1, \dots, \mathbf{y}_n)$, is constant w.r.t. $\mathbf{x}_1, \dots, \mathbf{x}_n \in \mathcal{X}$ and all $n \in \mathbb{N}_{>0}$.

To approximate a stationary policy using function approximation, Gaussian process (GP) theory provides a means; using features in a Gaussian linear model that defines a stationary process [\[Rasmussen and Williams, 2006\]](#). To approximate such feature spaces using neural networks, this can be achieved through a relatively wide final layer with a periodic activation function (f_{per}), which can be shown to satisfy the stationarity property [\[Meronen et al., 2021\]](#). Refer to Appendix C for technical details. To reconcile this approach with prior work such as SAC, we use the predictive distribution of our Gaussian process in lieu of a network directly predicting Gaussian moments. The policy is defined as $\mathbf{a} = \tanh(\mathbf{z}(\mathbf{s}))$, where $\mathbf{z}(\mathbf{s}) = \mathbf{W}\phi(\mathbf{s})$. The weights are factorized row-wise $\mathbf{W} = [\mathbf{w}_1, \dots, \mathbf{w}_{d_a}]^{\top}$, $\mathbf{w}_i = \mathcal{N}(\boldsymbol{\mu}_i, \boldsymbol{\Sigma}_i)$ to define a GP with independent actions. Using change-of-variables [\[Haarnoja et al., 2018\]](#), the policy is expressed per-action as

$$q(a_i \mid \mathbf{s}) = \mathcal{N} \left(z_i; \boldsymbol{\mu}_i^{\top} \phi(\mathbf{s}), \phi(\mathbf{s})^{\top} \boldsymbol{\Sigma}_i \phi(\mathbf{s}) \right) \cdot \left| \det \left(\frac{d\mathbf{a}_i}{d\mathbf{z}_i} \right) \right|^{-1}, \quad \phi(\mathbf{s}) = f_{\text{per}}(\tilde{\mathbf{W}}\phi_{\text{mlp}}(\mathbf{s})).$$

\tilde{W} are weights drawn from a distribution, e.g. a Gaussian, that also characterizes the stochastic process and ϕ_{mlp} is an arbitrary MLP. We refer to this heteroskedastic stationary model as `HETSTAT`.

Function approximation necessitates several additional practical implementation details of `CSIL`.

Function-approximated and regularized critic. Theorem 1 and Lemma 1 show that the log policy ratio is also a shaped critic. However, we found this was not effective in the function approximation setting. The critic is instead implemented as a standard MLP and pre-trained after the policy. For coherency, a useful inductive bias is to minimize the critic Jacobian w.r.t. the expert actions to approximate first-order optimality, i.e. $\min_{\phi} \mathbb{E}_{s,a \sim \mathcal{D}} [\nabla_a Q_{\phi}(s, a)]$, as an auxiliary loss during policy evaluation. Pretraining and regularization are ablated in Figures 43 and 45 in the Appendix.

Using the cloned policy as prior. While a uniform prior is used in the `CSIL` reward, in practice we found that finetuning the cloned policy with this prior lead to divergent policies. By replacing the uniform prior (i.e. maximum entropy regularization) with the initial cloned policy, this divergent behaviour was mitigated by adopting KL regularization. This KL regularization still retains a maximum entropy effect if the `BC` policy behaves like a stationary process. This approach matches prior work on KL -regularized deep RL from demonstrations, e.g. [Siegel et al., 2020, Rudner et al., 2021].

‘Faithful’ heteroscedastic regression loss. To fit a parametric pseudo-posterior to the expert dataset, we use the predictive distribution for conditional density estimation [Jankowiak et al., 2020] using heteroscedastic regression [Le et al., 2005]. A practical issue with heteroscedastic regression with function approximators is the incorrect modelling of data as noise [Seitzer et al., 2022]. This can be overcome with a ‘faithful’ loss function and modelling construction [Stirn et al., 2023], which achieves the desired minimization of the squared error in the mean and fits the predictive variance to model the residual errors. For more details see Appendix D.

Refining the coherent reward. The `HETSTAT` network we use is still an approximation of a stationary process, as shown in Figure 2. To ensure spurious reward values from approximation errors are not exploited during learning, it can be beneficial to refine, in a minimax fashion, the coherent reward with the additional data seen during learning. This minimax refinement both reduces the stationary approximation errors of the policy, while also improving the reward from the game-theoretic `IRL` perspective. For further details and intuition see Appendix E and G.

5. Experimental results

We evaluate `CSIL` against baseline methods on tabular and continuous state-action environments. The baselines are popular entropy-regularized imitation learning methods discussed in Section 2. Moreover, ablation studies are provided in Appendix L for the experiments in Section 5.2 and 5.3

5.1. Tabular inverse optimal control

To examine the performance of `CSIL` without approximations, we consider inverse optimal control in two tabular environments. One (‘dense’) has a uniform initial distribution across the state space and several goal states, while the other (‘sparse’) has one initial state, one goal state and one forbidden state with a large negative reward. Table 1 and Appendix K.1 show the results for the nominal and a ‘windy’ environment, which has a fixed dynamics disturbance to test the policy robustness. The results show that `CSIL` is effective across all settings, especially the sparse environment where many baselines produce policies that are brittle to disturbances and therefore covariate shift. Moreover, `CSIL` produces value functions similar to `GAIL` (Figures 22 and 26) while being a simpler algorithm.

MDP	Variant	Expert	BC	Classifier	ME-IRL	GAIL	IQLearn	PPIL	CSIL
Dense	Nominal	0.266	0.200	0.249	0.251	0.253	0.244	0.229	0.257
	Windy	0.123	0.086	0.103	0.111	0.105	0.104	0.104	0.107
Sparse	Nominal	1.237	1.237	1.237	1.131	1.237	1.237	1.237	1.237
	Windy	0.052	0.002	0.044	0.036	0.043	0.002	0.002	0.044

Table 1 | Inverse optimal control, combining `SPI` and known dynamics, in tabular `MDPs`. The ‘dense’ `MDP` has a uniform initial state distribution and four goal states. The ‘sparse’ `MDP` has one initial state, one goal state and one forbidden state. The agents are trained on the nominal `MDP`. The ‘windy’ `MDP` has a random disturbance across all states to evaluate the robustness of the policy. `CSIL` performs well across all settings despite being the simpler algorithm relative to the `IRL` baselines.

5.2. Continuous control from agent demonstrations

A common benchmark of deep imitation learning is learning MuJoCo [Todorov et al., 2012] Gym [Brockman et al., 2016] and `Adroit` [Rajeswaran et al., 2018] tasks from agent demonstrations. We evaluate not only online learning, but also offline learning, where a fixed dataset is used in lieu of environment interactions [Fu et al., 2020]. `Acme` [Hoffman et al., 2020] was used to implement `CSIL` and baselines, and expert data was obtained using `rlds` [Ramos et al., 2021] from existing sources [Orsini et al., 2021, Rajeswaran et al., 2018, Fu et al., 2020]. Returns are normalized with respect to reported expert and random performance [Orsini et al., 2021] (Table 2).

Online imitation learning. In this setting we used `DAC` (actor-critic `GAIL`), `IQLearn`, `PPIL`, `SQIL` and `PWIL` as entropy-regularized imitation learning baselines. We evaluate on the common benchmark of locomotion-based Gym tasks, using the `SAC` expert data generated by Orsini et al. [2021]. In this setting, Figures 3 and 27 show `CSIL` closely matches the best baseline performance across environments and dataset sizes. We also evaluate on the `Adroit` environments, which involve manipulation tasks with a complex 27-dimensional robot hand [Rajeswaran et al., 2018]. In this setting, Figures 4 and 28 show that saddle-point methods struggle, due to the instability of the optimization in high dimensions without careful regularization and hyperparameter selection [Orsini et al., 2021]. In contrast, `CSIL` is very effective, matching or surpasses `BC`, highlighting the benefit of coherency for both policy initialization and improvement. In the Appendix, Figure 28 includes `SAC` from demonstrations (`SACFD`) [Vecerik et al., 2017, Rajeswaran et al., 2018] as an oracle baseline with access to the true reward. `CSIL` exhibits greater sample efficiency than `SACFD`, presumably due to the `BC` initialization and the shaped reward, and often matches final performance.

Offline imitation learning. Another challenging setting for deep `RL` is *offline* learning, where the online interactions are replaced with a static dataset. Note that prior works have used ‘offline’ learning to describe the setting where only the demonstrations are learned from [Kostrikov et al., 2020, Arenz and Neumann,

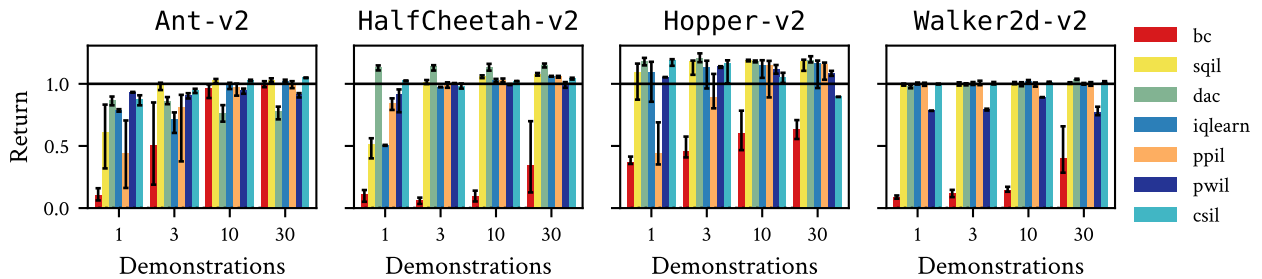


Figure 3 | Normalized performance of `CSIL` against baselines for online imitation learning for continuous control. Uncertainty intervals depict quartiles over 10 seeds. To assess convergence across seeds, performance is chosen using the highest 25th percentile of the episode return during learning.

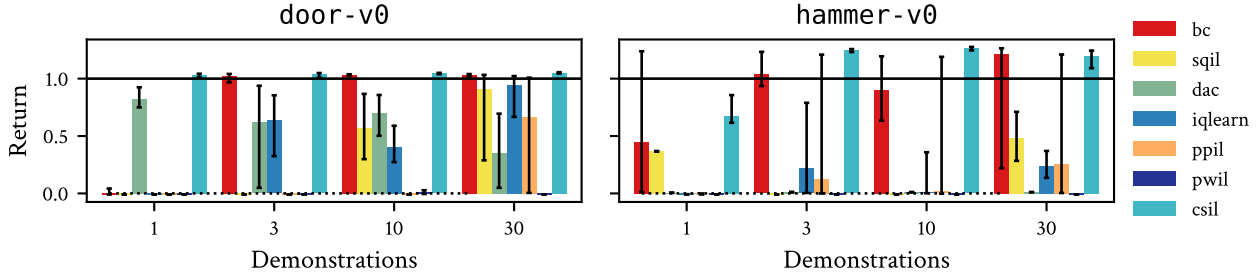


Figure 4 | Normalized performance of CSIL against baselines for online imitation learning for Adroit tasks. Uncertainty intervals depict quartiles over 10 seeds. To assess convergence across seeds, performance is chosen using the highest filtered 25th percentile of the return during learning.

2020, Garg et al., 2021, Viano et al., 2022], like in BC, such that the IL method becomes a form of regularized BC [Ziniu et al., 2022]. Standard offline learning is challenging primarily because the critic approximation can favour unseen state-actions, motivating appropriate regularization (e.g. [Kumar et al., 2020]). We use the full-replay datasets from the d4rl benchmark [Fu et al., 2020] of the Gym locomotion tasks for the offline dataset, so the offline and demonstration data is not the same. In this setting, Figures 5 and 29 demonstrate that offline learning is significantly harder than online learning, with no method solving the tasks with few demonstrations. This can be attributed to the lack of overlap between the offline and demonstration data manifesting as a sparse reward signal. However, with more demonstrations, CSIL is able to achieve reasonable performance. This is in part due to the strength of the initial BC policy, but CSIL can still demonstrate policy improvement in some cases (Figure 39). Figure 29 includes CQL [Kumar et al., 2020] as an oracle baseline, which has access to the true reward function. For some environments CSIL outperforms CQL with enough demonstrations.

5.3. Continuous control from human demonstrations from states and images

As a more realistic evaluation, we consider learning robot manipulation tasks such as picking (Lift), pick-and-place (PickPlaceCan) and insertion (NutAssemblySquare) from random initializations and mixed-quality human demonstrations using the robomimic datasets [Mandlekar et al., 2021], which also include image observations. The investigation of Mandlekar et al. [2021] considered offline RL and various forms of BC with extensive model selection. Instead, we investigate the applicability of imitation learning, using online learning with CSIL as an alternative to BC model selection. One aspect of these tasks is that they have a sparse reward based on success, which can be used to define an absorbing state. As observed in prior work [Kostrikov et al., 2019], in practice there is a synergy between absorbing states and the sign of the reward, where positive rewards encourage survival and negative rewards encourage minimum-time strategies. We found that CSIL was initially ill-suited to these goal-oriented tasks as the rewards are typically positive. In the same way that the AIRL reward can be designed for a given sign [Orsini et al., 2021], we can design negative CSIL rewards by recognising that the log policy ratio can have

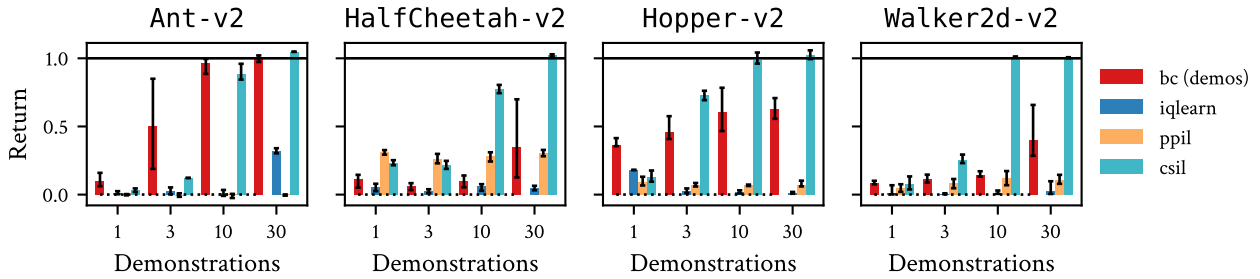


Figure 5 | Normalized performance of CSIL against baselines for offline imitation learning for Gym tasks. Uncertainty intervals depict quartiles over 10 seeds. To assess convergence across seeds, performance is chosen using the highest filtered 25th percentile of the episode return during learning.

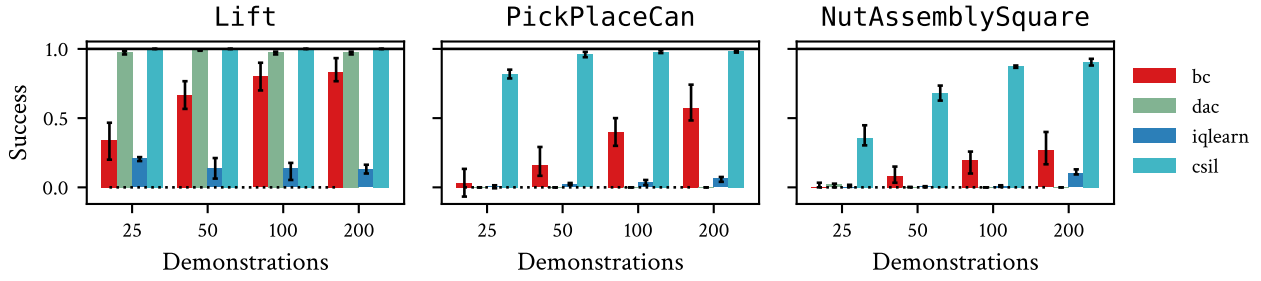


Figure 6 | Average success rate over 50 evaluations for online imitation learning for robomimic tasks. Uncertainty intervals depict quartiles over 10 seeds. To assess convergence across seeds, performance is chosen using the highest 25th percentile of the averaged success during learning.

its upper-bound subtracted (for further details, see Appendix F). These tasks are also more difficult due to the variance in the task initialization, requiring much larger function approximators than in Section 5.2. Moreover, success rate is measured over 50 random initialization. Figures 6 and 35 show the performance of CSIL and baselines, where up to 200 demonstrations are required to sufficiently solve the tasks. CSIL achieves effective performance and reasonable demonstration sample efficiency across all environments, while baselines such as DAC struggle to solve the harder tasks. Moreover, Figure 35 shows CSIL is more sample efficient than SACFD here as well. Figure 7 shows the performance on CSIL when scaled up to image-based observations, where the convolutional layers are frozen after the BC stage. CSIL was able to solve the simpler tasks in this setting, matching the model selection strategy of Mandlekar et al. [2021], demonstrating its scalability. Figure 36 shows offline state-based results with sub-optimal ('mixed human') demonstrations as offline data. While some improvement could be made on simpler tasks, on the whole it appears much harder to learn from offline human data. This supports previous observations that human interactions are sufficiently different from agent interactions to adversely affect learning algorithms [Orsini et al., 2021, Mandlekar et al., 2021].

6. Discussion

We have shown that 'coherency' is an effective approach to IL, by combining BC with IRL-based finetuning and using a shaped reward for which the BC policy is optimal. We have demonstrated the effectiveness of CSIL empirically across a range of settings, in particular for high-dimensional tasks and offline learning, due to CSIL's initialization of the policy and reward, and relative simplicity.

In Figure 34 of the Appendix, we investigate why baselines IQLearn and PPIL, both similar to CSIL, struggle in the high-dimensional and offline settings. Firstly, the sensitivity of the saddle-point optimization can be observed in the stability of the expert reward and critic values during learning. Secondly, we observe that the policy optimization does not minimize the BC objective, which is unintuitive and suggest the algorithms are lacking the quality of 'coherence' that CSIL has.

A current practical limitation of CSIL is understanding when the initial BC policy is viable as a coherent

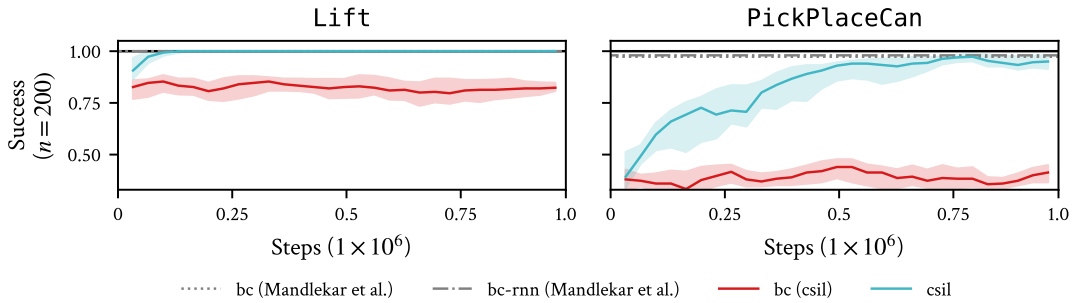


Figure 7 | Average success rate over 50 evaluations for image-based online imitation learning for robomimic tasks. Uncertainty intervals depict quartiles over 5 seeds. Baseline results obtained from Mandlekar et al. [2021]. BC (CSIL) denotes the performance of CSIL's initial policy for comparison.

reward. Our empirical results show that `CSIL` can solve complex control tasks using only one demonstration, where its `BC` policy is ineffective. However, if a demonstration-rich `BC` policy cannot solve the task (e.g. image-based `NutAssemblySquare`), `CSIL` also appears to be unable to solve the task. This suggests there is scope to improve the `BC` to make performance more consistent across more complex environments. An avenue for future work is to investigate the performance of `CSIL` with richer policy classes beyond `MLPs`, such as recurrent models, to assess the implications of the richer coherent reward.

Acknowledgements

We wish to thank Jost Tobias Springenberg, Markus Wulfmeier, Todor Davchev, Ksenia Konyushkova, Abbas Abdolmaleki and Matthew Hoffman for helpful insights and suggestions during the project. We would also like to thank Gabriel Dulac-Arnold and Sabela Ramos for help with setting up datasets and experiments, Luca Vivano for help reproducing `PPIL`, and Martin Riedmiller, Markus Wulfmeier, Oleg Arenz and Davide Tateo for feedback on the report draft.

References

Takayuki Osa, Joni Pajarinen, Gerhard Neumann, J Andrew Bagnell, Pieter Abbeel, Jan Peters, et al. An algorithmic perspective on imitation learning. *Foundations and Trends® in Robotics*, 2018.

Stefan Schaal. Is imitation learning the route to humanoid robots? *Trends in Cognitive Sciences*, 1999.

D. A. Pomerleau. Efficient training of artificial neural networks for autonomous navigation. *Neural Computation*, 1991.

Rudolph E. Kalman. When is a linear control system optimal? *Journal of Basic Engineering*, 1964.

Andrew Y. Ng and Stuart J. Russell. Algorithms for inverse reinforcement learning. In *International Conference on Machine Learning*, 2000.

P. Abbeel and A. Y. Ng. Apprenticeship learning via inverse reinforcement learning. In *International Conference on Machine Learning*, 2004.

Martin L Puterman. *Markov Decision Processes: Discrete Stochastic Dynamic Programming*. John Wiley & Sons, 2014.

Richard S Sutton and Andrew G Barto. *Reinforcement learning: An introduction*. MIT press, 2018.

Stéphane Ross and Drew Bagnell. A reduction of imitation learning and structured prediction to no-regret online learning. In *International Conference on Artificial Intelligence and Statistics*, 2011.

Boyuan Zheng, Sunny Verma, Jianlong Zhou, Ivor W Tsang, and Fang Chen. Imitation learning: Progress, taxonomies and challenges. *IEEE Transactions on Neural Networks and Learning Systems*, 2022.

Manu Orsini, Anton Raichuk, Léonard Hussenot, Damien Vincent, Robert Dadashi, Sertan Girgin, Matthieu Geist, Olivier Bachem, Olivier Pietquin, and Marcin Andrychowicz. What matters for adversarial imitation learning? In *Advances in Neural Information Processing Systems*, 2021.

Jan Peters, Katharina Mülling, and Yasemin Altün. Relative entropy policy search. In *Proceedings of the AAAI Conference on Artificial Intelligence*, 2010.

Roy Fox, Ari Pakman, and Naftali Tishby. Taming the noise in reinforcement learning via soft updates. In *Conference on Uncertainty in Artificial Intelligence*, 2016.

Herke Van Hoof, Gerhard Neumann, and Jan Peters. Non-parametric policy search with limited information loss. *Journal of Machine Learning Research*, 2017.

Abbas Abdolmaleki, Jost Tobias Springenberg, Yuval Tassa, Remi Munos, Nicolas Heess, and Martin Riedmiller. Maximum a Posteriori policy optimisation. In *International Conference on Learning Representations*, 2018.

Tuomas Haarnoja, Aurick Zhou, Pieter Abbeel, and Sergey Levine. Soft actor-critic: Off-policy maximum entropy deep reinforcement learning with a stochastic actor. In *International Conference on Machine Learning*, 2018.

Joan Bas-Serrano, Sebastian Curi, Andreas Krause, and Gergely Neu. Logistic Q -learning. In *International Conference on Artificial Intelligence and Statistics*, 2021.

Matteo Pirotta and Marcello Restelli. Inverse reinforcement learning through policy gradient minimization. In *Proceedings of the AAAI Conference on Artificial Intelligence*, 2016.

Giorgia Ramponi, Gianluca Drappo, and Marcello Restelli. Inverse reinforcement learning from a gradient-based learner. In *Advances in Neural Information Processing Systems*, 2020.

Yi-Feng Zhang, Fan-Ming Luo, and Yang Yu. Improve generated adversarial imitation learning with reward variance regularization. *Machine Learning*, 2022.

Siddharth Reddy, Anca D. Dragan, and Sergey Levine. SQIL: Imitation learning via regularized behavioral cloning. *arXiv:1905.11108*, 2019.

Kiante Brantley, Wen Sun, and Mikael Henaff. Disagreement-regularized imitation learning. In *International Conference on Learning Representations*, 2020.

Nived Rajaraman, Lin Yang, Jiantao Jiao, and Kannan Ramchandran. Toward the fundamental limits of imitation learning. *Advances in Neural Information Processing Systems*, 2020.

Stuart Russell. Learning agents for uncertain environments. In *Conference on Computational Learning Theory*, 1998.

Umar Syed and Robert E. Schapire. A game-theoretic approach to apprenticeship learning. In *Advances in Neural Information Processing Systems*, 2007.

Tian Xu, Ziniu Li, and Yang Yu. Error bounds of imitating policies and environments. *Advances in Neural Information Processing Systems*, 2020.

Brian D Ziebart. *Modeling purposeful adaptive behavior with the principle of maximum causal entropy*. Carnegie Mellon University, 2010.

Edwin T Jaynes. On the rationale of maximum-entropy methods. *Proceedings of the IEEE*, 1982.

Joseph Marino, Alexandre Piché, Alessandro Davide Ialongo, and Yisong Yue. Iterative amortized policy optimization. In *Advances in Neural Information Processing Systems*, 2021.

David Barber. *Bayesian reasoning and machine learning*. Cambridge University Press, 2012.

Konrad Rawlik, Marc Toussaint, and Sethu Vijayakumar. On stochastic optimal control and reinforcement learning by approximate inference. In *Robotics: Science and Systems*, 2013.

Joe Watson and Jan Peters. Inferring smooth control: Monte Carlo posterior policy iteration with Gaussian processes. In *Conference on Robot Learning*, 2022.

Alberto Maria Metelli, Matteo Pirotta, and Marcello Restelli. Compatible reward inverse reinforcement learning. In *Advances in Neural Information Processing Systems*, 2017.

Jonathon Ho and Stefan Ermon. Generative adversarial imitation learning. In *Advances in Neural Information Processing Systems*, 2016.

Justin Fu, Katie Luo, and Sergey Levine. Learning robust rewards with adversarial inverse reinforcement learning. In *International Conference on Learning Representations*, 2018a.

Seyed Kamyar Seyed Ghasemipour, Richard Zemel, and Shixiang Gu. A divergence minimization perspective on imitation learning methods. In *Conference on Robot Learning*, 2019.

Ilya Kostrikov, Kumar Krishna Agrawal, Debidatta Dwibedi, Sergey Levine, and Jonathan Tompson. Discriminator-actor-critic: Addressing sample inefficiency and reward bias in adversarial imitation learning. In *International Conference on Learning Representations*, 2019.

Ilya Kostrikov, Ofir Nachum, and Jonathan Tompson. Imitation learning via off-policy distribution matching. In *International Conference on Learning Representations*, 2020.

Divyansh Garg, Shuvam Chakraborty, Chris Cundy, Jiaming Song, and Stefano Ermon. IQ-learn: Inverse soft- Q learning for imitation. In *Advances in Neural Information Processing Systems*, 2021.

Luca Viano, Angeliki Kamoutsi, Gergely Neu, Igor Krawczuk, and Volkan Cevher. Proximal point imitation learning. In *Advances in Neural Information Processing Systems*, 2022.

Robert Dadashi, Leonard Hussenot, Matthieu Geist, and Olivier Pietquin. Primal Wasserstein imitation learning. In *International Conference on Learning Representations*, 2021.

Abdeslam Boularias, Jens Kober, and Jan Peters. Relative entropy inverse reinforcement learning. In *International Conference on Artificial Intelligence and Statistics*, 2011.

Markus Wulfmeier, Peter Ondruska, and Ingmar Posner. Maximum entropy deep inverse reinforcement learning. *arXiv preprint arXiv:1507.04888*, 2015.

Oleg Arenz, Hany Abdulsamad, and Gerhard Neumann. Optimal control and inverse optimal control by distribution matching. In *IEEE/RSJ International Conference on Intelligent Robots and Systems*, 2016.

Chelsea Finn, Sergey Levine, and Pieter Abbeel. Guided cost learning: Deep inverse optimal control via policy optimization. In *International Conference on Machine Learning*, 2016.

Tianwei Ni, Harshit Sikchi, Yufei Wang, Tejas Gupta, Lisa Lee, and Ben Eysenbach. f -IRL: Inverse reinforcement learning via state marginal matching. In *Conference on Robot Learning*, 2020.

Gergely Neu and Csaba Szepesvári. Apprenticeship learning using inverse reinforcement learning and gradient methods. In *Conference on Uncertainty in Artificial Intelligence*, 2007.

Paul Barde, Julien Roy, Wonseok Jeon, Joelle Pineau, Chris Pal, and Derek Nowrouzezahrai. Adversarial soft advantage fitting: Imitation learning without policy optimization. In *Advances in Neural Information Processing Systems*, 2020.

Rohit Jena, Changliu Liu, and Katia Sycara. Augmenting GAIL with BC for sample efficient imitation learning. In *Conference on Robot Learning*, 2020.

Haoran Xu, Xianyuan Zhan, Honglei Yin, and Huijing Qin. Discriminator-weighted offline imitation learning from suboptimal demonstrations. In *International Conference on Machine Learning*, 2022.

Alexis Jacq, Matthieu Geist, Ana Paiva, and Olivier Pietquin. Learning from a learner. In *International Conference on Machine Learning*, 2019.

Jan van Campenhout and Thomas Cover. Maximum entropy and conditional probability. *IEEE Transactions on Information Theory*, 1981.

Benjamin Guedj. A primer on PAC-Bayesian learning. In *Proceedings of the second congress of the French Mathematical Society*, 2019.

Pierre Alquier, James Ridgway, and Nicolas Chopin. On the properties of variational approximations of Gibbs posteriors. *Journal of Machine Learning Research*, 2016.

Jeremias Knoblauch, Jack Jewson, and Theodoros Damoulas. An optimization-centric view on Bayes' rule: Reviewing and generalizing variational inference. *Journal of Machine Learning Research*, 2022.

Hanbit Oh, Hikaru Sasaki, Brendan Michael, and Takamitsu Matsubara. Bayesian disturbance injection: Robust imitation learning of flexible policies for robot manipulation. *Neural Networks*, 2023.

Tim GJ Rudner, Cong Lu, Michael A Osborne, Yarin Gal, and Yee Teh. On pathologies in KL-regularized reinforcement learning from expert demonstrations. *Advances in Neural Information Processing Systems*, 2021.

Carl E. Rasmussen and Chris Williams. *Gaussian Processes for Machine Learning*. MIT Press, 2006.

Quoc V. Le, Alex J. Smola, and Stéphane Canu. Heteroscedastic Gaussian process regression. In *International Conference on Machine Learning*, 2005.

Martin Jankowiak, Geoff Pleiss, and Jacob Gardner. Parametric Gaussian process regressors. In *International Conference on Machine Learning*, 2020.

Andrew Y. Ng, Daishi Harada, and Stuart J. Russell. Policy invariance under reward transformations: Theory and application to reward shaping. In *International Conference on Machine Learning*, 1999.

Haoyang Cao, Samuel Cohen, and Lukasz Szpruch. Identifiability in inverse reinforcement learning. In *Advances in Neural Information Processing Systems*, 2021.

Justin Fu, Katie Luo, and Sergey Levine. Learning robust rewards with adversarial inverse reinforcement learning. In *International Conference on Learning Representations*, 2018b.

Matthieu Geist, Bruno Scherrer, and Olivier Pietquin. A theory of regularized Markov decision processes. In *International Conference on Machine Learning*, 2019.

David Roxbee Cox and Hilton David Miller. *The theory of stochastic processes*. CRC press, 1977.

Lassi Meronen, Martin Trapp, and Arno Solin. Periodic activation functions induce stationarity. In *Advances in Neural Information Processing Systems*, 2021.

Noah Siegel, Jost Tobias Springenberg, Felix Berkenkamp, Abbas Abdolmaleki, Michael Neunert, Thomas Lampe, Roland Hafner, Nicolas Heess, and Martin Riedmiller. Keep doing what worked: Behavior modelling priors for offline reinforcement learning. In *International Conference on Learning Representations*, 2020.

Maximilian Seitzer, Arash Tavakoli, Dimitrije Antic, and Georg Martius. On the pitfalls of heteroscedastic uncertainty estimation with probabilistic neural networks. In *International Conference on Learning Representations*, 2022.

Andrew Stirn, Hans-Hermann Wessels, Megan Schertzer, Laura Pereira, Neville E. Sanjana, and David A. Knowles. Faithful heteroscedastic regression with neural networks. In *International Conference on Artificial Intelligence and Statistics*, 2023.

Emanuel Todorov, Tom Erez, and Yuval Tassa. MuJoCo: A physics engine for model-based control. In *IEEE International Conference on Intelligent Robots and Systems*, 2012.

Greg Brockman, Vicki Cheung, Ludwig Pettersson, Jonas Schneider, John Schulman, Jie Tang, and Wojciech Zaremba. OpenAI Gym. *arXiv preprint arXiv:1606.01540*, 2016.

Aravind Rajeswaran, Vikash Kumar, Abhishek Gupta, Giulia Vezzani, John Schulman, Emanuel Todorov, and Sergey Levine. Learning complex dexterous manipulation with deep reinforcement learning and demonstrations. In *Robotics: Science and Systems*, 2018.

Justin Fu, Aviral Kumar, Ofir Nachum, George Tucker, and Sergey Levine. D4rl: Datasets for deep data-driven reinforcement learning. *arXiv preprint arXiv:2004.07219*, 2020.

Matthew W Hoffman, Bobak Shahriari, John Aslanides, Gabriel Barth-Maron, Nikola Momchev, Danila Sinopalnikov, Piotr Stańczyk, Sabela Ramos, Anton Raichuk, Damien Vincent, et al. Acme: A research framework for distributed reinforcement learning. *arXiv preprint arXiv:2006.00979*, 2020.

Sabela Ramos, Sertan Girgin, Léonard Huszenot, Damien Vincent, Hanna Yakubovich, Daniel Toyama, Anita Gergely, Piotr Stanczyk, Raphael Marinier, Jeremiah Harmsen, et al. Rlds: An ecosystem to generate, share and use datasets in reinforcement learning. *arXiv preprint arXiv:2111.02767*, 2021.

Mel Vecerik, Todd Hester, Jonathan Scholz, Fumin Wang, Olivier Pietquin, Bilal Piot, Nicolas Heess, Thomas Rothörl, Thomas Lampe, and Martin Riedmiller. Leveraging demonstrations for deep reinforcement learning on robotics problems with sparse rewards. *arXiv preprint arXiv:1707.08817*, 2017.

Oleg Arenz and Gerhard Neumann. Non-adversarial imitation learning and its connections to adversarial methods. *arxiv preprint arxiv:2008.03525*, 2020.

Li Ziniu, Xu Tian, Yu Yang, and Luo Zhi-Quan. Rethinking ValueDice – Does it really improve performance? ICLR Blog Track, <https://iclr-blog-track.github.io/2022/03/25/rethinking-valuedice/>, 2022.

Aviral Kumar, Aurick Zhou, George Tucker, and Sergey Levine. Conservative Q-learning for offline reinforcement learning. *Advances in Neural Information Processing Systems*, 2020.

Ajay Mandlekar, Danfei Xu, Josiah Wong, Soroush Nasiriany, Chen Wang, Rohun Kulkarni, Li Fei-Fei, Silvio Savarese, Yuke Zhu, and Roberto Martín-Martín. What matters in learning from offline human demonstrations for robot manipulation. In *Conference on Robot Learning*, 2021.

Konrad Zołna, Alexander Novikov, Ksenia Konyushkova, Caglar Gulcehre, Ziyu Wang, Yusuf Aytar, Misha Denil, Nando de Freitas, and Scott Reed. Offline learning from demonstrations and unlabeled experience. In *Offline Reinforcement Learning Workshop, NeurIPS*, 2020.

Geon-Hyeong Kim, Seokin Seo, Jongmin Lee, Wonseok Jeon, HyeongJoo Hwang, Hongseok Yang, and Kee-Eung Kim. DemoDICE: Offline imitation learning with supplementary imperfect demonstrations. In *International Conference on Learning Representations*, 2022.

Marc Peter Deisenroth, Gerhard Neumann, and Jan Peters. A survey on policy search for robotics. *Foundations and Trends in Robotics*, 2013.

Yecheng Ma, Andrew Shen, Dinesh Jayaraman, and Osbert Bastani. Versatile offline imitation from observations and examples via regularized state-occupancy matching. In *International Conference on Machine Learning*, 2022.

Firas Al-Hafez, Davide Tateo, Oleg Arenz, Guoping Zhao, and Jan Peters. LS-IQ: Implicit reward regularization for inverse reinforcement learning. In *International Conference on Learning Representations*, 2023.

Andrew Szot, Amy Zhang, Dhruv Batra, Zsolt Kira, and Franziska Meier. BC-IRL: Learning generalizable reward functions from demonstrations. In *International Conference on Learning Representations*, 2023.

Fumihiro Sasaki and Ryota Yamashina. Behavioral cloning from noisy demonstrations. In *International Conference on Learning Representations*, 2021.

Deepak Ramachandran and Eyal Amir. Bayesian inverse reinforcement learning. In *International Joint Conference on Artificial Intelligence*, 2007.

Jaedeug Choi and Kee-Eung Kim. MAP inference for Bayesian inverse reinforcement learning. *Advances in Neural Information Processing Systems*, 2011.

Giuseppe Da Prato and Jerzy Zabczyk. *Stochastic equations in infinite dimensions*. Cambridge University Press, 2014.

Chris Chatfield. *The analysis of time series: An introduction*. Chapman and Hall, 1989.

Jeremiah Liu, Zi Lin, Shreyas Padhy, Dustin Tran, Tania Bedrax Weiss, and Balaji Lakshminarayanan. Simple and principled uncertainty estimation with deterministic deep learning via distance awareness. In *Advances in Neural Information Processing Systems*, 2020.

John Schulman. Approximating KL divergence. <http://joschu.net/blog/kl-approx.html>, 2020.

Shengyang Sun, Guodong Zhang, Jiaxin Shi, and Roger Grosse. Functional variational Bayesian neural networks. In *International Conference on Learning Representations*, 2019.

Joe Watson, Jihao Andreas Lin, Pascal Klink, and Jan Peters. Neural linear models with functional Gaussian process priors. In *Third Symposium on Advances in Approximate Bayesian Inference*, 2021.

Div99. IQ-Learn implementation. <https://github.com/Div99/IQ-Learn>, 2021.

Yihong Wu. Lecture notes for ECE598YW: Information-theoretic methods in high-dimensional statistics. Yale University, 2016.

James Bradbury, Roy Frostig, Peter Hawkins, Matthew James Johnson, Chris Leary, Dougal Maclaurin, George Necula, Adam Paszke, Jake VanderPlas, Skye Wanderman-Milne, and Qiao Zhang. JAX: Composable transformations of Python+NumPy programs, 2018. URL <http://github.com/google/jax>.

lviano. Proximal point imitation learning implementation. <https://github.com/lviano/p2il>, 2022.

Lasse Espeholt, Hubert Soyer, Remi Munos, Karen Simonyan, Vlad Mnih, Tom Ward, Yotam Doron, Vlad Firoiu, Tim Harley, Iain Dunning, et al. Impala: Scalable distributed deep-RL with importance weighted actor-learner architectures. In *International conference on machine learning*, 2018.

A. Extended related work

This section discusses more of the relevant prior works and in more detail.

Generative adversarial imitation learning (**GAIL**) [Ho and Ermon, 2016] combines the game-theoretic **IRL** objective with causal entropy regularization and convex regularization of the reward. This primal optimization problem can be transformed into a dual objective, which has the interpretation of minimizing a divergence between the expert and imitator’s stationary distributions, where the divergence corresponds to the choice of convex reward regularization. Choosing regularization that reduced the reward to a classification problem corresponds to the Jensen-Shannon (JS) divergence. While **GAIL** used on-policy **RL**, **DAC** [Kostrikov et al., 2019] used off-policy actor critic methods (e.g. **SAC**) in an adhoc fashion for greater sample efficiency. **ORIL** [Zolna et al., 2020] adopts a classification-based reward in the offline setting. Kostrikov et al. [2019] also note that the **GAIL** classifier can be used in different forms to produce rewards with different forms. **AIRL** [Fu et al., 2018b] highlight that the **GAIL** reward is shaped by the dynamics if the **MDP** following the shaping theory of Ng and Russell [2000], and use additional approximators that disentangle the shaping terms. **NAIL** [Arenz and Neumann, 2020] replaces the minimax nature of adversarial learning with a more stable max-max approach using expectation maximization-like optimization on a lower-bound of the **KL** divergence between policies. Its reward function is defined, as with **AIRL**, as the log density ratio of the stationary distributions of the expert and policy, regularized by the causal entropy. **NAIL** and **CSIL** therefore have similar reward structures, however while **CSIL**’s reward can be obtained from **BC** and prior design, **NAIL** requires iterative density ratio estimation during learning. Ghasemipour et al. [2019] investigate the performance of **AIRL** with different f -divergences, and corresponding reward regularization, beyond JS such as the forward and reverse **KL** divergence. Ghasemipour et al. [2019] discuss the connection between the log density ratio and **AIRL**, **GAIL** and their proposed methods. Ghasemipour et al. [2019] also connect **BC** to **IRL**, but from the divergence perspective rather than the likelihood perspective, as the conditional **KL** divergence between policies can be used for **BC**.

A separate line of study uses the convex duality in a slightly different fashion for ‘discounted distribution correction estimation’ (**DICE**) methods. **valuedICE** uses the Donsker-Varadhan representation to transform the **KL** minimization problem into an alternative form, and a change of variables to represent the log ratio of the stationary distributions as with an implicit representation using the Bellman operator. However, this alternative form is still a saddle-point problem like **GAIL**. The final objective is more amenable to off-policy optimization. **DemodICE** [Kim et al., 2022] considers the offline setting and incorporates **KL**-regularization into the **DICE** framework which simplifies optimization. Due to the offline setting, the reward is obtained using a pretrained classifier. Policy improvement reduces to weighted **BC**, like in many **KL**-regularized **RL** methods [Deisenroth et al., 2013, Abdolmaleki et al., 2018]. **SmodICE** [Ma et al., 2022] is closely related to **DemodICE**, but focuses on matching the state distribution and therefore does not rely on expert actions. In their offline **Gym** experiments, **SmodICE** and **demodICE** required of expert demonstrations in the hundreds, whereas **CSIL** has demonstrated online and offline imitators can succeed with around 30.

Inverse soft Q -learning (**IQLearn**) [Garg et al., 2021] combined the game-theoretic **IRL** objective, entropy-regularized actor-critic (**SAC**), convex reward regularization and implicit rewards to perform **IRL** using only the critic by maximizing the expert’s implicit reward. While Garg et al. [2021] claim their method is non-adversarial, it is still derived from the game-theoretic objective, and for continuous control the **IQLearn** implementation requires shaping the implicit reward using online samples, like **GAIL**. Moreover, the implementation replaces the minimization of the initial value with the value evaluated for the expert samples. For **SAC**, in which the value function is computed by evaluating the critic with the policy, this amounts to shaping the critic to have a local maxima around the expert samples. We found this implementation detail to be crucial to reproduce the results for few demonstrations.

Proximal point imitation learning (**PPIL**) [Viano et al., 2022] combines the game-theoretic and linear

programming forms of `IRL`, along with entropy-regularized actor-critic `RL`, to derive an effective method with convergence guarantees. Its construction yields a single objective (the dual) for optimizing the reward and critic jointly in a more stable fashion, rather than alternating updates like in `DAC`, but unlike `IQLearn` it has an explicit reward model. For continuous control, its implementation builds on `SAC` and `IQLearn`, including the aforementioned tricks, but with two key differences: an explicit reward function and minimization of the ‘logistic’, rather than squared, Bellman error [Bas-Serrano et al., 2021].

In the context of these works, `CSIL` has two key distinctions. One is the reward hypothesis space in the form of the log policy ratio, which is derived from `KL`-regularized `RL`, as opposed to a classifier-based reward or critic-as-classifier implicit reward. Secondly, the consequence of this coherent reward is that it can be pretrained using `BC` and the `BC` policy can be used as reference policy. While `BC` pretraining could be incorporated into prior methods in an adhoc fashion, their optimization objectives to do not guarantee that coherency is maintained. This is demonstrated in Figure 34, where `IQLearn` and `PPIL` combined with `BC` pretraining and `KL` regularization do not converge like `CSIL`.

Concurrent work, least-squares inverse Q -learning (`LS-IQ`) [Al-Hafez et al., 2023], addresses the undocumented regularization of `IQLearn` by minimizing a mixture divergence which yields to desired regularization terms and better treatment of absorbing states. The treatment moves away from entropy-regularized `RL` view and instead opts for explicit regularization critics instead.

[Szot et al. \[2023\]](#), in concurrent work, use the bi-level optimization view of `IRL` to optimize the maximum entropy reward through an upper-level behavioral cloning loss using ‘meta’ gradients. This approach achieves coherency through the top-level loss while also regularizing the learned reward. However, this approach is restricted to on-policy `RL` algorithms that directly use the reward rather than actor-critics methods that use a Q function, so it is less sample efficient.

[Brantley et al. \[2020\]](#) propose disagreement-regularized imitation learning, which trains an ensemble of policies via `BC` and uses their predictive variance to define a proxy reward. This work shares the same motivation as `CSIL`, coherency and policy recovery. Moreover, the use of ensembles is similar to `CSIL`’s stationary policies, as both models are inspired by Bayesian modelling and exhibit meaningful uncertainty quantification. Unlike `CSIL`, the method is not motivated by reward shaping and the reward is obtained by thresholding the predictive variance to ± 1 , rather than assume a the likelihood values are meaningful.

‘Noisy’ `BC` [[Sasaki and Yamashina, 2021](#)] is tangentially related to `CSIL`, as it uses the `BC` loglikelihood as a proxy reward to finetune a `BC` policy trained on perturbed demonstrations by mode seeking via policy gradient updates.

Soft Q -imitation learning (`SQL`) [[Reddy et al., 2019](#)] uses binary rewards for the demonstration and interaction transitions, bypassing the complexity of standard `IRL`. The benefit of this approach comes from the critic learning policy recovery strategies from the credit assignment. This approach has no theoretical guarantees, and the simplistic nature of the reward does not encourage stable convergence in practice.

[Barde et al. \[2020\]](#) proposed adversarial soft advantage fitting (`ASAF`), an adversarial approach that constructs the classifier using two policies over trajectories or transitions. This approach is attractive as the classification step performs the policy update, so no policy evaluation step is required. While this approach has clear connections to regularized behavioral cloning, its uncertain how it can perform policy recovery without any credit assignment. Moreover, this method has no convergence guarantees.

`CSIL` adopts a Bayesian-style approach to its initial `BC` policy by specifying a prior policy, but uses the predictive distribution rather than a likelihood to fit the demonstration data. This is in contrast to Bayesian `IRL` [[Ramachandran and Amir, 2007](#)], where the prior is place over the reward function as a means of reasoning about its ambiguity. As the reward is an unobserved abstract quantity, the exponentiated critic is adopted as a pseudo-likelihood and approximate inference is required to estimate the posterior reward. This

use of a pseudo-likelihood means that Bayesian `IRL` and `ME-IRL` are not so different in practice, especially when using point estimates of the posterior [Choi and Kim, 2011].

B. Likelihoods and priors in imitation learning

The pseudo-posterior perspective in this work was inspired by van Campenhout and Cover [1981], who identify that effective likelihoods arise from relevant functions that describe a distribution. With this in mind, we believe it is useful to see `IRL` as extending `BC` from a myopic, state-independent likelihood to one that encodes the causal, state-dependent nature of the problem as done `ME-IRL`, essentially incorporating the structure of the `MDP` into the regression problem [Neu and Szepesvári, 2007]. This perspective has two key consequences. One is the importance of the prior, which provides important regularization. For example, Ziniu et al. [2022] have previously showed that the `valuedICE` does not necessarily outperform `BC` as previously reported, but rather matches `BC` with appropriate regularization. Moreover, the `MIMIC-EXP` formulation of `BC` of Rajaraman et al. [2020] proposes a stationary-like `BC` policy,

$$\pi(a | s) = \begin{cases} p_{\mathcal{D}}(a | s) \text{ if } s \in \mathcal{D}, \text{ where } p_{\mathcal{D}} \text{ denotes conditional density estimation of } \mathcal{D}, \\ \mathcal{U}_{\mathcal{A}}(a) \text{ otherwise.} \end{cases}$$

Stationary policies have been seldom considered in entropy-regularized `RL` but is a major component of this work. The second consequence is the open-question of how to define effective likelihoods for imitation learning. `ME-IRL` and other prior works uses feature matching which, while an appropriate constraint, raises the additional question of which features are needed. The use of a classifier in `AIRL` has proved highly effective, but not always straightforward to implement in practice without regularization and hyperparameter tuning. Much of `IQLearn`'s empirical success for continuous tasks arises from the shaping of the critic-as-likelihood through the expert and on-policy regularization terms.

This work addresses the likelihood design problem through the idea of coherence and the inversion analysis in Theorem 1, which informs the function-approximated critic regularization described in Section 4. An open question is how these design choices could be further improved, as the ablation study in Figure 45 shows that the benefit of the critic regularization is not universal.

C. Parametric stationary processes

The effectiveness of `CSIL` is down to its stationary policy design. This section briefly summarizes the definition of stationary processes and how they can be approximated with `MLPs` following the work of Meronen et al. [2021].

While typically discussed for temporal stochastic processes whose input is time, stationary processes (Definition 2) are those whose statistics do not vary with their input. In machine learning, these processes are useful as they allow us to design priors that are consistent per input but capture correlations (e.g. smoothness) across inputs, which can be used for regularization in regression and classification [Rasmussen and Williams, 2006]. In the continuous setting, stationarity can be defined for linear models, i.e. $y = \mathbf{w}^\top \phi(\mathbf{x})$, $\mathbf{w} \sim \mathcal{N}(\mu, \Sigma)$, through their kernel function $\mathcal{K}(\mathbf{x}, \mathbf{x}') = \phi(\mathbf{x})^\top \phi(\mathbf{x}')$, the feature inner product. For stationary kernels, the kernel depends only on a relative shift $\mathbf{r} \in \mathbb{R}^d$ between inputs, i.e. $\mathcal{K}(\mathbf{r}) = \phi(\mathbf{x})^\top \phi(\mathbf{x} + \mathbf{r})$. By combining the kernel with the weight prior of the linear model, we can define the covariance function, e.g. $\mathcal{C}(\mathbf{r}) = \phi(\mathbf{x})^\top \Sigma \phi(\mathbf{x} + \mathbf{r})$. Boschner's theorem [Da Prato and Zabczyk, 2014] states that the covariance function of a stationary process can be represented as the Fourier transform of a positive finite measure. If the measure has a density, it is known as the spectral density $S(\omega)$, and it is a Fourier dual of the covariance function if the necessary conditions apply, known as the Wiener-Khinchin

theorem [Chatfield, 1989],

$$\mathcal{C}(\mathbf{r}) = \frac{1}{(2\pi)^d} \int_{\mathbb{R}^d} S(\boldsymbol{\omega}) \exp(i\boldsymbol{\omega}^\top \mathbf{r}) d\mathbf{r}, \quad S(\boldsymbol{\omega}) = \int_{\mathbb{R}^d} \mathcal{C}(\mathbf{r}) \exp(-i\boldsymbol{\omega}^\top \mathbf{r}) d\boldsymbol{\omega}. \quad (8)$$

To use this theory to design stationary function approximators, we can use the Wiener-Khintchin theorem to design function approximators that produce Monte Carlo approximation of stationary kernels. Firstly, we consider only the last layer of the `MLP`, such that it can be viewed as a linear model. Secondly, Meronen et al. [2021] describe several periodic activation functions that produce products of the form $\exp(i\boldsymbol{\omega}^\top \mathbf{r})$, such that the inner product of the whole feature space performs a Monte Carlo approximation of the integral. We implemented sinusoidal, triangular and periodic ReLU activations (see Figure 3 of Meronen et al. [2021]) as a policy architecture hyperparameter. Thirdly, the input into the stationary kernel approximation should be small (e.g. < 20), as the stationary behaviour is dictated by \mathbf{r} , and this distance becomes less meaningful in higher dimensions. This means the `MLP` feature space that feeds into the last layer should be small or have a ‘bottleneck’ architecture to compress the internal representation. Finally, we require a density to represent the spectral density, which also defines the nature of the stationary process. We use a Gaussian, but other distributions such as a Student- t or Cauchy could be used if ‘rougher’ processes are desired. In summary, the last layer activations take the form $f_p(\mathbf{W}\phi(\mathbf{x}))$, where f_p is the periodic activation function of choice, \mathbf{W} are weights sampled from the distribution of choice and $\phi(\mathbf{x})$ is an arbitrary (bottlenecked) `MLP` feature space of choice.

Related work combining stationary kernel approximations with `MLPs` have constrained the feature space with a residual architecture and spectral normalization to bound the upper and lower Lipschitz constant [Liu et al., 2020], to prevent these features overfitting. We found we did not need this to achieve approximate stationarity (e.g. Figure 2), which avoided the need for environment-dependent policy architectures and the risk of underfitting.

A crucial practical detail is that the sampled weights \mathbf{W} should be trained and not kept constant, as the theory suggests. In practice, we did not observe the statistics of these weights changing significantly during training, while training this weight layer reduced underfitting enough for significantly more effective `BC` performance.

D. Faithful heteroscedastic regression

This section summarizes the approach of Stirn et al. [2023]. The faithful objective combines the mean squared error (`MSE`) and negative loglikelihood `NLLH` loss with a careful construction of the heteroscedastic model. The loss is

$$\mathcal{L}(\mathcal{D}, \boldsymbol{\theta}) = \mathbb{E}_{s, \mathbf{a} \sim \mathcal{D}} \left[(\mathbf{a} - \boldsymbol{\mu}_{\boldsymbol{\theta}}(s))^2 - \log \tilde{q}(\mathbf{a} \mid s) \right], \quad \tilde{q}(\mathbf{a} \mid s) = \mathcal{N}(\text{sg}(\boldsymbol{\mu}_{\boldsymbol{\theta}}(s)), \boldsymbol{\Sigma}_{\boldsymbol{\theta}}(s)), \quad (9)$$

where `sg`(\cdot) denotes the stop gradient operator. Moreover, for the models ‘shared torso’ (e.g. features), the gradient is stopped between the torso and the predictive variance, so that the features are only trained to satisfy the `MSE` objective. Figure 8 illustrates the impact of the alternative loss function and model adjustments. Note that the faithful objective is not strictly necessary for `BC` or `CSIL`, and is mitigating a potential issue seen in practice. The issue of modelling ‘signal’ as noise when using heteroscedastic function approximators is poorly understood, and depends on model architecture, initialization and the dataset considered. While motivated by 1D toy examples, it was observed during development that the faithful objective is beneficial for `CSIL`’s downstream performance.

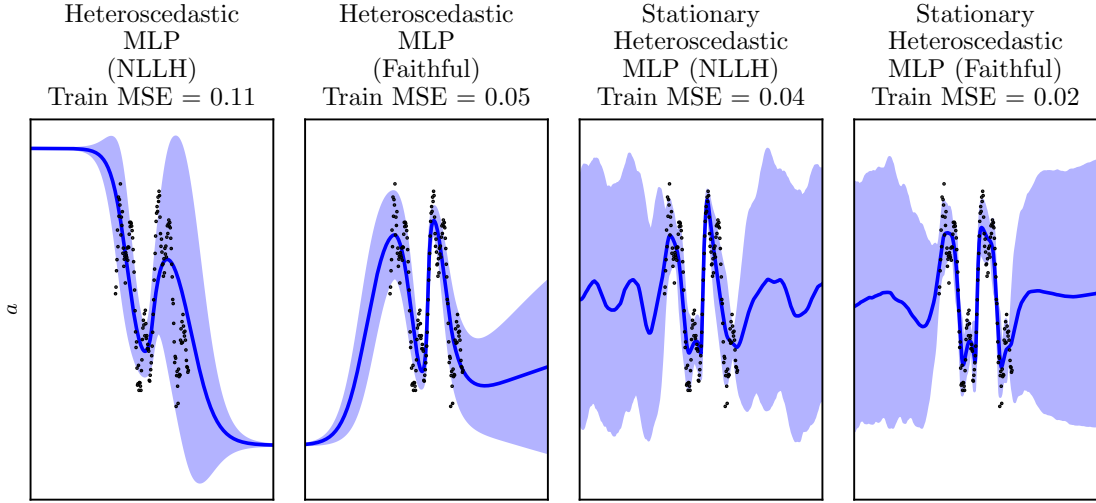


Figure 8 | We repeat the regression problem from Figure 2 to highlight the effect of ‘faithful’ heteroscedastic regression. The `NLLH` objective has a tendency to model ‘signal’ as noise, which is most clearly seen in the heteroscedastic `MLP`. For both models, the faithful heteroscedastic loss reduces the mean prediction error significantly without affecting uncertainty quantification.

E. Reward refinement and function-space relative entropy estimation

In the function approximation setting, we refine the reward model with additional non-expert samples. Motivated by Theorem 2, we maximize the objective using samples from the replay buffers

$$\mathcal{J}_r(\theta) = \mathbb{E}_{s, a \sim \mathcal{D}} \left[\alpha \log \frac{q_\theta(a | s)}{p(a | s)} \right] - \mathbb{E}_{s, a \sim \rho_\pi} \left[\alpha \log \frac{q_\theta(a | s)}{p(a | s)} \right]. \quad (10)$$

If the behaviour policy π is $q_\theta(a | s)$, we can view the second term as a Monte Carlo estimation of the relative KL divergence between q and p . This estimator can suffer greatly from bias, as the KL should always be non-negative. To counteract this, we construct an unbiased, positively-constrained estimator following Schulman [2020], using $\mathbb{E}_{x \sim q(\cdot)}[R(x)^{-1}] = \int p(x) dx = 1$ and $\log(x) \leq x - 1$,

$$\mathbb{D}_{\text{KL}}[q(\mathbf{x}) || p(\mathbf{x})] = \mathbb{E}_{\mathbf{x} \sim q(\cdot)}[\log R(\mathbf{x})] = \mathbb{E}_{\mathbf{x} \sim q(\cdot)}[R(\mathbf{x})^{-1} - 1 + \log R(\mathbf{x})],$$

This estimator results in replacing the second term of Equation 10 with

$$\mathbb{E}_{s, a \sim \rho_\pi} [r_\theta(s, a)] \rightarrow \mathbb{E}_{s, a \sim \rho_\pi} [r_\theta(s, a) - \alpha + \alpha \exp(-r_\theta(s, a)/\alpha)].$$

This objective is maximized concurrently with policy evaluation, using samples from the replay buffer. This reward refinement is similar to behavioral cloning via function-space variational inference (e.g. [Sun et al., 2019, Watson et al., 2021]), enforcing the prior using the prior predictive distribution rather than the prior weight, distribution.

In practice, the samples are taken from a replay buffer of online and offline data, so the action samples are actually taken from a different distribution to q_θ . However, we still found the adjust objective effective for reward regularization. Without it, the saddle-point refinement was less stable. Appendix G illustrates this refinement in a simple setting. Figure 44 ablates this component, where its effect is most beneficial when there are fewer demonstrations.

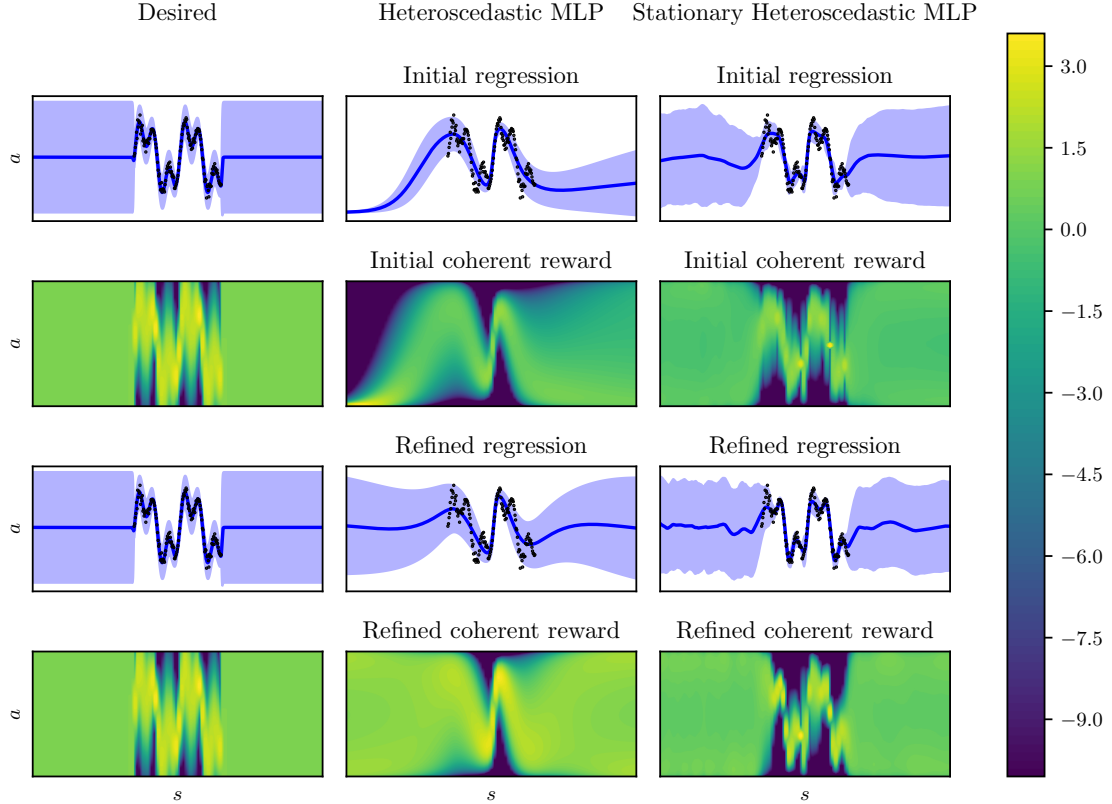


Figure 9 | We extend the regression problem from Figure 2 to highlight the effect of reward refinement detailed in Section E from the BC and IRL perspective. Refining the coherent reward with a minimax objective results in a BC policy that appears more stationary, as seen in the heteroscedastic MLP. The stationary heteroscedastic policy is also refined, but to a lesser degree, as its stationary quality is still an approximation. The colourmap is shared between contour plots, and rewards are clipped at -10 to improve the visual colour range. Regression uncertainty is one standard deviation.

F. Bounding the coherent reward

The coherent reward $\alpha(\log q(\mathbf{a} \mid \mathbf{s}) - \log p(\mathbf{a} \mid \mathbf{s}))$ can be upper bounded if $p(\mathbf{a} \mid \mathbf{s}) > 0$ whenever $q(\mathbf{a} \mid \mathbf{s}) > 0$. The bound is policy dependent. We make use of the bound in the continuous setting where we use a tanh-transformed Gaussian policy. We add a small bias term σ_{\min}^2 to the predictive variance in order to define the Gaussian likelihood upper bound. Inconveniently, the tanh change of variables term in the loglikelihood $-\sum_{i=1}^{d_a} \log(1 - \tanh^2(u))$ [Haarnoja et al., 2018] has no upper bound in theory, as the ‘latent’ action $u \in [-\infty, \infty]$, but in the Acme implementation this loglikelihood is bounded for numerical stability due to the inverse tanh operation. For action dimension d_a and uniform prior across action range $[-1, 1]^{d_a}$ and $\alpha = d_a^{-1}$, the upper bound is $r(\mathbf{s}, \mathbf{a}) \leq \frac{1}{d_a}(-0.5d_a \log 2\pi\sigma_{\min}^2 + c + d_a \log 2) = -0.5 \log \pi\sigma_{\min}^2/2 + \tilde{c}$, where c, \tilde{c} depends on the tanh clipping term.

G. Visualizing reward refinement

To provide intuition on Theorem 2 and connect it to reward refinement (Appendix E) we build on the regression example from Figure 2 by viewing it as a continuous contextual bandit problem, i.e. a single-state MDP with no dynamics. Outside of the demonstration state distribution, we desire that the reward is uniformly zero, as we have no data to inform action preference. Figure 9 shows the result of applying CSIL and reward refinement to this MDP, where the state distribution is uniform. The ‘desired’ BC fit exhibits a coherent reward with the desired qualities, and the HETSTAT policy approximates this desired

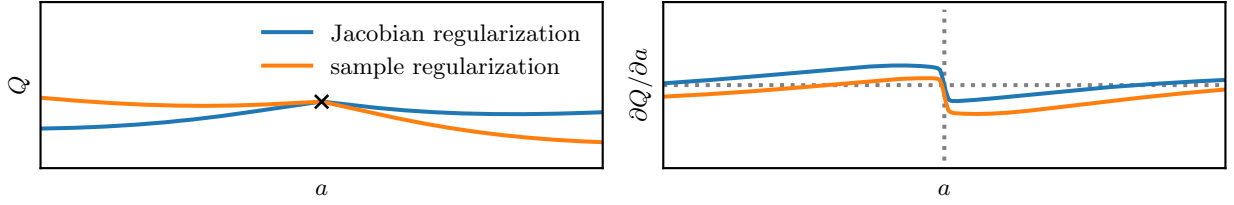


Figure 10 | Illustrating the two forms of critic regularization on a toy 1D problem for critic $Q(a)$ with regression target \mathbf{x} . Jacobian regularization minimizing the squared gradient, and corresponds to **CSIL**. Sample regularization minimizes sampled nearby actions, and corresponds to **IQLearn** and **PPIL**. Both approaches shape the critic to have zero gradient around the target action, denoted by the dotted lines. A standard two layer **MLP** with 256 units and **ELU** actions is used for approximation.

policy. The heteroskedastic **MLP** exhibits undesirable out-of-distribution (OOD) behaviour, where arbitrary regions have strongly positive or negative reward. Reward refinement improves the coherent reward of the heteroscedastic **MLP** to be more uniform OOD, which in turn makes the regression fit look more like a stationary policy. This is the intuition behind Theorem 2, which shows that κL -regularized **BC** corresponds to a game-theoretic **IRL** objective lower bound with the coherent reward.

H. Critic regularization

For the function approximation setting, **CSIL** requires an auxiliary loss term during learning to incorporate coherency. The full critic objective is

$$\min_{\phi} \mathbb{E}_{s,a \sim \mathcal{D}_R} [(\mathcal{Q}_\phi(s, a) - \mathcal{Q}^*(s, a))^2] + \mathbb{E}_{s,a \sim \mathcal{D}} [\|\nabla_a \mathcal{Q}_\phi(s, a)\|^2],$$

where \mathcal{Q}^* denotes the target Q values and \mathcal{D}_R denotes the replay buffer, that combines demonstrations \mathcal{D} and additional samples. The motivation is to shape the critic such that the demonstration actions are first-order optimal by minimizing the squared Frobenius norm of the action Jacobian.

IQLearn and **PPIL** adopt similar regularization, but one that is less explicit. Equation 10 of [Garg et al. \[2021\]](#) is

$$\max_{\phi} \mathbb{E}_{s,a \sim \mathcal{D}_R} [f \left(\mathcal{Q}_\phi(s, a) - \gamma \mathbb{E}_{s' \sim \mathcal{P}(\cdot | s, a)} [\mathcal{V}_\phi^\pi(s')] \right)] - (1 - \gamma) \mathbb{E}_{s \sim \mu_0} [\mathcal{V}_\phi^\pi(s)],$$

where $\mathcal{V}_\phi^\pi(s) = \mathcal{Q}(s, a')$, $a' \sim \pi(\cdot | s)$ and f is the concave function defining the implicit reward regularization. In the implementation [\[Div99, 2021\]](#), the ‘v0’ objective variant replaces the initial distribution μ_0 with the demonstration state distribution. This trick is deployed to improve regularization without affecting optimality (Section 5.3, [Kostrikov et al. \[2020\]](#)). If the policy is matching the expert actions with its mode, then this term is shaping a local maximum by minimizing the critic at action samples around the expert. However, if the policy is not accurately matching the expert actions, the effect of this term is harder to reason about. In Figure 10, we illustrate these two forms from critic regularization on a toy example, demonstrating that both can produce local maximums in the critic.

I. Theoretical results

This section provides derivations and proofs for the theoretical results in the main text.

I.1. Relative entropy regularization for reinforcement learning

This section re-derives KL -regularized RL and ME-IRL in a shared notation for the reader's reference.

Reinforcement learning. We consider the discounted, infinite-horizon setting with a hard KL constraint on the policy update with bound ϵ ,

$$\max_q \mathbb{E}_{\mathbf{s}_{t+1} \sim \mathcal{P}(\cdot | \mathbf{s}, \mathbf{a}), \mathbf{a} \sim q(\cdot | \mathbf{s}), \mathbf{s}_0 \sim \mu_0(\cdot)} [\sum_t \gamma^t r(\mathbf{s}_t, \mathbf{a}_t)] \quad \text{s.t.} \quad \mathbb{E}_{\mathbf{s} \sim \nu_q(\cdot)} [\mathbb{D}_{\text{KL}}[q(\mathbf{a} | \mathbf{s}) || p(\mathbf{a} | \mathbf{s})]] \leq \epsilon.$$

This constrained objective is transcribed into the following Lagrangian objective following [Van Hoof et al. \[2017\]](#), using the discounted stationary joint distribution $d(\mathbf{s}, \mathbf{a}) = q(\mathbf{a} | \mathbf{s}) \nu(\mathbf{s}) = (1 - \gamma) \rho(\mathbf{s}, \mathbf{a})$,

$$\begin{aligned} \mathcal{L}(d, \lambda_1, \lambda_2, \lambda_3) = & (1 - \gamma)^{-1} \int_{\mathcal{S} \times \mathcal{A}} d(\mathbf{s}, \mathbf{a}) r(\mathbf{s}, \mathbf{a}) \, d\mathbf{s} \, d\mathbf{a} + \lambda_1 \left(1 - \int_{\mathcal{S} \times \mathcal{A}} d(\mathbf{s}, \mathbf{a}) \, d\mathbf{s} \, d\mathbf{a} \right) \\ & + \int_{\mathcal{S}} \lambda_2(\mathbf{s}') \left(\int_{\mathcal{S} \times \mathcal{A}} \gamma \mathcal{P}(\mathbf{s}' | \mathbf{s}, \mathbf{a}) d(\mathbf{s}, \mathbf{a}) \, d\mathbf{s} \, d\mathbf{a} + (1 - \gamma) \mu_0(\mathbf{s}') - \int_{\mathcal{A}} d(\mathbf{s}', \mathbf{a}') \, d\mathbf{a}' \right) \, d\mathbf{s}' \\ & + \lambda_3 \left(\epsilon - \int_{\mathcal{S}} \nu(\mathbf{s}) \int_{\mathcal{A}} q(\mathbf{a} | \mathbf{s}) \log \frac{q(\mathbf{a} | \mathbf{s})}{p(\mathbf{a} | \mathbf{s})} \, d\mathbf{a} \, d\mathbf{s} \right), \end{aligned}$$

where λ_2 is a function for an infinite-dimensional constraint. Solving for $\partial \mathcal{L}(q, \lambda_1, \lambda_2, \lambda_3) / \partial d = 0$,

$$q(\mathbf{a} | \mathbf{s}) \propto \exp(\underbrace{\alpha^{-1} (r(\mathbf{s}, \mathbf{a}) + \gamma \mathbb{E}_{\mathbf{s}' \sim \mathcal{P}(\cdot | \mathbf{s}, \mathbf{a})} [\mathcal{V}(\mathbf{s}')] - \mathcal{V}(\mathbf{s}))}_{\mathcal{Q}(\mathbf{s}, \mathbf{a})} p(\mathbf{a} | \mathbf{s}),$$

with $\alpha = (1 - \gamma) \lambda_3$ and $\lambda_2(\mathbf{s}) = (1 - \gamma) \mathcal{V}(\mathbf{s})$, where \mathcal{V} can be interpreted as the soft value function,

$$\mathcal{V}(\mathbf{s}) = \alpha \log \int_{\mathcal{A}} \exp \left(\frac{1}{\alpha} \mathcal{Q}(\mathbf{s}, \mathbf{a}) \right) p(\mathbf{a} | \mathbf{s}) \, d\mathbf{a} \quad \text{as} \quad \int_{\mathcal{A}} q(\mathbf{a} | \mathbf{s}) \, d\mathbf{a} = 1.$$

To obtain the more convenient lower bound of the soft Bellman equation, we combine importance sampling and Jensen's inequality to the soft Bellman equation

$$\begin{aligned} \mathcal{V}(\mathbf{s}) &= \alpha \log \int_{\mathcal{A}} \exp \left(\frac{1}{\alpha} \mathcal{Q}(\mathbf{s}, \mathbf{a}) \right) \frac{p(\mathbf{a} | \mathbf{s})}{q(\mathbf{a} | \mathbf{s})} q(\mathbf{a} | \mathbf{s}) \, d\mathbf{a}, \\ &\geq \mathbb{E}_{\mathbf{a} \sim q(\cdot | \mathbf{s})} \left[\mathcal{Q}(\mathbf{s}, \mathbf{a}) - \alpha \log \frac{q(\mathbf{a} | \mathbf{s})}{p(\mathbf{a} | \mathbf{s})} \right]. \end{aligned}$$

This derivation is for the 'hard' KL constraint. In many implementations, including ours, the constraint is 'softened' where λ_3 and therefore α is a fixed hyperparameter.

Inverse reinforcement learning. As mentioned in Section 2 and Definition 1, ME-IRL is closely related to KL -regularized RL , but with the objective and a constraint reversed,

$$\min_q \mathbb{E}_{\mathbf{s} \sim \nu_q(\cdot)} [\mathbb{D}_{\text{KL}}[q(\mathbf{a} | \mathbf{s}) || p(\mathbf{a} | \mathbf{s})]] \quad \text{s.t.} \quad \mathbb{E}_{\mathbf{s}, \mathbf{a} \sim \rho_q} [\phi(\mathbf{s}, \mathbf{a})] = \mathbb{E}_{\mathbf{s}, \mathbf{a} \sim \mathcal{D}} [\phi(\mathbf{s}, \mathbf{a})].$$

The constrained optimization is therefore transcribed into a similar Lagrangian,

$$\begin{aligned}\mathcal{L}(d, \lambda_1, \lambda_2, \boldsymbol{\lambda}_3) = & \int_{\mathcal{S}} \nu(\mathbf{s}) \int q(\mathbf{a} \mid \mathbf{s}) \log \frac{q(\mathbf{a} \mid \mathbf{s})}{p(\mathbf{a} \mid \mathbf{s})} d\mathbf{a} d\mathbf{s} + \lambda_1 \left(1 - \int_{\mathcal{S} \times \mathcal{A}} d(\mathbf{s}, \mathbf{a}) d\mathbf{s} d\mathbf{a} \right) \\ & + \int_{\mathcal{S}} \lambda_2(\mathbf{s}') \left(\int_{\mathcal{S} \times \mathcal{A}} \gamma \mathcal{P}(\mathbf{s}' \mid \mathbf{s}, \mathbf{a}) d(\mathbf{s}, \mathbf{a}) d\mathbf{s} d\mathbf{a} + (1 - \gamma) \mu_0(\mathbf{s}') - \int_{\mathcal{A}} d(\mathbf{s}', \mathbf{a}') d\mathbf{a}' \right) d\mathbf{s}' \\ & + \boldsymbol{\lambda}_3^\top \left((1 - \gamma)^{-1} \int_{\mathcal{S} \times \mathcal{A}} d(\mathbf{s}, \mathbf{a}) \phi(\mathbf{s}, \mathbf{a}) d\mathbf{s} d\mathbf{a} - \mathbb{E}_{\mathbf{s}, \mathbf{a} \sim \mathcal{D}} [\phi(\mathbf{s}_t, \mathbf{a}_t)] \right).\end{aligned}$$

The consequence of this change is that the likelihood temperature is now implicit in the reward model $r(\mathbf{s}, \mathbf{a}) = (1 - \gamma)^{-1} \boldsymbol{\lambda}_3^\top \phi(\mathbf{s}, \mathbf{a})$ due to the Lagrange multiplier weights, and this reward model is used in the soft Bellman equation in place of the true reward. The reward model is jointly optimized to minimize the apprenticeship error by matching the feature expectation.

I.2. Proof for Theorem 1

Theorem 1. (KL-regularized policy improvement inversion). *Let p and q_α be the prior and pseudo-posterior policy given by posterior policy iteration (Equation 4). The critic can be expressed as*

$$\mathcal{Q}(\mathbf{s}, \mathbf{a}) = \alpha \log \frac{q_\alpha(\mathbf{a} \mid \mathbf{s})}{p(\mathbf{a} \mid \mathbf{s})} + \mathcal{V}_\alpha(\mathbf{s}), \quad \mathcal{V}_\alpha(\mathbf{s}) = \alpha \log \int_{\mathcal{A}} \exp \left(\frac{1}{\alpha} \mathcal{Q}(\mathbf{s}, \mathbf{a}) \right) p(\mathbf{a} \mid \mathbf{s}) d\mathbf{a}. \quad (6)$$

Substituting into the KL-regularized Bellman equation lower-bound from Equation 2,

$$r(\mathbf{s}, \mathbf{a}) = \alpha \log \frac{q_\alpha(\mathbf{a} \mid \mathbf{s})}{p(\mathbf{a} \mid \mathbf{s})} + \mathcal{V}_\alpha(\mathbf{s}) - \gamma \mathbb{E}_{\mathbf{s}' \sim \mathcal{P}(\cdot \mid \mathbf{s}, \mathbf{a})} [\mathcal{V}_\alpha(\mathbf{s}')]. \quad (7)$$

The $\mathcal{V}_\alpha(\mathbf{s})$ term is the ‘soft’ value function. We assume $q_\alpha(\mathbf{a} \mid \mathbf{s}) = 0$ whenever $p(\mathbf{a} \mid \mathbf{s}) = 0$.

Proof. Equation 6 is derived by rearranging the posterior policy update in Equation 4. Equation 7 is derived by substituting the critic expression from Equation 6 into the KL-regularized Bellman equation (Equation 3),

$$\begin{aligned}\underbrace{\alpha \log \frac{q_\alpha(\mathbf{a} \mid \mathbf{s})}{p(\mathbf{a} \mid \mathbf{s})} + \mathcal{V}_\alpha(\mathbf{s})}_{\mathcal{Q}(\mathbf{s}, \mathbf{a})} = & r(\mathbf{s}, \mathbf{a}) + \gamma \mathbb{E}_{\mathbf{s}' \sim \mathcal{P}(\cdot \mid \mathbf{s}, \mathbf{a}), \mathbf{a}' \sim q_\alpha(\cdot \mid \mathbf{s}')} \left[\underbrace{\alpha \log \frac{q_\alpha(\mathbf{a}' \mid \mathbf{s}')}{p(\mathbf{a}' \mid \mathbf{s}')} + \mathcal{V}_\alpha(\mathbf{s}')}_{\mathcal{Q}(\mathbf{s}', \mathbf{a}')} - \underbrace{\alpha \log \frac{q_\alpha(\mathbf{a}' \mid \mathbf{s}')}{p(\mathbf{a}' \mid \mathbf{s}')} + \mathcal{V}_\alpha(\mathbf{s}')}_{\mathcal{Q}(\mathbf{s}, \mathbf{a})} \right].\end{aligned}$$

□

I.3. Proof for Theorem 2

Theorem 2 relies on the data processing inequality (Lemma 2) to connect the function-space KL seen in CSIL with the weight-space KL used in regularized BC.

Assumption 1. (Realizability) *The optimal policy can be expressed by the parametric policy $q_\theta(\mathbf{a} \mid \mathbf{s})$.*

Lemma 2. (Data processing inequality, Wu [2016], Theorem 4.1). *For two stochastic processes parameterized with finite random variables $\mathbf{w} \sim p(\cdot)$, $\mathbf{w} \in \mathcal{W}$ and shared hypothesis spaces $p(\mathbf{y} \mid \mathbf{x}, \mathbf{w})$, the conditional f -divergence in function space at points $\mathbf{X} \in \mathcal{X}^L$, $L \in \mathbb{Z}_+$ is upper bounded by the f -divergence in parameter space,*

$$\mathbb{D}_f[q(\mathbf{w}) \parallel p(\mathbf{w})] = \mathbb{D}_f[q(\mathbf{Y}, \mathbf{w} \mid \mathbf{X}) \parallel p(\mathbf{Y}, \mathbf{w} \mid \mathbf{X})] \geq \mathbb{D}_f[q(\mathbf{Y} \mid \mathbf{X}) \parallel p(\mathbf{Y} \mid \mathbf{X})].$$

Theorem 2. (Coherent inverse reinforcement learning as KL -regularized behavioral cloning). A KL -regularized game-theoretic IRL objective, with policy $q_{\theta}(\mathbf{a} \mid \mathbf{s})$ and coherent reward parameterization $r_{\theta}(\mathbf{s}, \mathbf{a}) = \alpha(\log q_{\theta}(\mathbf{a} \mid \mathbf{s}) - \log p(\mathbf{a} \mid \mathbf{s}))$ where $\alpha \geq 0$, is lower bounded by a scaled KL -regularized behavioral cloning objective and a constant term when the optimal policy, posterior and prior share a hypothesis space $p(\mathbf{a} \mid \mathbf{s}, \mathbf{w})$ and finite parameters \mathbf{w} ,

$$\begin{aligned} \mathbb{E}_{\mathbf{s}, \mathbf{a} \sim \mathcal{D}} [r_{\theta}(\mathbf{s}, \mathbf{a})] - \mathbb{E}_{\mathbf{a} \sim q_{\theta}(\cdot \mid \mathbf{s}), \mathbf{s} \sim \mu_{q_{\theta}}(\cdot)} [r_{\theta}(\mathbf{s}, \mathbf{a}) - \beta(\log q_{\theta}(\mathbf{a} \mid \mathbf{s}) - \log p(\mathbf{a} \mid \mathbf{s}))] \geq \\ \alpha (\mathbb{E}_{\mathbf{s}, \mathbf{a} \sim \mathcal{D}} [\log q_{\theta}(\mathbf{a} \mid \mathbf{s})] - \lambda \mathbb{D}_{\text{KL}}[q_{\theta}(\mathbf{w}) \parallel p(\mathbf{w})] + \mathbb{E}_{\mathbf{s}, \mathbf{a} \sim \mathcal{D}} [\log p(\mathbf{a} \mid \mathbf{s})]). \end{aligned}$$

where $\lambda = (\alpha - \beta)/\alpha$ and $\mathbb{E}_{\mathbf{s}, \mathbf{a} \sim \mathcal{D}} [\log p(\mathbf{a} \mid \mathbf{s})]$ is constant. The regression objective bounds the IRL objective for a worst case on-policy state distribution $\mu_q(\mathbf{s})$, which motivates its scaling through β . If \mathcal{D} has sufficient coverage, no RL finetuning or KL regularization is required, so $\beta = \alpha$. If \mathcal{D} does not have sufficient coverage, then let $\beta < \alpha$ so $\lambda > 0$ to regularize the BC fit and finetune the policy with RL accordingly with additional soft policy iteration steps.

Proof. We begin with the KL -regularized game-theoretic IRL objective,

$$\mathcal{J}(r, \pi) = \mathbb{E}_{\mathbf{s}, \mathbf{a} \sim \mathcal{D}} [r(\mathbf{s}, \mathbf{a})] - \mathbb{E}_{\mathbf{s}, \mathbf{a} \sim \rho_{\pi}} \left[r(\mathbf{s}, \mathbf{a}) - \beta \log \frac{\pi(\mathbf{a} \mid \mathbf{s})}{p(\mathbf{a} \mid \mathbf{s})} \right].$$

Substituting the coherent reward from Theorem 1, the objective becomes

$$\mathcal{J}(\theta, \pi) = \mathbb{E}_{\mathbf{s}, \mathbf{a} \sim \mathcal{D}} \left[\alpha \log \frac{q_{\theta}(\mathbf{a} \mid \mathbf{s})}{p(\mathbf{a} \mid \mathbf{s})} \right] - \mathbb{E}_{\mathbf{s}, \mathbf{a} \sim \rho_{\pi}} \left[\alpha \log \frac{q_{\theta}(\mathbf{a} \mid \mathbf{s})}{p(\mathbf{a} \mid \mathbf{s})} - \beta \log \frac{\pi(\mathbf{a} \mid \mathbf{s})}{p(\mathbf{a} \mid \mathbf{s})} \right].$$

Due to the realizability assumption (Assumption 1), the optimal policy π_{θ_*} can be obtained through maximum likelihood estimation $\theta_* = \arg \max_{\theta} \mathbb{E}_{\mathbf{s}, \mathbf{a} \sim \mathcal{D}} [\log q_{\theta}(\mathbf{s}, \mathbf{a})]$. With this assumption, the left hand term performs maximum likelihood estimation of the optimal policy. Therefore, combined with the coherent reward which is derived from policy inversion, we replace the inner policy optimization of π with the maximum likelihood solution of q_{θ} , resulting in a simpler objective $\tilde{\mathcal{J}}$ in terms of only θ ,

$$\tilde{\mathcal{J}}(\theta) = \mathbb{E}_{\mathbf{s}, \mathbf{a} \sim \mathcal{D}} \left[\alpha \log \frac{q_{\theta}(\mathbf{a} \mid \mathbf{s})}{p(\mathbf{a} \mid \mathbf{s})} \right] - \mathbb{E}_{\mathbf{a} \sim q_{\theta}(\cdot \mid \mathbf{s}), \mathbf{s} \sim \mu_{q_{\theta}}} \left[(\alpha - \beta) \log \frac{q_{\theta}(\mathbf{a} \mid \mathbf{s})}{p(\mathbf{a} \mid \mathbf{s})} \right].$$

The right-hand term contains a conditional KL divergence, which we can replace with an upper-bound using the data processing inequality from Lemma 2 and the weight-space KL . This weight-space KL is constant w.r.t. the state distribution expectation, and we introduce the scale factor $\lambda = (\alpha - \beta)/\alpha$. The resulting lower-bound objective is proportional to the regularized behavioural cloning objective proposed in Equation 5,

$$\tilde{\mathcal{J}}(\theta) \geq \alpha (\mathbb{E}_{\mathbf{s}, \mathbf{a} \sim \mathcal{D}} [\log q_{\theta}(\mathbf{a} \mid \mathbf{s})] - \lambda \mathbb{D}_{\text{KL}}[q_{\theta}(\mathbf{w}) \parallel p(\mathbf{w})] + C), \quad C = \mathbb{E}_{\mathbf{s}, \mathbf{a} \sim \mathcal{D}} [-\log p(\mathbf{a} \mid \mathbf{s})].$$

□

The intuition from Theorem 2 is that the KL regularization during BC achieves reward shaping similar to the IRL saddle-point solution when using the coherent reward. The lower bound's 'tightness' depends on the data processing inequality. The weight-space KL is 'global' regularization, rather than state-dependent. Therefore, rather than providing a tight lower bound, this result is more to demonstrate that KL -regularized BC provides effective reward shaping from the game-theoretic perspective. We visualize this phenomena in Appendix G to reinforce the result.

Task	Random return	Expert return
HalfCheetah-v2	-282	8770
Hopper-v2	18	2798
Walker2d-v2	1.6	4118
Ant-v2	-59	5637
Humanoid-v2	123	9115
door-expert-v0	-56	2882
hammer-expert-v0	-274	12794

Table 2 | Expert and random policy returns used to normalize the performance for Gym and Adroit tasks. Taken from [Orsini et al. \[2021\]](#).

J. Implementation and experimental details

The tabular experiments are implemented in `jax` automatic differentiation and linear algebra library [[Bradbury et al., 2018](#)]. The continuous state-action experiments are implemented in `acme`, using `jax`. One feature of `acme` is distributed training, where we use 4 concurrent actors to speed up the wall clock time of learning. `IQLearn` and `PPIL` were re-implemented based on the open-source implementations as reference [[Div99, 2021](#), [lviano, 2022](#)]. `CSIL`, `IQLearn` and `PPIL` shared a combined implementation as ‘soft’ imitation learning algorithms due to their common structure and to facilitate ablation studies. Baselines `DAC`, `SQIL`, `PWIL`, `SACFD` and `CQL` are implemented in `acme`. We used a stochastic actor for learning and a deterministic actor (i.e. evaluating the mean action) for evaluation.

Due to the common use of `SAC` as the base `RL` algorithm, most implementation shared common standard hyperparameters. The policy and critic networks were two layers of 256 units with `ELU` activations. Learning rates were $3e-4$, the batch size was 256 and the target network smoothing coefficient was 0.005. One difference to standard `RL` implementations is the use of `layernorm` in the critic, which is adopted in some algorithm implementations in `acme` and was found to improve performance. For the inverse temperature α , for most methods we used the adaptive strategy based on a lower bound on the policies entropy. `IQLearn` and `PPIL` both have a fixed temperature strategy that we tuned in the range $[1.0, 0.3, 0.1, 0.03, 0.01]$. `CSIL` also has a fixed temperature strategy, but applied to the `KL` penalty. In practice they are very similar, so we swept the same range. We also investigated a hard `KL` bound and adaptive temperature strategy, but there was no performance improvement to warrant the extra complexity. `CSIL`’s `HETSTAT` policies had an additional bottleneck layer of 12 units and a final layer of 256 units with stationary activations. For

Experiment	Algorithm					
	DAC	PWIL	SQIL	IQLearn	PPIL	CSIL
Online Gym	$\mathbb{H}(\pi)$	$\mathbb{H}(\pi)$	$\mathbb{H}(\pi)$	0.01	0.01	0.01
Offline Gym	$\mathbb{H}(\pi)$	$\mathbb{H}(\pi)$	$\mathbb{H}(\pi)$	0.03	0.03	0.1
Online Humanoid-v2	$\mathbb{H}(\pi)$	$\mathbb{H}(\pi)$	$\mathbb{H}(\pi)$	0.01	0.01	0.01
Online Adroit	$\mathbb{H}(\pi)$	$\mathbb{H}(\pi)$	$\mathbb{H}(\pi)$	0.03	0.03	0.1
Online robomimic	$\mathbb{H}(\pi)$	-	-	0.1	-	0.1
Offline robomimic	-	-	-	-	-	1.0
Image-based robomimic	-	-	-	-	-	0.3

Table 3 | Entropy regularization used across methods and environments. Values refer to a fixed temperature while $\mathbb{H}(\pi)$ refers to the adaptive temperature scheme which ensures the policy entropy is at least equal to $-d_a$, where d_a is the dimension of the action space.

Experiment	Pretraining hyperparameters			
	$n(\pi)$	$\lambda(\pi)$	$n(Q)$	$\lambda(Q)$
Online and offline Gym	25000	1e-3	5000	1e-3
Online Humanoid-v2	500	1e-3	5000	1e-3
Online Adroit	25000	1e-4	5000	1e-3
Online and offline robomimic	50000	1e-4	2000	1e-3
Image-based robomimic	25000	1e-4	2000	1e-3

Table 4 | `CSIL`’s pretraining hyperparameters for the policy (π) and critic (Q), listing the learning rate (λ) and number of iterations (n).

the `Gym` tasks, triangular activations were used. For `robomimic` tasks, periodic ReLU activations were used. `IQLearn`, `PPIL` and `CSIL` all have single critics rather than dual critics, while the other baselines had dual critics to match the standard `SAC` implementation. We tried dual critics to stabilize `IQLearn` and `PPIL`, but this did not help. `CSIL`’s reward finetuning learning rate was 1e-3. As the reward model was only being finetuned with non-expert samples, we did not find this hyperparameter to be very sensitive. For `robomimic`, larger models were required with two layers of 1024 units. The `HETSTAT` policies increased accordingly with a 1024 unit final layer and 48 units for the bottleneck layer.

For `DAC`, we used the hyperparameters and regularizers recommended by [Orsini et al. \[2021\]](#), including spectral normalization for the single hidden layer discriminator with 64 units. `IQLearn` has a smaller actor learning rate of 3e-5 and the open-source implementation has the option of different value function regularizers per task [[Div99, 2021](#)]. We used ‘v0’ regularization for all environments, which minimizes the averaged value function at the expert samples. In the original `IQLearn` experiments, this regularizer is tuned per environment [[Div99, 2021](#)]. `PPIL` shares the same smaller actor learning rate of 3e-5 and the open-source implementation also uses 20 critic updates for every actor update, which we maintained. The implementation of `PPIL` borrows the same value function regularization as `IQLearn`, so we used ‘v0’ regularization for all environments [[lviano, 2022](#)]. For `SACFD`, we swept the demo-to-replay ratio across [0.1, 0.01]. For `adroit` the ratio was 0.01 and for `robomimic` it was 0.1.

The major implementation details of `CSIL` are discussed in Sections 4, C, D and E. The pretraining hyperparameters are listed in Table 4. While the critic is not too important for performance (Figure 43), appropriate policy pretraining is crucial. In lieu of training a regularization hyperparameter, we instead opted for early stopping. As a result, there is a trade-off between `BC` accuracy and policy entropy. In the online setting, if the policy is trained too long, then the entropy is reduced too far and there is not enough exploration for `RL`. As a result, the policy pretraining hyperparameters need tuning when action dimension and datasets size change significantly to ensure the `BC` fit is sufficient for downstream performance. For `robomimic`, we used negative `CSIL` rewards that were scaled by 0.5 to ensure they lie around $[-1, 0]$. For vision-based `robomimic`, the CNN torso was a impala-style [[Espeholt et al., 2018](#)] `Acme ResNetTorso` down to a `LayerNorm MLP` with 48 output units, `ELU` activations, orthogonal weight initialization and final `tanh` activation. [Mandlekar et al. \[2021\]](#) used a larger `ResNet18`. As in [Mandlekar et al. \[2021\]](#), image augmentation was achieved with random crops from 84 down to 76. Pixel values were normalized to [-0.5, 0.5]. For memory reasons, the batch size was reduced to 128. The implementations of `IQLearn`, `PPIL` and `CSIL` combined equally-sized mini-batches from the expert and non-expert replay buffers for learning the reward, critic and policy. We did not investigate tuning this ratio.

Regarding computational resources, the main experiments were run using `acme` which implements distributed learning. As a result, our ‘learner’ (policy evaluation and improvement) run on a single TPU v2. We ran four actors to interact in to environment. Depending on the algorithm, there were also one or more evaluators. For vision-based tasks, we used A100 GPUs for the vision-based policies.

K. Experimental results

This section includes additional experimental results from Section 5. Videos of the simulation studies are available at www.sites.google.com/view/coherentsoftimitationlearning.

K.1. Inverse optimal control

This section shows the converged value function, stationary distribution and ‘windy’ stationary distribution for the tabular setting results from Table 1. ‘Oracle classifier’ constructs an offline classifier-based reward separating the states and actions with- and without demonstration data, in the spirit of methods such as `sQIL` and `ORIL` [Zolna et al., 2020]. No optimization was conducted on the windy environment, just evaluation to assess the policy robustness to disturbance. We use the viridis colourmap, so yellow regions have a larger value than blue regions.

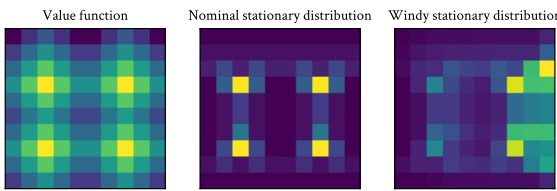


Figure 11 | Expert on the dense MDP.

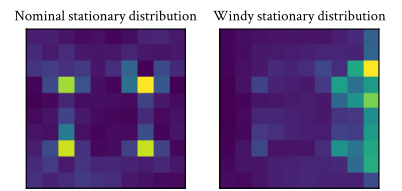


Figure 12 | bc on the dense MDP.

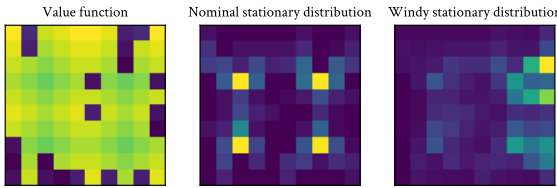


Figure 13 | Oracle classifier on the dense MDP.

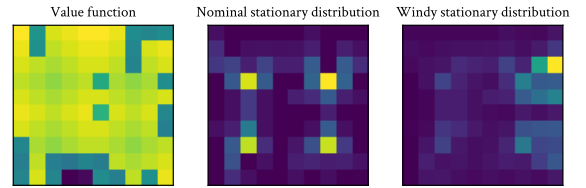


Figure 14 | GAIL on the dense MDP.

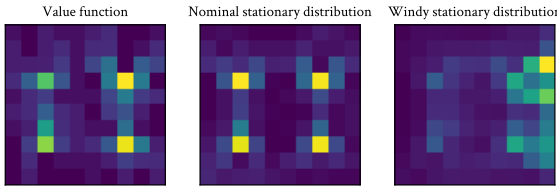


Figure 15 | iQLearn on the dense MDP.

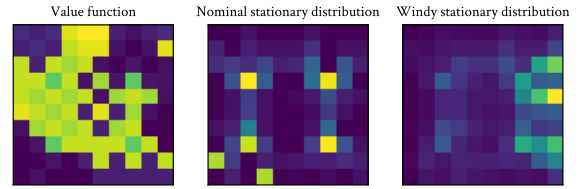


Figure 16 | PPIL on the dense MDP.

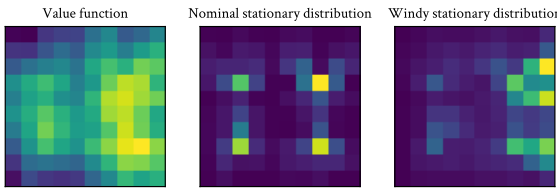


Figure 17 | ME-IRL on the dense MDP.

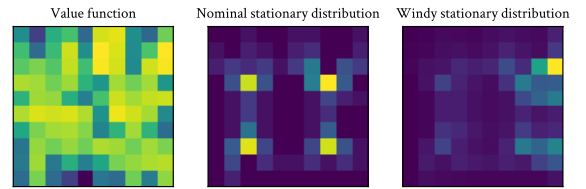


Figure 18 | CSIL on the dense MDP.

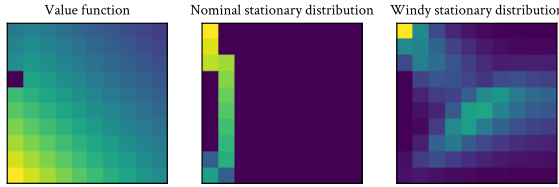


Figure 19 | Expert on the sparse MDP.

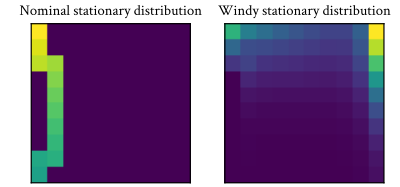


Figure 20 | BC on the sparse MDP.

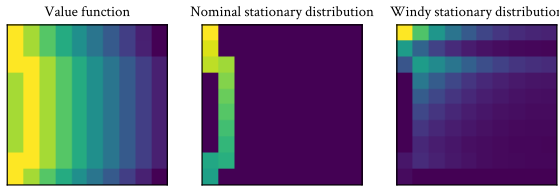


Figure 21 | Oracle classifier on the sparse MDP.

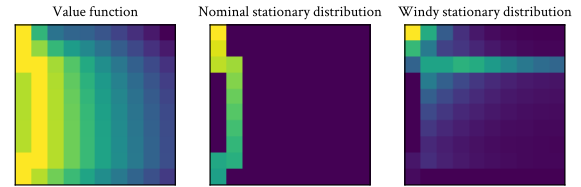


Figure 22 | GAIL on the sparse MDP.

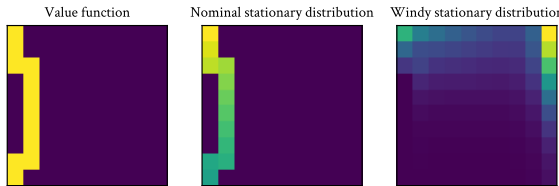


Figure 23 | iQLearn on the sparse MDP.

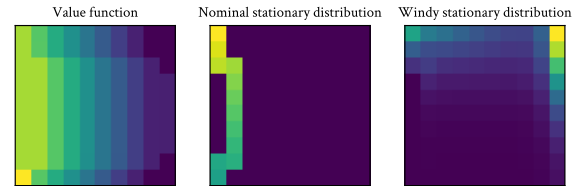


Figure 24 | PPIL on the sparse MDP.

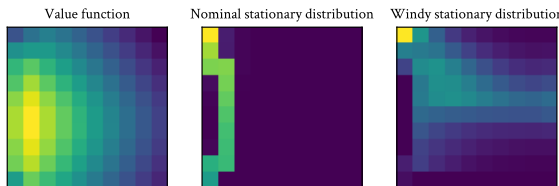


Figure 25 | ME-IRL on the sparse MDP.

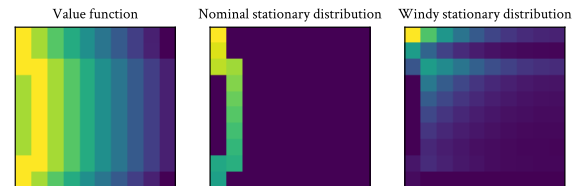


Figure 26 | CSIL on the sparse MDP.

K.2. Continuous control from agent demonstrations

Step-wise results. Figure 27, 28 and 29 show step-wise performance curves, as opposed to the demonstration-wise results in the main paper. For online experiments, steps refers to the actor and learner, while for offline experiments steps corresponds to the learner.

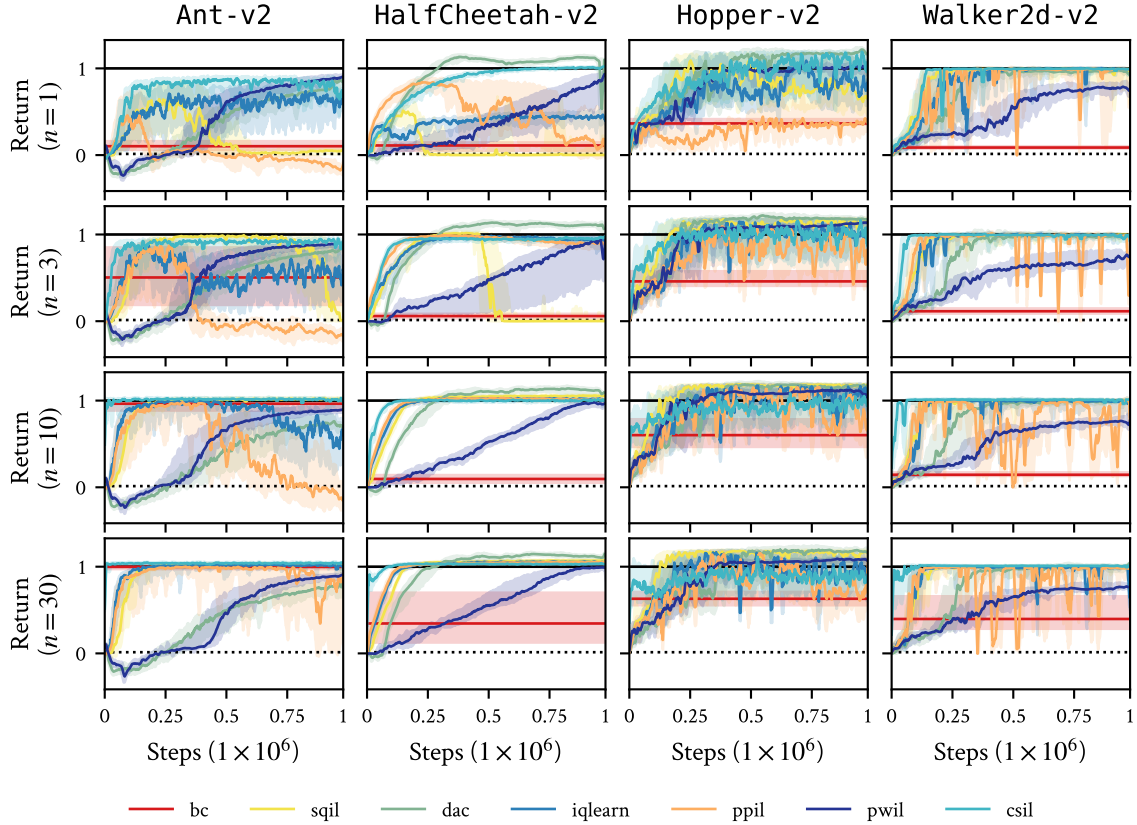


Figure 27 | Normalized performance of CSIL against baselines for online imitation learning on MuJoCo Gym tasks. Uncertainty intervals depict quartiles over 10 seeds. CSIL exhibits stable convergence with both sample and demonstration efficiency. BC here is applied to the demonstration dataset. n refers to demonstration trajectories.

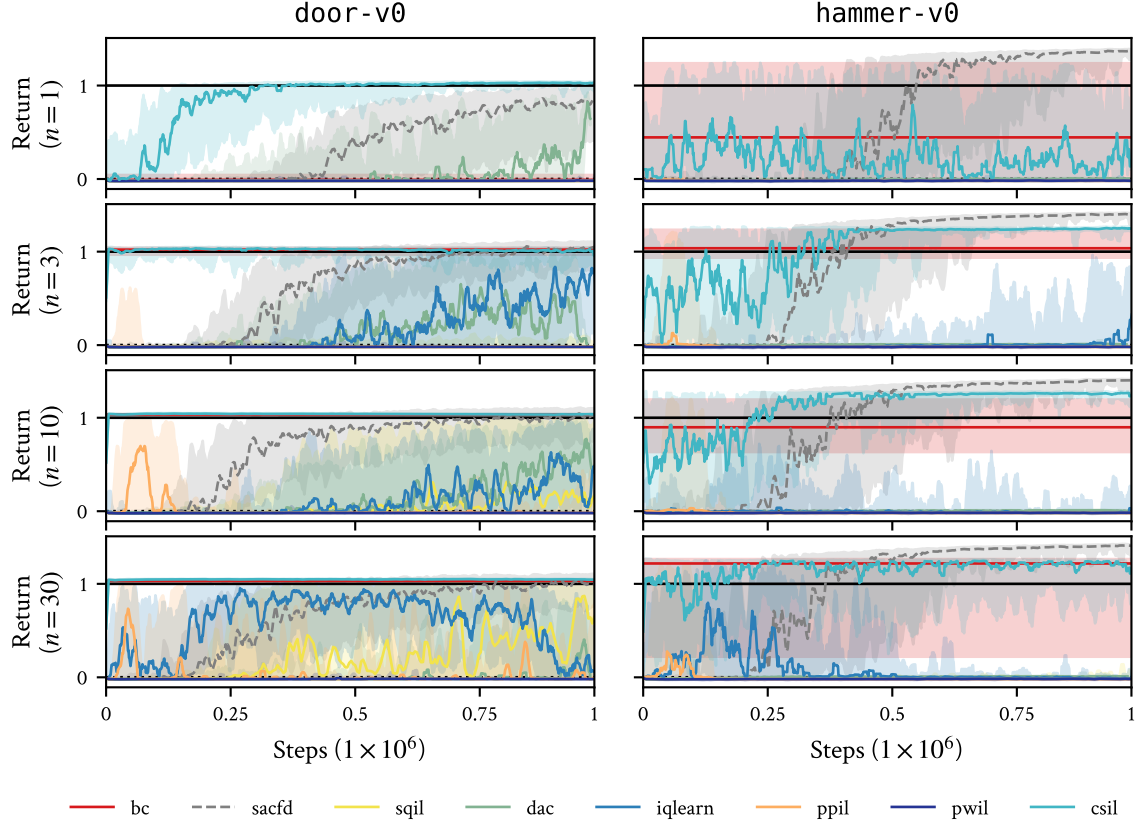


Figure 28 | Normalized performance of CSIL against baselines for online imitation learning for Adroit tasks. Uncertainty intervals depict quartiles over 10 seeds. CSIL exhibits stable convergence with both sample and demonstration efficiency. Many baselines cannot achieve stable convergence due to the high-dimensional action space. SACFD is an oracle baseline that combines the demonstrations with the true (shaped) reward. n refers to demonstration trajectories.

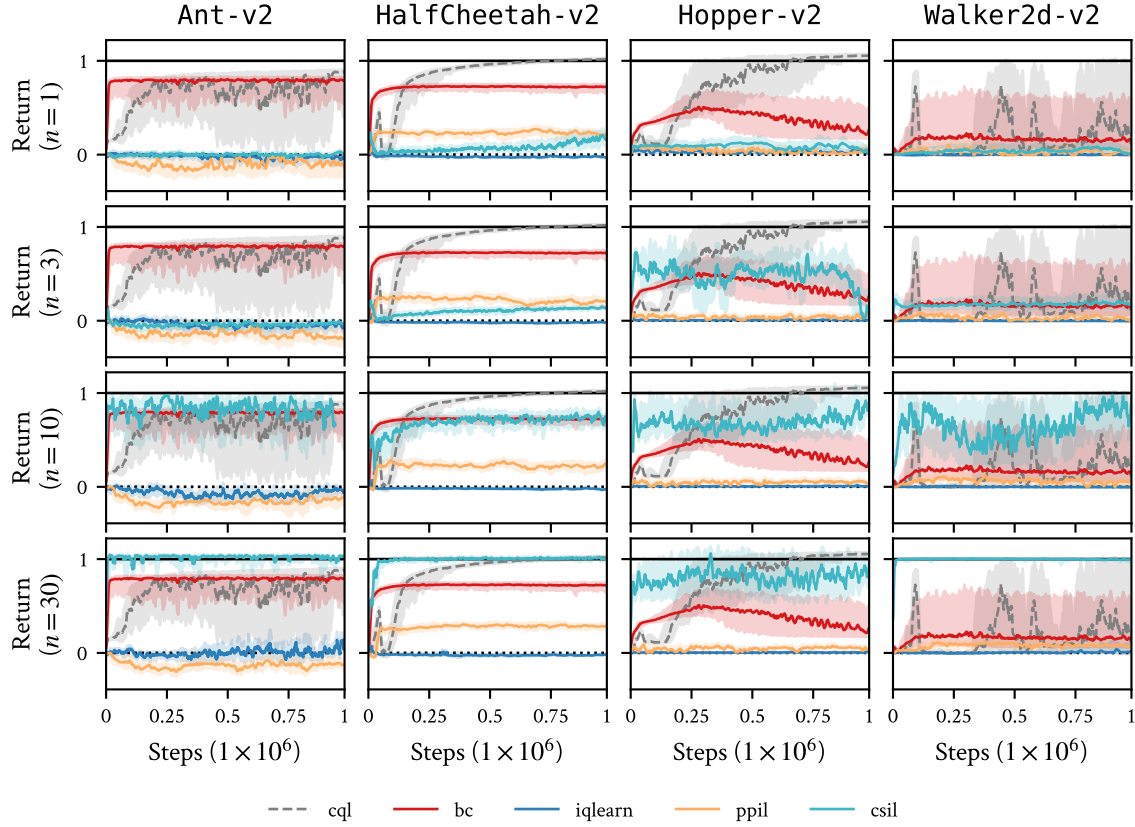


Figure 29 | Normalized performance of CSIL against baselines for *offline* imitation learning for Gym tasks. Uncertainty intervals depict quartiles over 10 seeds. While all methods struggle in this setting compared to online learning, CSIL manages convergence with enough demonstrations. CQL is an oracle baseline using the true rewards. The BC baseline is trained to the whole offline dataset, not just demonstrations. n refers to demonstration trajectories.

Humanoid-v2 results. We evaluated CSIL and baselines on the high-dimensional Humanoid-v2 locomotion task in Figure 30. We found that CSIL struggled to solve this task due to difficulty for BC to perform well at this task, even when using all 200 of the available demonstrations in the dataset.

One aspect of Humanoid-v2 to note is that a return of around 5000 (around 0.5 normalized) corresponds to the survival / standing bonus, rather than actual locomotion (around 9000). While the positive nature of the coherent reward enabled learning the stabilize, this was not consistent across seeds. We also found it difficult to reproduce baseline results due to IQLearn’s instability, which we also reproduced on the author’s implementation [Div99, 2021].

In theory, BC should be able to approximate the original optimal agent’s policy with sufficient demonstrations. We believe the solution may be additional BC regularization, as the environment has a 376 dimensional state space.

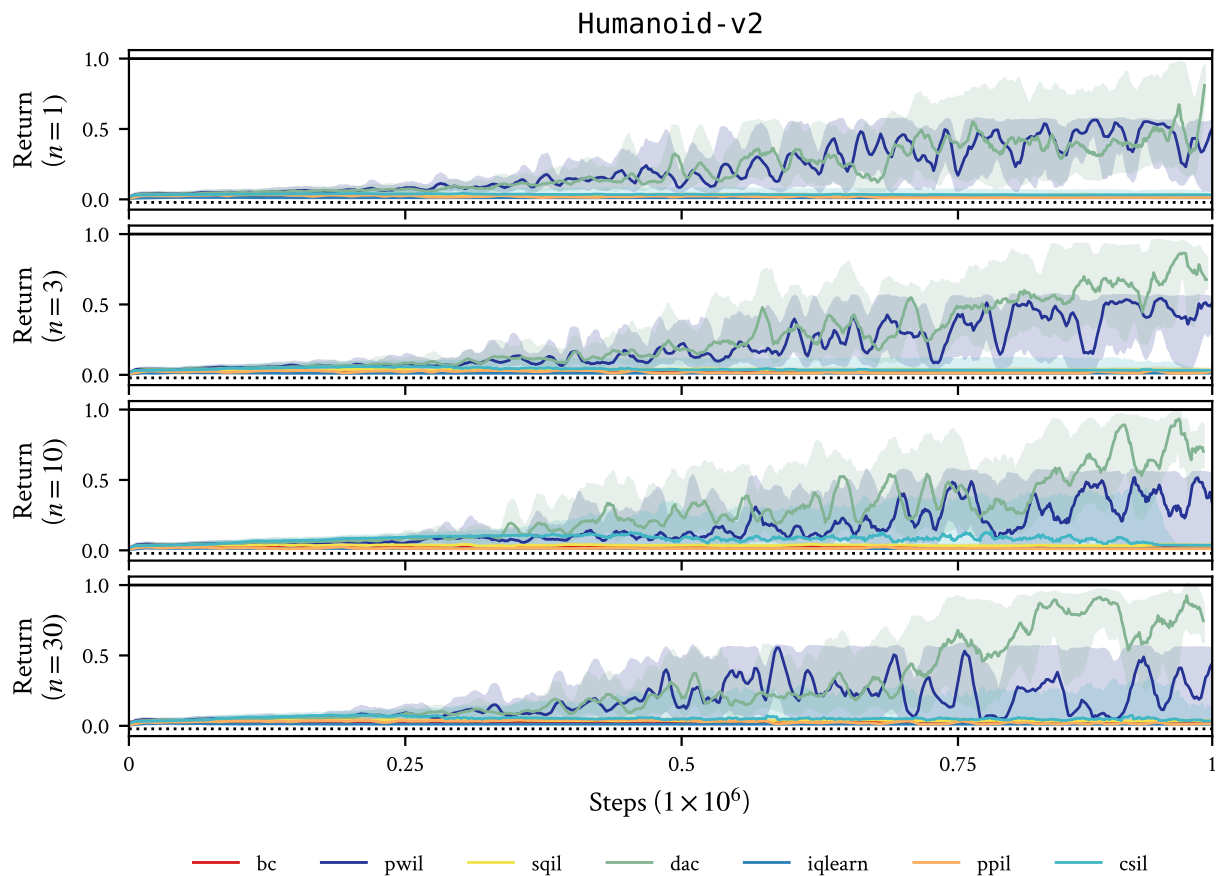


Figure 30 | Normalized performance of CSIL against baselines for online imitation learning for Humanoid-v2. Uncertainty intervals depict quartiles over 10 seeds. n refers to demonstration trajectories.

Performance improvement of coherent imitation learning A desired quality of `csIL` is its ability to match or exceed its initial `bc` policy. Figures 31, 32 and 33 show the performance of `csIL` relative to its initial `bc` policy. Empirical, `csIL` indeed matches or exceeds the initial `bc` policy across environments.

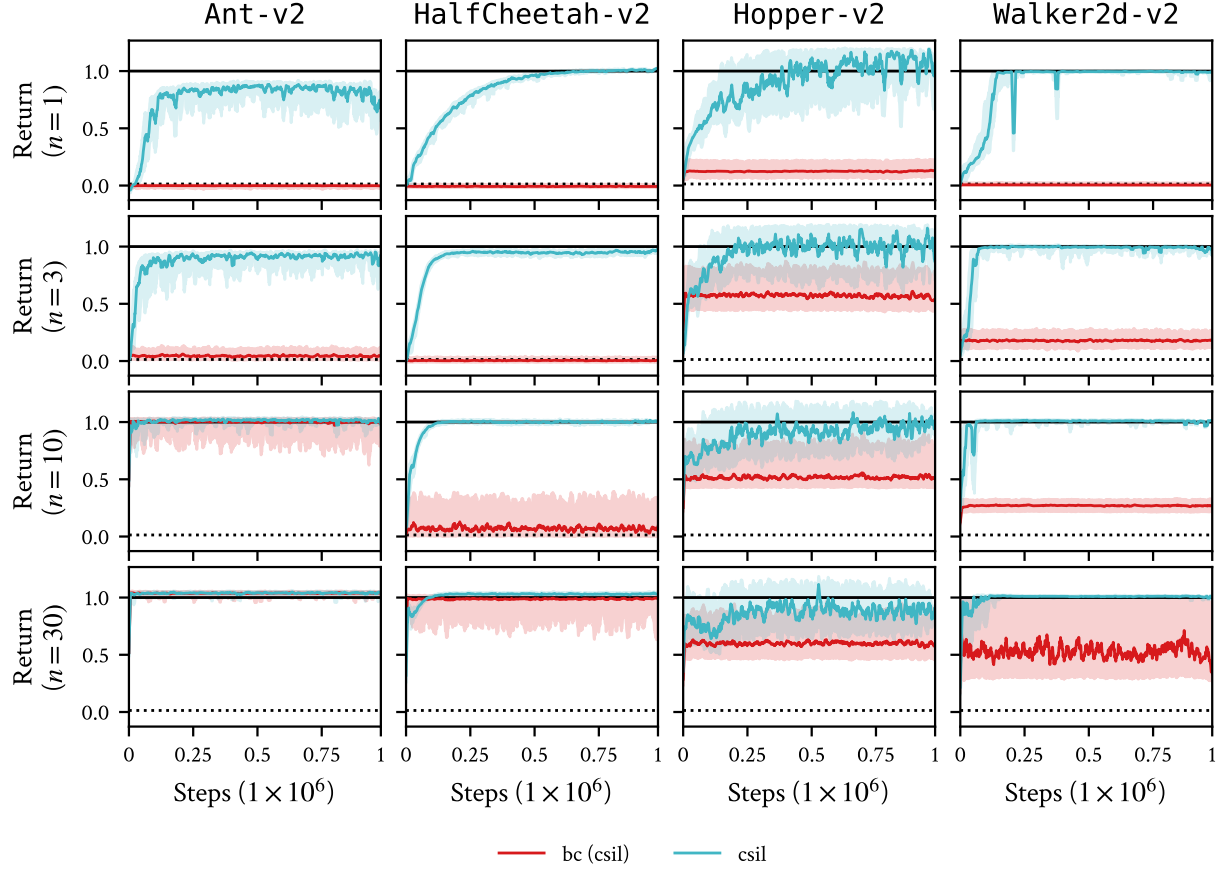


Figure 31 | Normalized performance of `csIL` for online Gym tasks against its `bc` initialization. Uncertainty intervals depict quartiles over 10 seeds. n refers to demonstration trajectories.

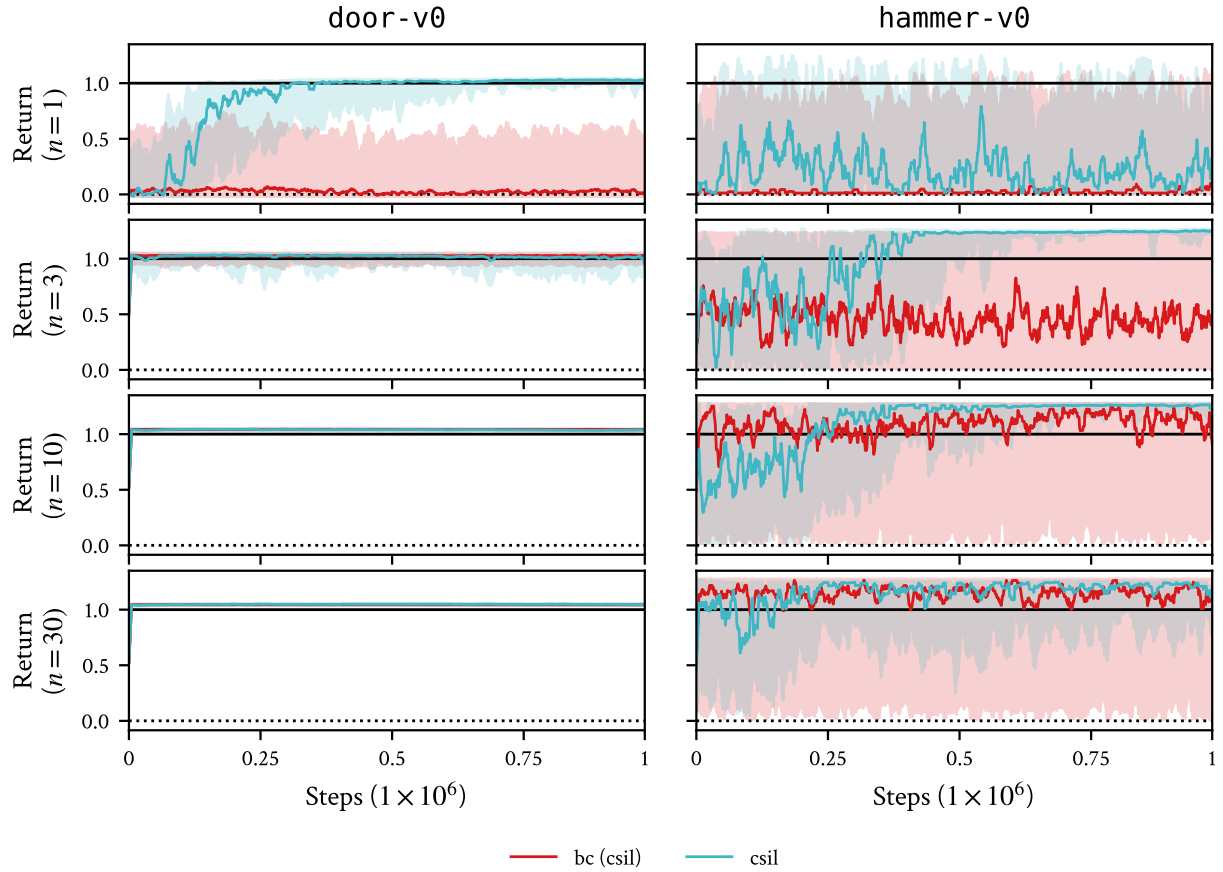


Figure 32 | Normalized performance of CSIL for online Adroit tasks against its BC initialization. Uncertainty intervals depict quartiles over 10 seeds. n refers to demonstration trajectories.

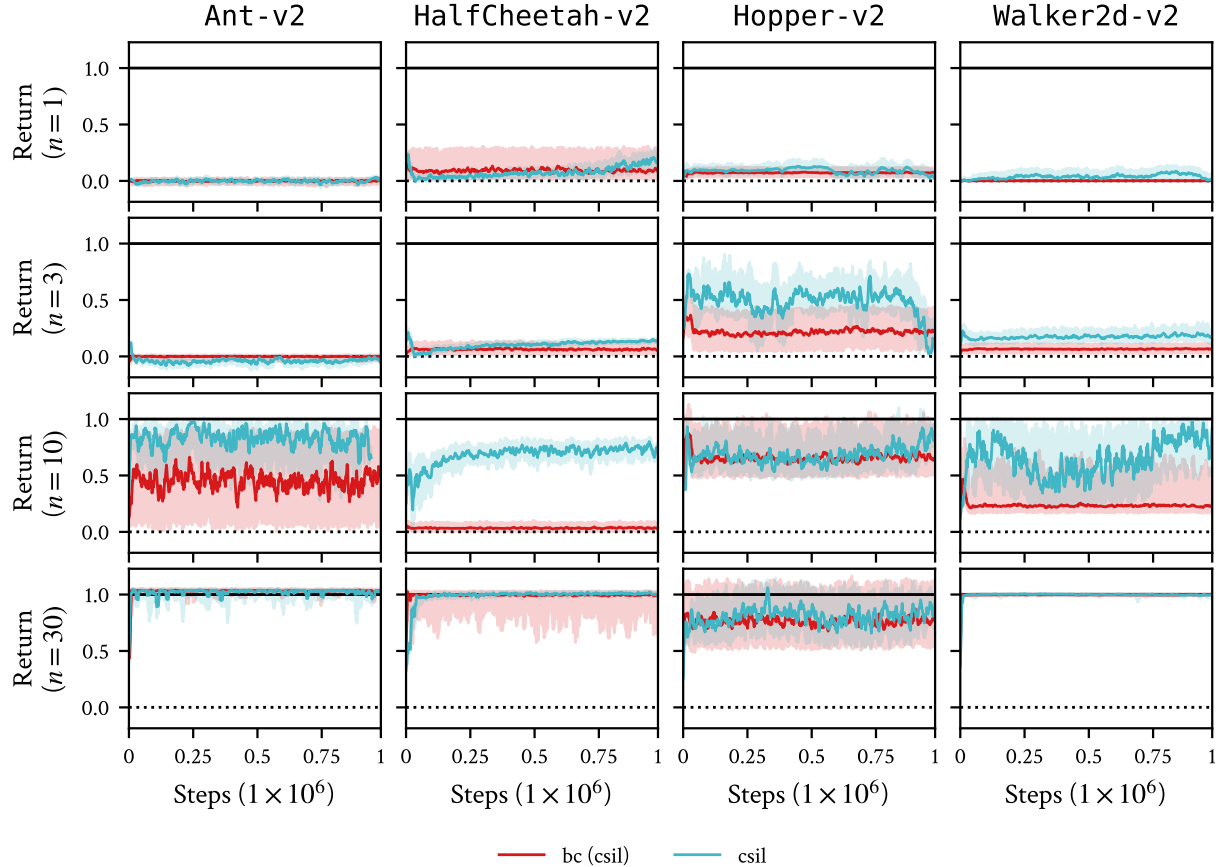


Figure 33 | Normalized performance of CSIL for offline Gym tasks against its BC initialization. Uncertainty intervals depict quartiles over 10 seeds. n refers to demonstration trajectories.

Divergence in minimax soft imitation learning To investigate the performance issues in IQLearn and PPIL relative to CSIL, we monitor a few key diagnostics during training for online door-v0 and offline Ant-v2 in Figure 34. One key observation is the drift in the BC accuracy. We attribute this to the instability in the reward or critic due to the saddle-point optimization.

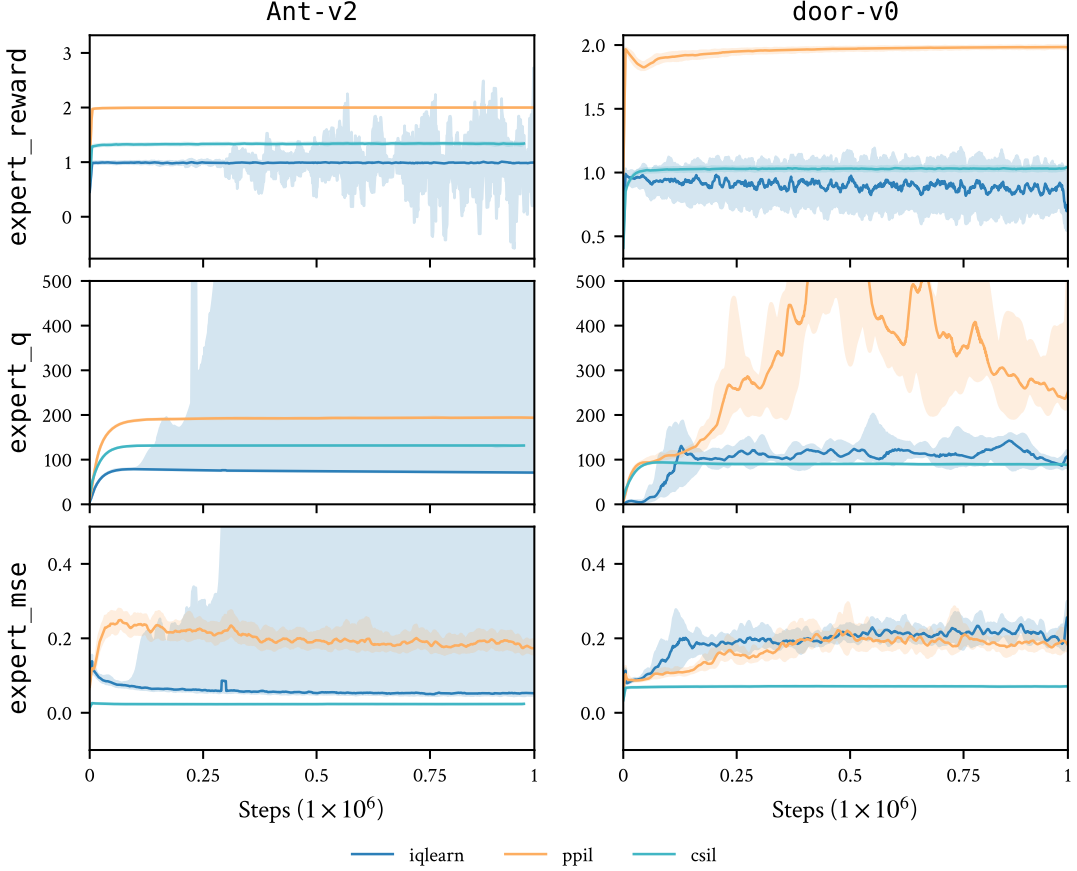


Figure 34 | We investigate the weakness of `iQLearn` and `PPIL` for offline learning (`Ant-v2`) and high-dimensional action spaces (`door-v0`). Compared to `CSIL`, `iQLearn` and `PPIL` have less stable and effective Q values, in particular for the expert demonstrations, which results in the policy not inaccurately predicting the demonstration actions (`expert_mse`).

K.3. Continuous control from human demonstrations

Figure 35 shows performance on the online setting w.r.t. learning steps and Figure 36 shows the offline performance w.r.t. learning steps. For online learning, `CSIL` consistently more sample efficient than the oracle baseline `SACFD`, presumably due to `BC` pretraining and `CSIL`'s shaped reward w.r.t. `robomimic`'s sparse reward on success. `CSIL` was also able to surpass [Mandlekar et al. \[2021\]](#)'s success rate on `NutAssemblySquare`. For offline learning from suboptimal human demonstrations, it appears to be a much harder setting for `CSIL` to improve on the initial `BC` policy, especially for harder tasks.

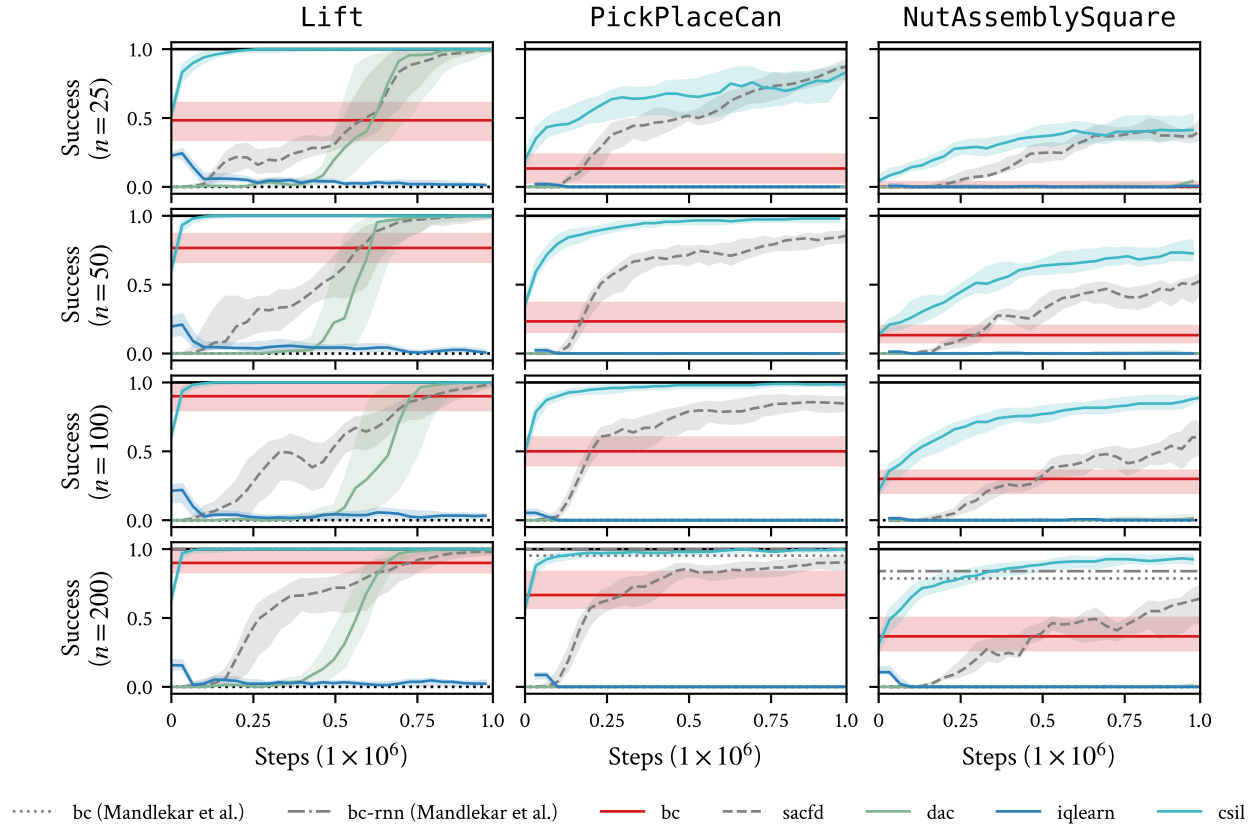


Figure 35 | Average success rate over 50 evaluations for online imitation learning for `robomimic` tasks. Uncertainty intervals depict quartiles over 10 seeds. The `bc` policy is trained on the demonstration data. n refers to demonstration trajectories.

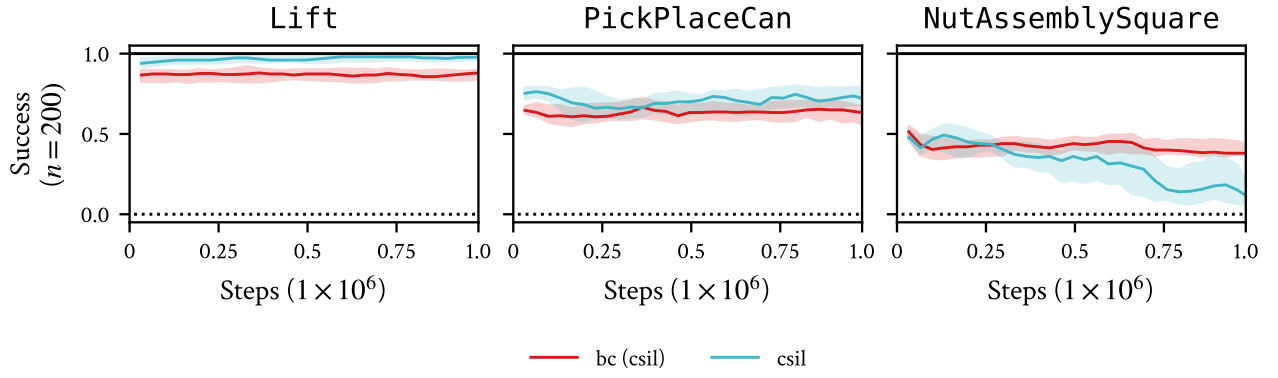


Figure 36 | Average success rate over 50 evaluations for *offline* imitation learning for `robomimic` tasks. Uncertainty intervals depict quartiles over 10 seeds. This experiment shows that learning from suboptimal offline demonstrations is much harder than on-policy data. It is also harder to use the KL regularization to ensure improvement over the initial policy. n refers to demonstration trajectories.

L. Ablation studies

This section includes ablation studies for the `CSIL` algorithm and baselines.

L.1. Baselines with behavioral cloning pretraining

To assess the importance of BC pretraining, we evaluate the performance of `IQLearn` and `PPIL` with BC pretraining in Figure 37. While difficult to see across all experiments, there is a small drop in performance at the beginning of training as the policy ‘unlearns’ as the critic and reward are randomly initialized since there is no notion of coherency.

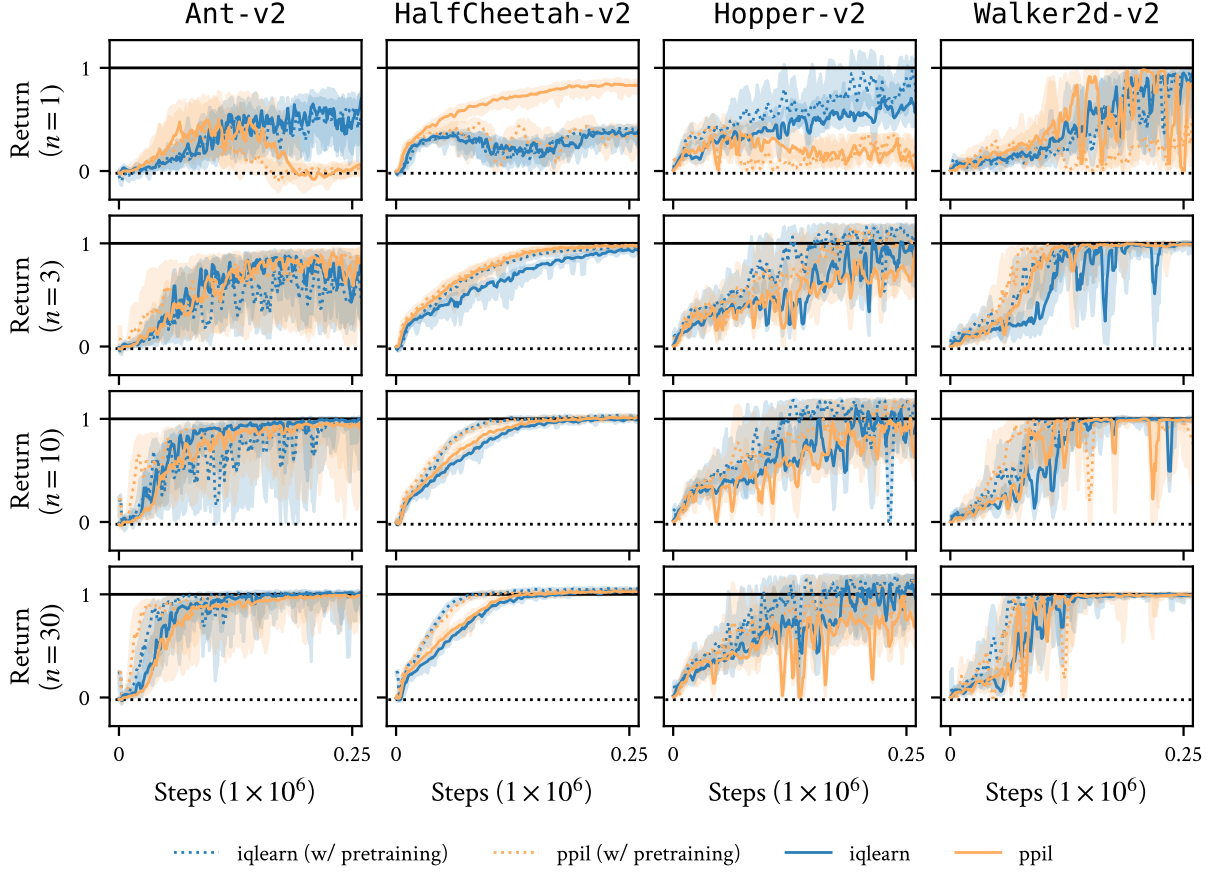


Figure 37 | Normalized performance of `IQLearn` and `PPIL` for online Gym tasks with BC pretraining. Uncertainty intervals depict quartiles over 10 seeds. n refers to demonstration trajectories.

L.2. Baselines with behavioral cloning pretraining and and KL regularization

To bring `IQLearn` and `PPIL` closer to `CSIL`, we implement the baselines with BC pretraining and KL regularization, but with `SAC`-style policies rather than `HETSTAT`. We evaluate on the harder tasks, online `Adroit` and offline `Gym`, to see if these features contribute sufficient stability to solve the task. Both Figure 38 and Figure 39 show increase in initial performance, it is not enough to completely stabilize the algorithms.

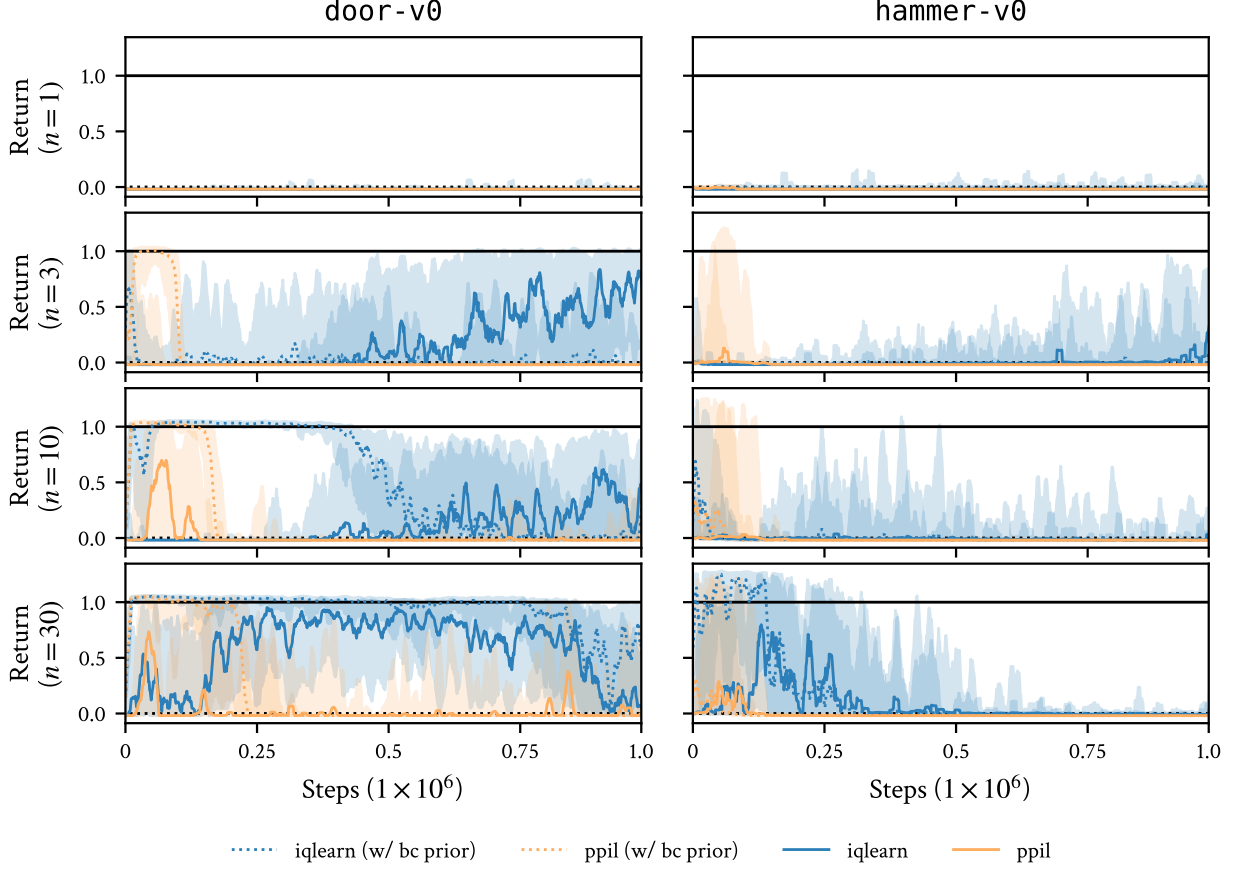


Figure 38 | Normalized performance of **IQLearn** and **PPIL** for online **Adroit** tasks with **BC** pretraining. Uncertainty intervals depict quartiles over 10 seeds. n refers to demonstration trajectories.

L.3. Baselines with heteroscedastic stationary policies

To investigate the impact of **HETSTAT** policies alone, we evaluated **PPIL** and **IQLearn** with **HETSTAT** policies on the online Gym tasks in Figure 40. There is not a significant discrepancy between **MLP** and **HETSTAT** policies.

L.4. Baselines with pretrained heteroscedastic stationary policies as priors

To bring **IQLearn** and **PPIL** closer to **CSIL**, we implement the baselines with **BC** pretraining, **HETSTAT** policies and **KL** regularization with stationary policies. We evaluate on the harder tasks, online **Adroit** and offline **Gym**, to see if these features contribute sufficient stability to solve the task. Both Figure 41 and Figure 42 show an increase in performance, especially with increasing number of demonstrations, but it is ultimately not enough to completely stabilize the algorithms to the degree seen in **CSIL**.

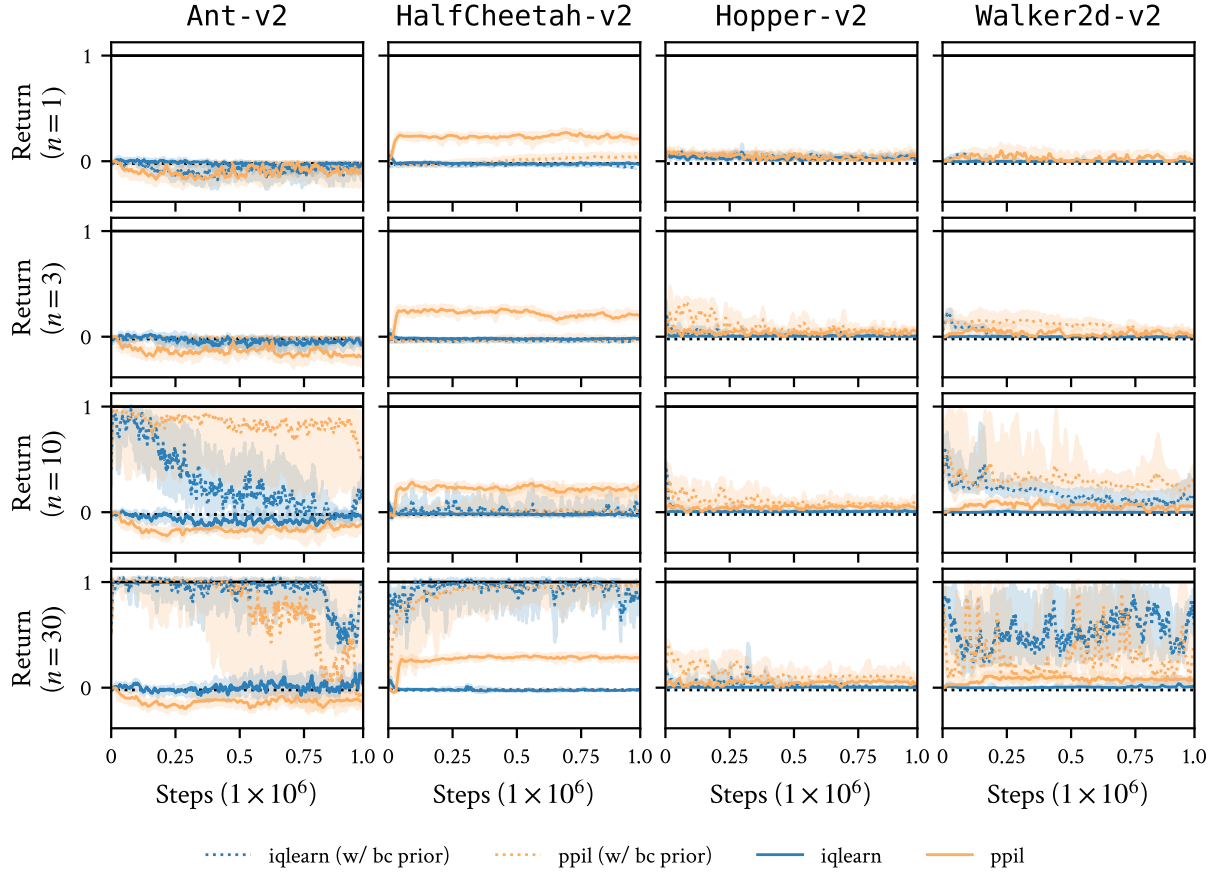


Figure 39 | Normalized performance of **iQLearn** and **PPIL** for offline Gym tasks with BC pretraining. Uncertainty intervals depict quartiles over 10 seeds. n refers to demonstration trajectories.

L.5. Importance of critic pretraining

To ablate the importance of critic pretraining, Figure 43 shows the performance difference on online Gym tasks. Critic pretraining provides only a minor performance improvement.

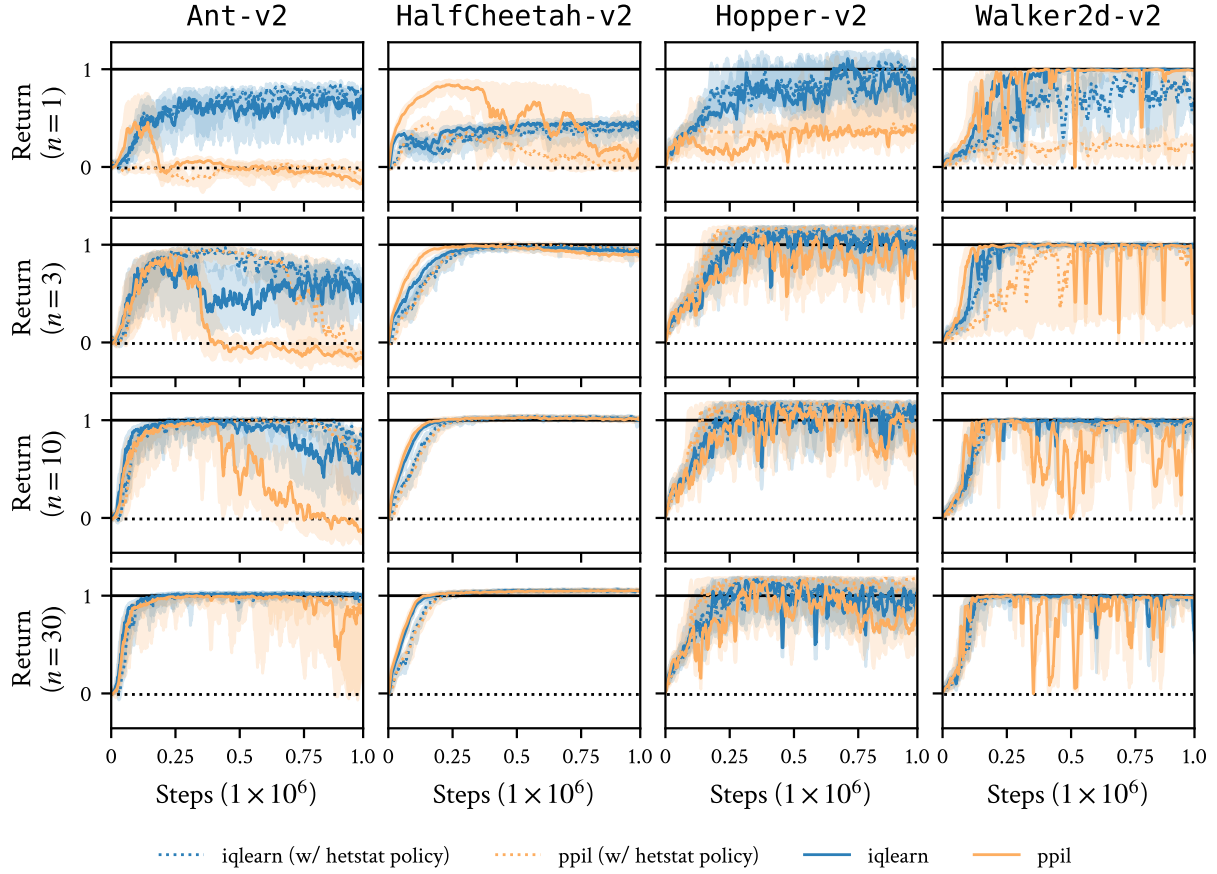


Figure 40 | Normalized performance of **iQLearn** and **PPIL** for online Gym tasks with **HETSTAT** policies. Uncertainty intervals depict quartiles over 10 seeds. n refers to demonstration trajectories.

L.6. Importance of reward finetuning

To ablate the importance of reward finetuning, Figure 44. shows the performance difference on online Gym tasks. Reward finetuning is crucial in the setting of few demonstration trajectories, as the imitation reward is sparse and therefore csil is more susceptible to approximation errors in stationarity. It is also important for reducing performance variance and ensuring stable convergence.

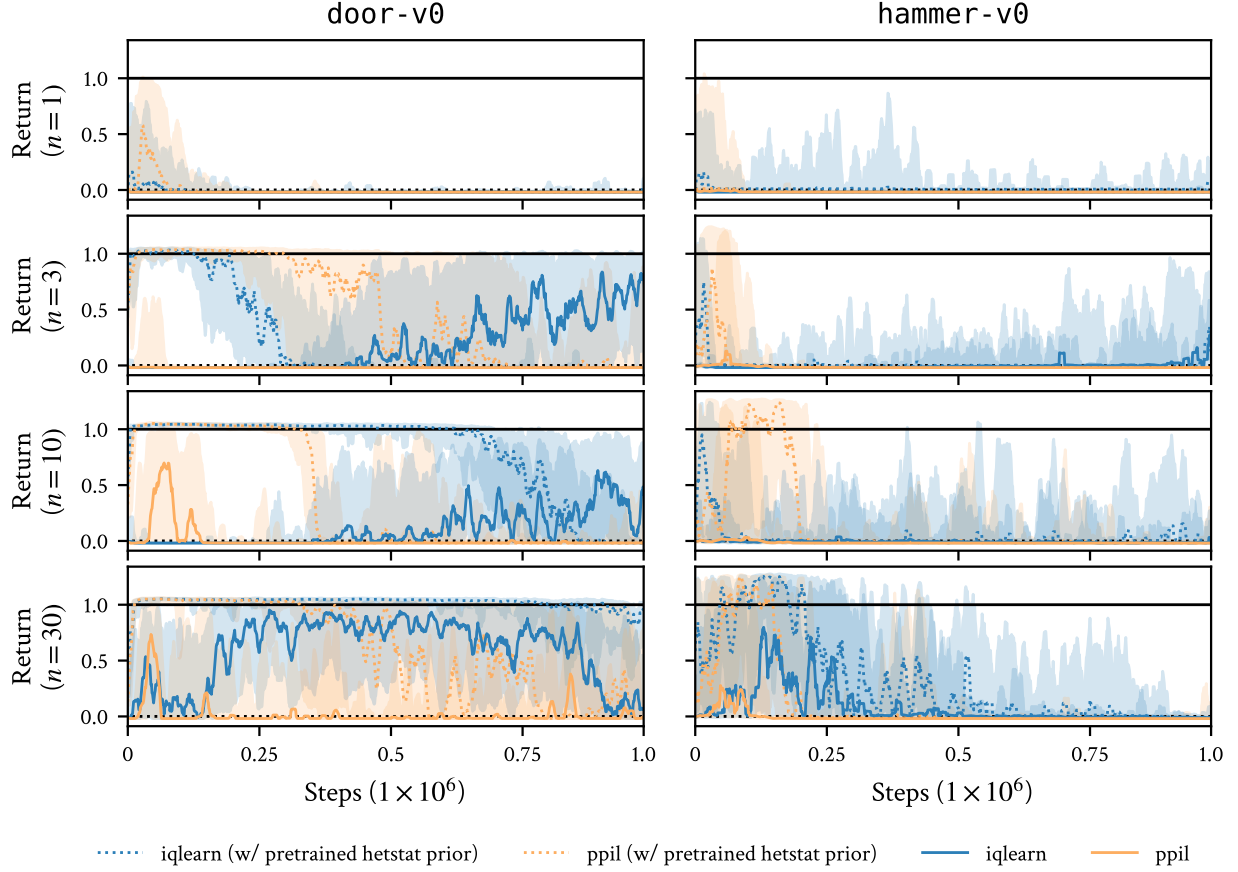


Figure 41 | Normalized performance of **IQLearn** and **PPIL** for online **Adroit** tasks with pretrained **HETSTAT** policies and **KL**-regularization. Uncertainty intervals depict quartiles over 10 seeds. n refers to demonstration trajectories.

L.7. Importance of critic regularization

To ablate the importance of critic Jacobian regularization, Figure 45. shows the performance difference on online Gym tasks. The regularization has several benefits. One is faster convergence, as it encodes the coherency inductive bias into the critic. A second is stability, as it encodes first-order optimality w.r.t. the expert demonstrations, mitigating errors in policy evaluation. The inductive bias also appears to reduce performance variance. One observation is that the performance of **Ant-v2** improves without the regularization. This difference could be because the regularization encourages imitation rather than apprenticeship-style learning where the agent improves on the expert.

L.8. Stationary and non-stationary policies

One important ablation for **CSIL** is evaluating the performance with standard **MLP** policies like those used by the baselines. We found that this setting was not numerically stable enough to complete an ablation experiment. Due to the spurious behaviour (e.g. as shown in Figure 2), the loglikelihood values used in the reward varied significantly in magnitude, destabilizing learning significantly, leading to policies that could no longer be numerically evaluated. This result means that stationarity is a critical component of the **CSIL** implementation.

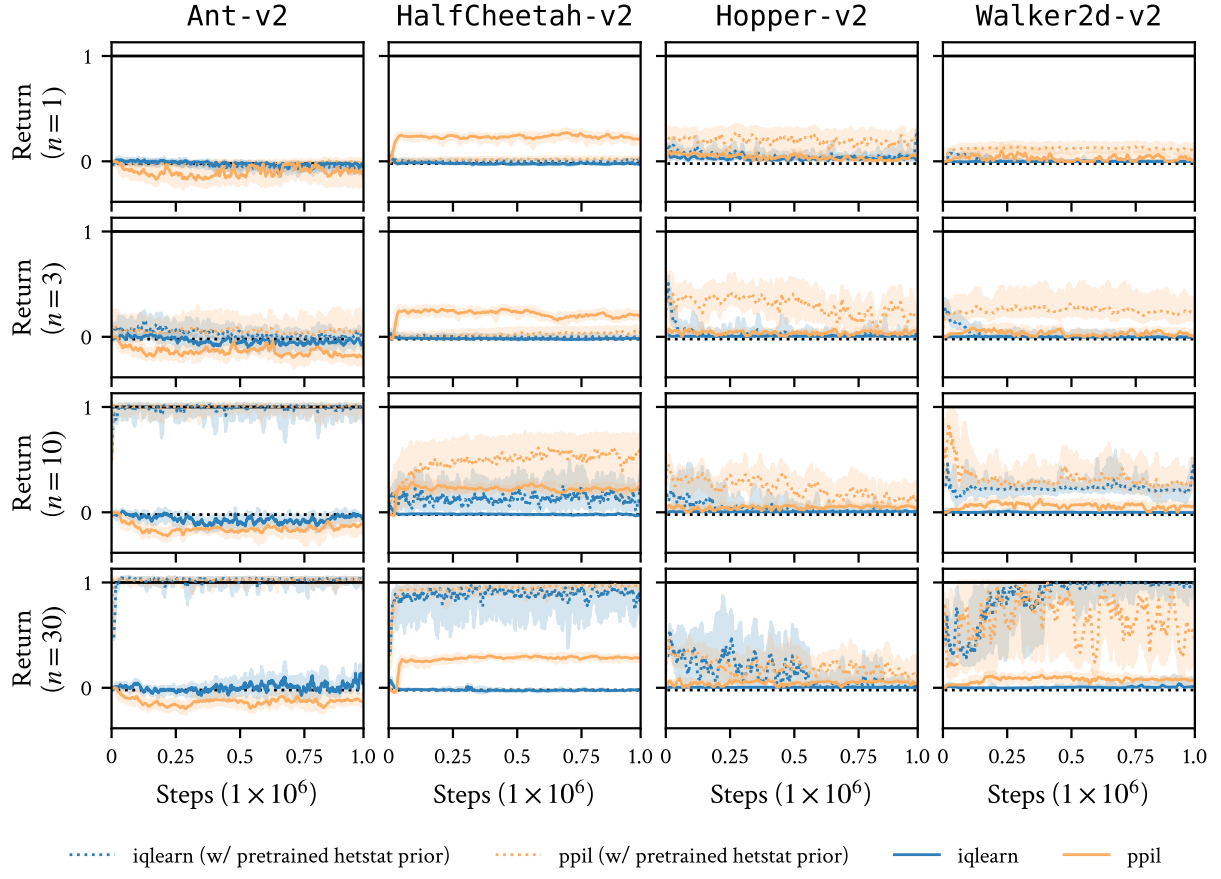


Figure 42 | Normalized performance of `iqlearn` and `ppil` for offline Gym tasks with pretrained `HETSTAT` policies and KL -regularization. Uncertainty intervals depict quartiles over 10 seeds. n refers to demonstration trajectories.

L.9. Effectiveness of constant rewards

Many imitation rewards typically encode an inductive bias of positivity or negativity, which encourage survival or ‘minimum time’ strategies respectively [Kostrikov et al., 2019]. We ablate `CSIL` with this inductive bias for survival tasks (`Hopper-v2` and `Walker-v2`) and minimum-time tasks (`robomimic`). Figure 46 shows that positive-only rewards are sufficient for `Hopper-v2` but not for `Walker-v2`. Figure 47 shows that negative-only rewards is effective for the simpler tasks (`Lift`) but not the harder tasks (`NutAssemblySquare`).

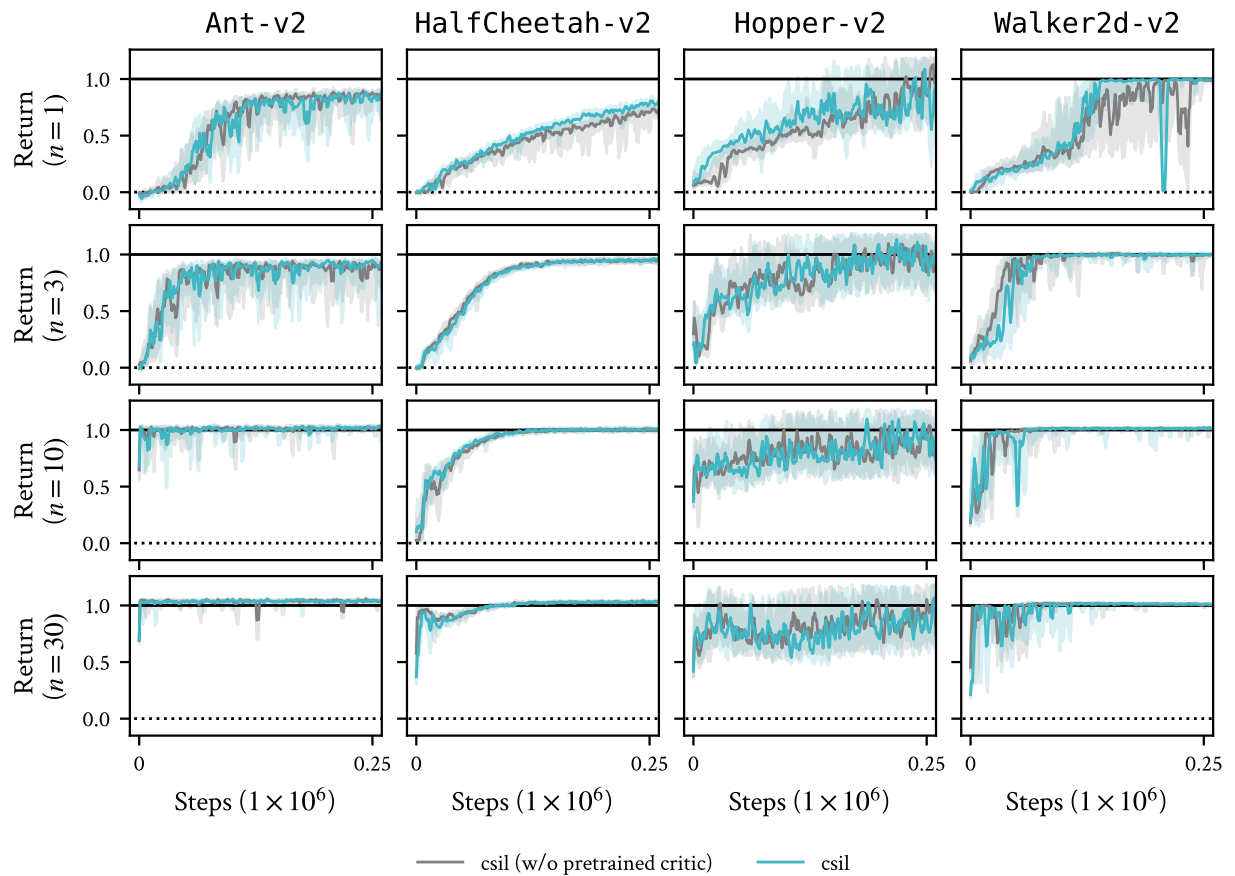


Figure 43 | Normalized performance of `csil` for online Gym tasks a critic pretraining ablation. Uncertainty intervals depict quartiles over 10 seeds. n refers to demonstration trajectories.

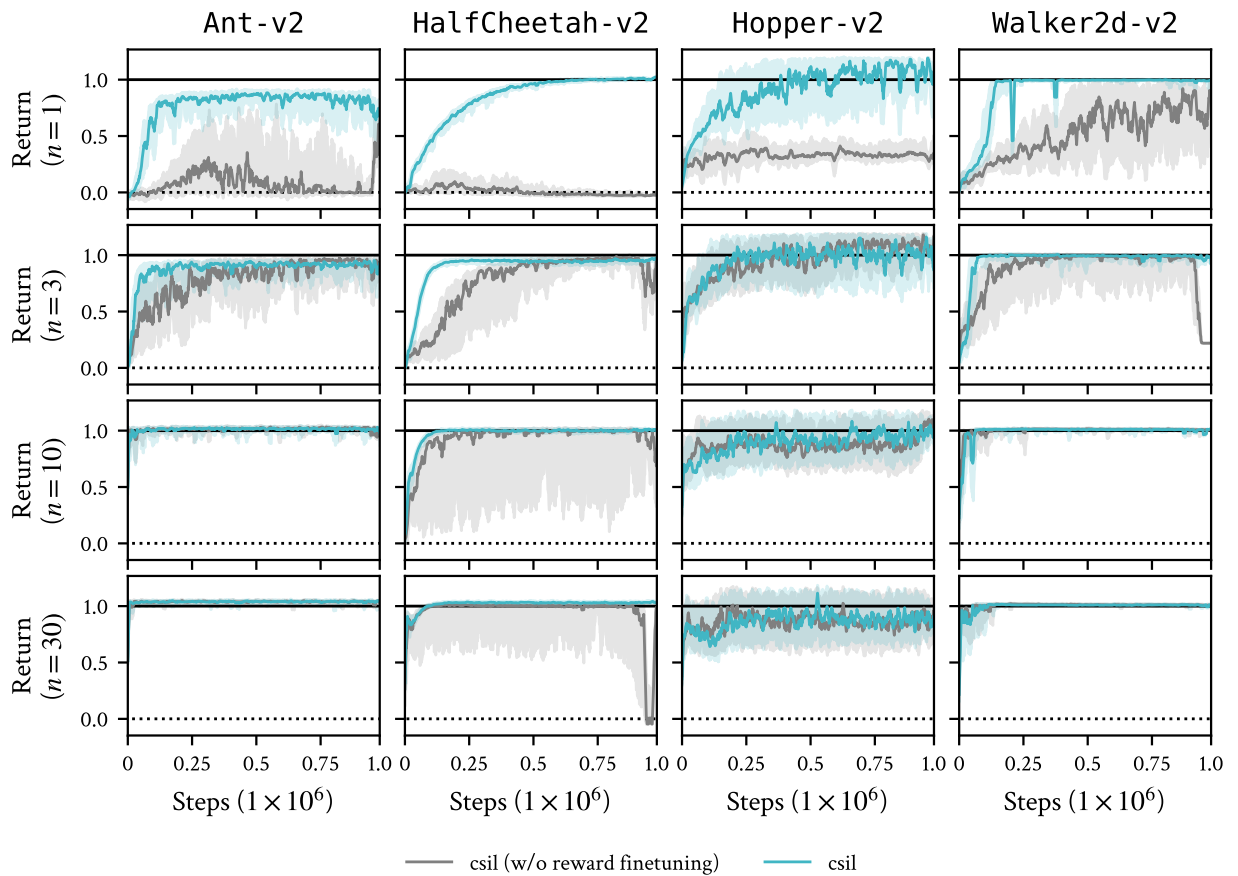


Figure 44 | Normalized performance of `csil` for online Gym tasks with a reward finetuning ablation. Uncertainty intervals depict quartiles over 10 seeds. Refinement is most important in the low demonstration setting where the initial BC policy and coherent reward is less defined, and therefore the initial policy is poor and the coherent reward is more susceptible to exploitation of the stationary approximation errors. n refers to demonstration trajectories.

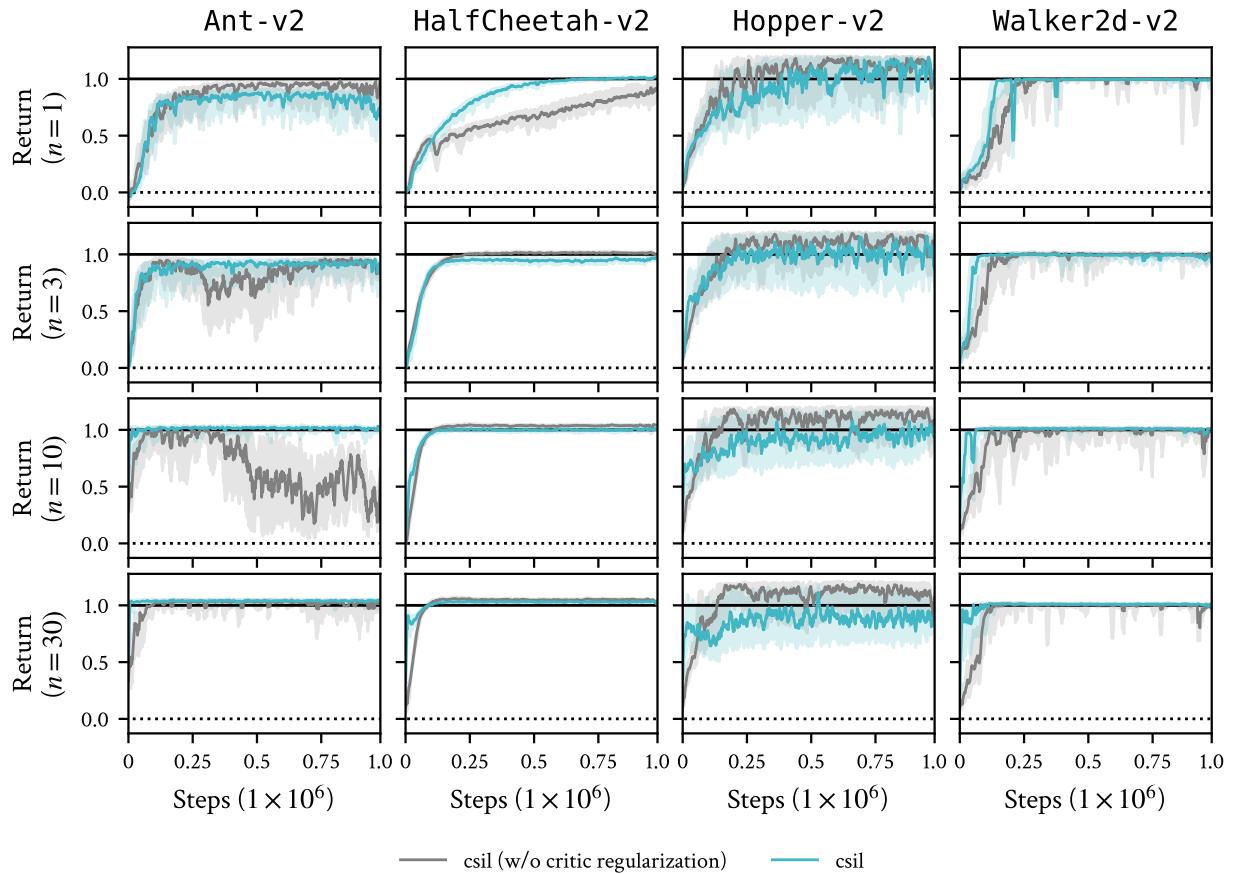


Figure 45 | Normalized performance of `csil` for online MuJoCo Gym without regularizing the critic Jacobian. Uncertainty intervals depict quartiles over 10 seeds. The benefit of this regularization is somewhat environment dependent, but clearly regularizes learning to the demonstrations effectively in many cases. Performance reduction is likely due to underfitting during policy evaluation due to the regularization. n refers to demonstration trajectories.

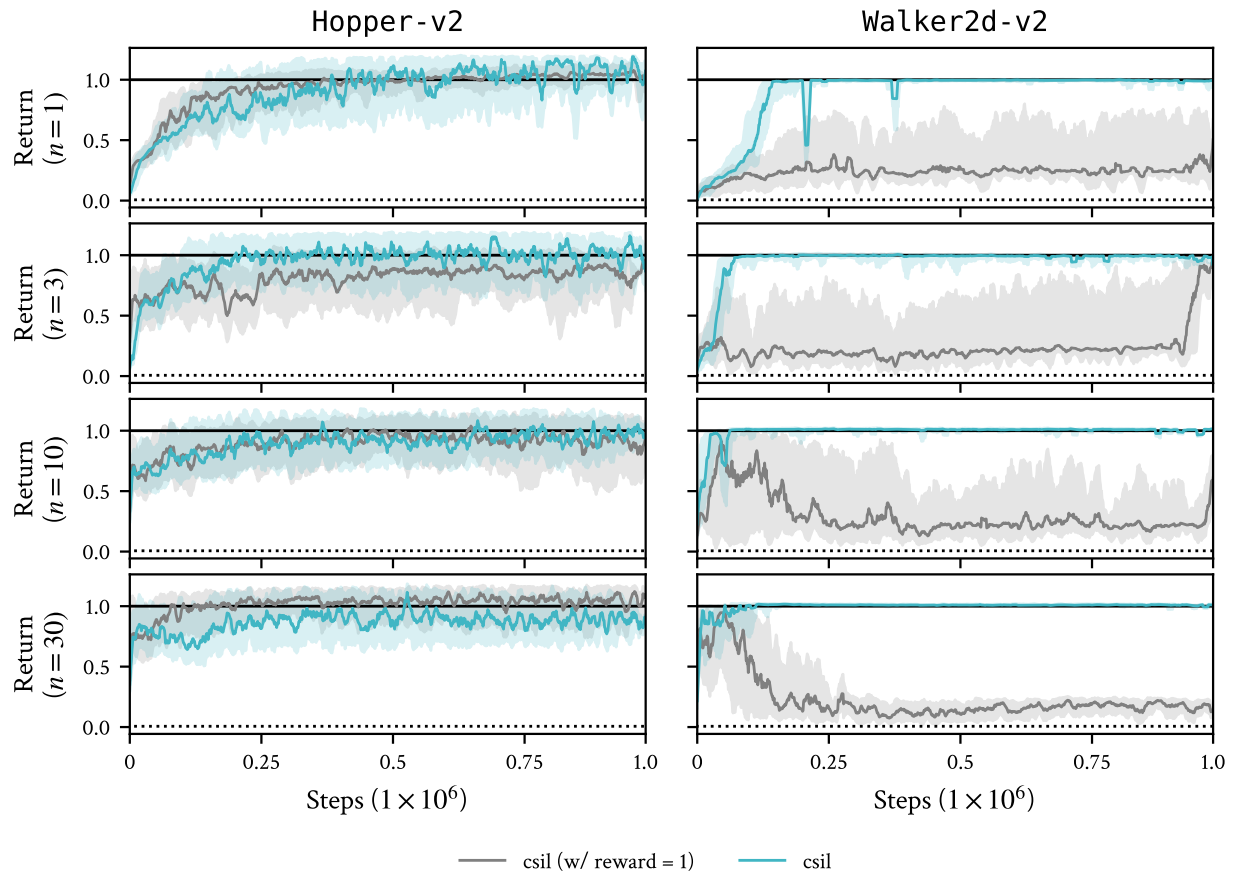


Figure 46 | Online MuJoCo Gym tasks with absorbing states where `CSIL` is given a constant +1 reward function. Uncertainty intervals depict quartiles over 10 seeds. While this is sometimes enough to solve the task (due to the absorbing state), the `CSIL` reward performs equal or better. n refers to demonstration trajectories.

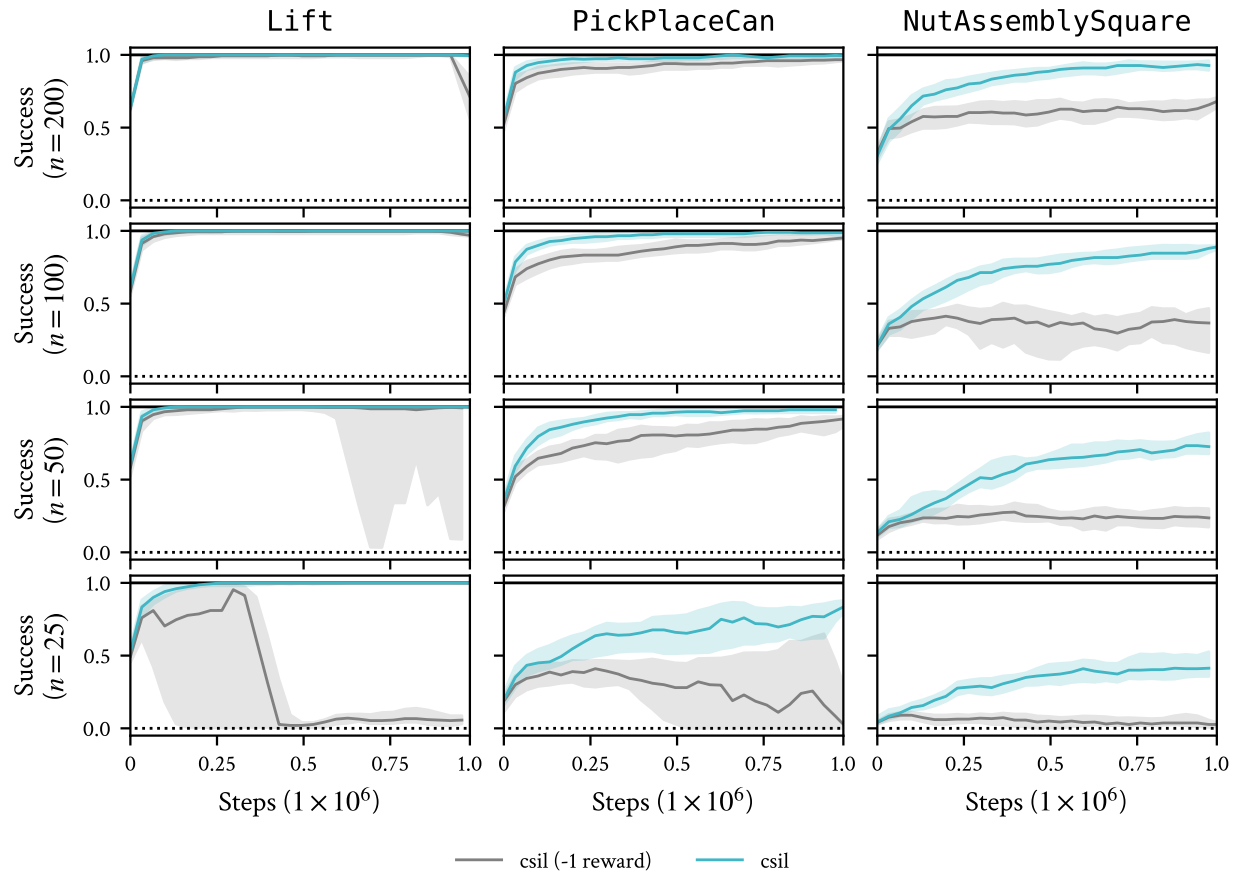


Figure 47 | Online robomimic tasks where CSIL is given a constant -1 reward function. Uncertainty intervals depict quartiles over 10 seeds. While a constant reward is sometimes enough to solve the task (due to the absorbing state), the CSIL reward performs roughly equal or better, with lower performance variance. n refers to demonstration trajectories.